The
PHILOSOPHICAL MAGAZINE

FIRST PUBLISHED IN 1798

L. 46 SEVENTH SERIES No. 381 October 1955

UNIVERSITY OF HAWAII
LIBRARY
NOV 25 '55

A Journal of Theoretical Experimental and Applied Physics

EDITOR
PROFESSOR N. F. MOTT, M.A., D.Sc., F.R.S.

EDITORIAL BOARD
SIR LAWRENCE BRAGG, O.B.E., M.C., M.A., D.Sc., F.R.S.
SIR GEORGE THOMSON, M.A., D.Sc., F.R.S.
PROFESSOR A. M. TYNDALL, C.B.E., D.Sc., F.R.S.

PRICE 15s. 0d.
Annual Subscription £8 0s. 0d. payable in advance

D AND PUBLISHED BY TAYLOR & FRANCIS LTD., RED LION COURT, FLEET ST., LONDON, E.C.4

Announcing a New International Journal on

FLUID MECHANICS

Taylor & Francis, Ltd. (*Publishers*), in consultation with the Editor of the Philosophical Magazine, propose shortly to start a new international journal dealing with **Fluid Mechanics,** under the Editorship of Dr. G. K. Batchelor (Cambridge). A notice giving particulars of the policy of the proposed journal will appear shortly.

To be printed and published by

TAYLOR & FRANCIS, LTD.
RED LION COURT, FLEET STREET
LONDON, E.C. 4

ALERE FLAMMAM

CXVIII. *The Four Possible Waves in a Magneto-Ionic Medium*

By J. H. Piddington
Division of Radiophysics, C.S.I.R.O., Sydney, Australia*

[Received June 20, 1955]

Summary

It is well known that several different types of waves may be transmitted through a magneto-ionic medium ; that is, ionized gas permeated by a steady magnetic field. Foremost is the pair of radio waves whose properties are so well described by the ' magneto-ionic theory ' of Appleton and others. More recently several hydromagnetic (or magneto-hydrodynamic) waves have been studied. A ' plasma ' or electron-pressure wave has received little attention except in the simple case of zero magnetic field. Finally there are sound waves which may propagate in any gas.

The relationship between these various waves is disclosed : the magneto-ionic medium is quadruply refracting, transmitting four, and only four, different waves. The hydromagnetic ordinary and extraordinary waves are identical with the radio O and E waves, the latter being the simple limiting case of the former when heavy ion motion is negligible. The other two waves comprise a ' magnetic sound ' wave (a type of hydro-magnetic wave) and a ' magnetic plasma ' (P) wave.

The P wave is discussed in some detail, using transport equations. Its velocity and polarization are determined within certain ranges and its spontaneous growth and decay are considered. Examples of P waves in the solar atmosphere are given. If, as seems probable, these waves can grow, then they may cause the O and E waves to grow and so provide an explanation of non-thermal solar radio noise.

The effect of electron pressure on the O and E waves is determined quantitatively.

§ 1. Introduction

A MAGNETO-IONIC medium, comprising ionized gas permeated by a steady magnetic field, may transmit magneto-ionic waves which are electromagnetic waves associated with oscillations of the ions. Radio physicists are well acquainted with the ' magneto-ionic theory ' of Appleton (1932) and others which has proved so satisfactory in explaining radio wave transmission in the ionosphere and the solar atmosphere. According to this theory the magneto-ionic medium is doubly refracting, transmitting an ' ordinary ' (O) and ' extraordinary ' (E) wave. In the present paper it is shown that the magneto-ionic medium is in fact not doubly but *quadruply* refracting.

---

* Communicated from Commonwealth Scientific and Industrial Research Organization.

The original magneto-ionic theory was developed to deal with waves of such high (radio) frequencies that perturbations of the heavy ions of the gas may be neglected.* Furthermore, both electron and heavy ion thermal motions and the resulting pressures of the electron gas and heavy ion gas are neglected.† If we continue to neglect gas pressure but decrease the wave frequency until heavy ion motion is important the two waves change gradually into hydromagnetic (or magneto-hydrodynamic) waves (Aström 1950, Piddington 1955 a). The O and E waves retain their identity throughout the frequency change,‡ but become more complex when heavy ion motion is considered. In fact the radio O and E waves are really simple limiting cases of hydromagnetic O and E waves when heavy ion motion is neglected.

In addition to the O and E waves, two others may propagate in the magneto-ionic medium provided the gas is not at absolute zero temperature. These waves depend in part on the elastic forces resulting from compression of the gas (either as a whole or the electron gas alone). The waves vanish when these forces are neglected. Nevertheless they are true electromagnetic waves, having associated electric and magnetic fields and a Poynting flux indicating a flow of electromagnetic energy. One of the waves appears at hydromagnetic frequencies and probably does not propagate in the higher frequency part of the spectrum. The other occurs at radio frequencies ; it is not yet clear how far into the low-frequency spectrum this wave may extend.

The low-frequency wave (which might be called a ‘ magnetic sound ’ or S wave) makes its appearance when thermal motions of the heavy gas particles, both ions and atoms, are taken into account ; that is when the whole gas has a finite pressure (Piddington 1955 a). It may be considered either as a third hydromagnetic wave or as a sound wave disturbed by the steady magnetic field. It differs considerably from the other two hydromagnetic waves : the gas movement tends to be longitudinal rather than transverse and the velocity is of the order of the velocity of sound rather than the familiar ‘ hydromagnetic velocity ’. When propagation is along the magnetic field the wave is almost a pure sound wave, having an associated electric field only.

The S wave has already been discussed in some detail and the (fourth degree) dispersion equation for a magneto-ionic medium with all four waves present has been given and discussed (Piddington 1955 b). In the present paper we will, for simplicity, confine ourselves to (radio) frequencies where heavy ion motion may be neglected. This eliminates the S wave and reduces the O and E waves to the relatively simple form of radio waves instead of hydromagnetic waves.

---

* The effects of heavy ions on wave polarization has been investigated by Baker and Green (1933).

† Electron motions are considered insofar as they cause collisions with heavy ions and atoms and so absorption of the waves by a scattering process.

‡ Although there may be portions of the spectrum where the refractive index of a particular wave is an imaginary quantity so that the wave cannot propagate.

The fourth (high-frequency) magneto-ionic wave appears when electron thermal motions and electron gas pressure are taken into account. At the frequencies concerned the medium may be regarded as triply refracting.

It is the object of the present paper to

(*a*) present the overall picture of the four magneto-ionic waves ;

(*b*) indicate the characteristics of the fourth magneto-ionic wave ;

(*c*) show the effects of electron pressure on the O and E waves ; it is not certain that this effect is negligible in regions of high temperature such as the solar corona ;

(*d*) consider the possibilities of spontaneous growth of the fourth magneto-ionic wave and its effectiveness in generating solar radio emission.

§ 2. PLASMA OSCILLATIONS AND WAVES

The reason for the neglect of the third magneto-ionic wave may be traced historically. When the magneto-ionic theory was developed, electron pressure terms were omitted for simplicity and the great success of the theory seemed to justify this step, at least as far as propagation in the ionosphere was concerned. This is so as far as the O and E waves are concerned, but what was not realized was that the omission entirely removed one root from the dispersion equation and one possible wave from the medium.

In the meantime a new type of electrical oscillation was studied, not as a wave travelling through the ionosphere, but as a stationary oscillation in a discharge tube. This is usually called a plasma or space-charge oscillation (Tonks and Langmuir 1929). Expressed mathematically in the form exp $i(\omega t - kx)$ for variation in time t and space x it has the restriction that k is zero or imaginary. Seeking standing waves in a magneto-ionic medium Martyn (1947) found two as opposed to Tonks and Langmuir's one. However, neither of these two corresponds to the earlier wave ; they are the O and E waves in a particular part of the spectrum where the real part of k is zero. A change in frequency or electron density will cause them to propagate through the gas. To these two must be added the third ‘ plasma ’ (P) wave which continues to exist when a steady magnetic field is added. The presence of three stationary oscillatory modes was noted by Westfold (1949) and the presence of three travelling waves may be inferred from Bailey's (1948) equations, although these have been complicated by the introduction of a steady electron drift so that there seem to be twelve different waves present. The nature of all these ‘ waves ’ has been discussed briefly elsewhere* (Piddington 1955 b).

When electron pressure is considered, the P wave (which might be called a ‘ magnetic plasma ’ wave) becomes a travelling *electromagnetic* wave and the medium triply refracting. The dispersion equation is now of the third degree and considerably more difficult to discuss as it does not factorize.

The P wave has been studied for propagation along the magnetic field, when it becomes a pure electric wave and quite independent of the two electromagnetic waves O and E. Thomson and Thomson (1933) found the dispersion equation

$$\frac{k^2}{\omega^2}=\frac{\beta m}{\kappa T}(1-X)$$

where m, T, e and N_0 are the electron mass, temperature, charge and density, κ is Boltzmann's constant, $X=4\pi N_0e^2/m\omega^2$ and β is a constant, equal to unity in this case. Electrostatic units are used. Bohm and Gross (1949 a) derived a similar equation starting from Boltzmann's equations instead of using transport methods ; they found $\beta=\frac{1}{3}$. The P wave has also been studied by Gross (1951) for the case of propagation perpendicular to the magnetic field. He finds some surprising results and incidentally demonstrates that the use of Boltzmann's equations in the extended (3 wave) magneto-ionic theory is likely to prove too difficult mathematically. Whatever the inaccuracy entailed, the use of transport methods seems justified at least in a preliminary survey.

§ 3. THE DISPERSION EQUATION

The equations necessary to describe the three magneto-ionic waves are Maxwell's field equations and Maxwell's momentum transfer equation for an electron gas. For the time being collisions of electrons with heavy ions are neglected. The equations are

$$\text{curl }\mathbf{H}=4\pi c^{-1}\mathbf{j}+c^{-1}\frac{\partial \mathbf{E}}{\partial t}, \qquad (1)$$

$$\text{curl }\mathbf{E}=-c^{-1}\frac{\partial \mathbf{H}}{\partial t}, \qquad (2)$$

$$\text{div }\mathbf{E}=-4\pi Ne, \qquad (3)$$

$$m\frac{d\mathbf{v}}{dt}+N^{-1}\text{ grad }p_e+e(\mathbf{E}+c^{-1}\mathbf{v}\times\mathbf{H})=0. \qquad (4)$$

---

* The general dispersion equation, derived for a stationary observer in a magneto-ionic medium, is of the fourth degree in k^2 or ω^2. Each type of wave is represented by two waves moving in opposite directions but otherwise identical. When the observer moves relative to the gas he sees waves which have undergone a Lorentz transformation and the pairs of waves are no longer identical. In addition the drift of the gas or observer appears to introduce further waves ; these are not real, however : they have velocity equal to the drift velocity and mean, physically, that any stationary irregularity in the gas appears as a travelling wave when seen by a moving observer.

Here $\mathbf{H}$, $\mathbf{E}$ and $\mathbf{j}$ are respectively the magnetic and electric fields and the current density and $\mathbf{v}$, N and p_e the electron gas velocity, density and pressure. For small oscillations about a steady state, products of two variables may be neglected so that eqn. (4) becomes

$$\frac{\partial \mathbf{v}}{\partial t}+N_0^{-1}\tau \operatorname{grad} n+\frac{e}{m}\mathbf{E}+\mathbf{v}\times\mathbf{\Omega}=0 \qquad . \quad . \quad . \quad . \quad . \quad . \quad (5)$$

where $n=N-N_0$, $\mathbf{H}_0$ is the steady part of $\mathbf{H}$, and $\mathbf{\Omega}=\mathbf{H}_0e/mc$. Also grad p_e has been replaced by $m\tau$ grad n where τ is one-third the mean square random velocity of the electrons, and electron temperature fluctuations are neglected.

$$\mathbf{j}=-N_0e\mathbf{v}. \quad . \quad . \quad . \quad . \quad . \quad . \quad . \quad . \quad . \quad . \quad (6)$$

Consider a right-handed system of axes (x, y, z) and a plane wave of the form exp $i(\omega t-kx)$ propagated along Ox. Let $\mathbf{\Omega}$ have components Ω_L and Ω_T along Ox and Oz respectively. The vector equations may be written in terms of the perturbation components $v_{x,y,z}$, $E_{x,y,z}$ and $H_{x\,y\,z}$, of N and of the wave frequency and wave number. They become:

$$\left.\begin{aligned} i\omega v_x+\Omega_T v_y+e/mE_x-ikN_0^{-1}\tau n=0 \\ i\omega v_y+\Omega_L v_z-\Omega_T v_x+e/mE_y=0 \\ i\omega v_z-\Omega_L v_y+e/mE_z=0 \end{aligned}\right\} \quad . \quad . \quad . \quad . \quad (7)$$

$$\left.\begin{aligned} 4\pi N_0 e v_x-i\omega E_x=0 \\ 4\pi N_0 e v_y-i\omega E_y+ickH_z=0 \\ 4\pi N_0 e v_z-i\omega E_z-ickH_y=0 \end{aligned}\right\} \quad . \quad . \quad . \quad . \quad (8)$$

$$\left.\begin{aligned} ckE_z+\omega H_y=0 \\ ckE_y-\omega H_z=0 \end{aligned}\right\} \quad . \quad . \quad . \quad . \quad . \quad . \quad . \quad . \quad (9)$$

$$ikE_x-4\pi ne=0. \quad . \quad . \quad . \quad . \quad . \quad . \quad . \quad . \quad (10)$$

Using eqns. (9) and introducing the function X, defined above, eqns. (8) reduce to

$$\left.\begin{aligned} \omega m X v_x &= ieE_x \\ \omega m X v_y &= ieE_y\left(1-\frac{c^2k^2}{\omega^2}\right) \\ \omega m X v_z &= ieE_z\left(1-\frac{c^2k^2}{\omega^2}\right). \end{aligned}\right\} \quad . \quad . \quad . \quad . \quad . \quad . \quad (11)$$

These equations and (10) may be used to eliminate $\mathbf{v}$ and n from (7); the new variables $Y_L=\Omega_L/\omega, Y_T=\Omega_T/\omega$ are introduced.

$$\left.\begin{aligned} \left(1-X-\frac{\tau k^2}{\omega^2}\right)E_x-iY_T\left(1-\frac{c^2k^2}{\omega^2}\right)E_y=0 \\ \left(1-X-\frac{c^2k^2}{\omega^2}\right)E_y-iY_L\left(1-\frac{c^2k^2}{\omega^2}\right)E_z+iY_TE_x=0 \\ \left(1-X-\frac{c^2k^2}{\omega^2}\right)E_z+iY_L\left(1-\frac{c^2k^2}{\omega^2}\right)E_y=0. \end{aligned}\right\} \quad . \quad (12)$$

Eliminating **E** we have the dispersion equation

$$\left(1-X-\frac{\tau k^2}{\omega^2}\right)\left\{\left(1-X-\frac{c^2k^2}{\omega^2}\right)^2-Y_L^2\left(1-\frac{c^2k^2}{\omega^2}\right)^2\right\}-Y_T^2\left(1-\frac{c^2k^2}{\omega^2}\right)\left(1-X-\frac{c^2k^2}{\omega^2}\right)=0. \qquad (13)$$

The basic equations used above are similar to those employed by Bailey (1948) with his steady drift velocity omitted. Equation (13) may be derived from Bailey's full (twelfth degree) dispersion equation by reducing the drift velocity to zero. The preceding derivation was given to avoid the confusion due to the ion drift and because eqns. (7) to (12) are needed later to determine the form of the P wave.

Equation (13) is of the third degree in k^2 indicating three pairs of electromagnetic waves ; these are the O, E and P waves. When $\tau=0$ one pair of waves disappears and, as Bailey has shown, the equation reduces to the well-known magneto-ionic equation.

To introduce the remaining (S) magneto-ionic wave, eqn. (6) is replaced by $\mathbf{j}=N_0e(\mathbf{v}'-\mathbf{v})$ where $\mathbf{v}'$ is the positive ion perturbation velocity and is given by another equation similar to (4) describing heavy ion momentum transfer. The dispersion equation is then of the fourth degree indicating four pairs of waves. This equation is difficult to use and if the S wave is to be studied some simplifying assumptions are desirable. A convenient simplification is effected by introducing the electrical conductivity tensor (Piddington 1955 a) in place of the two equations of momentum transfer. At the low frequencies concerned the displacement current may also be neglected and the properties of the three waves then found without excessive difficulty.

§ 4. LONGITUDINAL AND TRANSVERSE PROPAGATION

In the special cases of propagation along and perpendicular to the magnetic field, eqn. (13) factorizes. In each case two of the modes remain linked with a quadratic dispersion equation, while the third separates out.

For longitudinal propagation ($Y_T=0$) the P wave separates out ; its dispersion equation, with the effect of electron collisions with heavy particles included (frequency ν sec^{-1}), is

$$\frac{k^2}{\omega^2}=\tau^{-1}(1-X-iZ)$$

where $Z=\nu/\omega$. This shows the way in which electron collisions cause wave attenuation, just as found earlier by Bohm and Gross (1949 b) using a microscopic treatment. The wave velocity is $(\tau/1-X)^{1/2}$ which differs by a fixed factor from that found by Bohm and Gross whose dispersion equation is

$$\frac{k^2}{\omega^2}=\frac{1}{3\tau}(1-X-iZ).$$

The O and E waves are exactly as in the simple magneto-ionic theory being unaffected by electron pressure.

When propagation is perpendicular to the magnetic field ($Y_L=0$) the O wave separates out, once again unaffected by the electron pressure term. The E and P waves are linked in a quadratic equation whose roots are (writing Y for Y_T) :

$$\frac{k^2}{\omega^2}=\frac{1}{2}\left\{(1-X)\left(\frac{1}{\tau}+\frac{1}{c^2}\right)-\frac{Y^2}{\tau}\right\}\pm\frac{1}{2}\left\{(1-X)\left(\frac{1}{\tau}-\frac{1}{c^2}\right)-\frac{Y^2}{\tau}\right\}$$
$$\times\left[1+\frac{4Y^2X}{c^2\tau\{(1-X)(1/\tau-1/c^2)-Y^2/\tau\}^2}\right]^{1/2}.$$

The positive sign corresponds to the P wave and the negative to the E wave. The equation simplifies for very small values of the second term in square brackets. When $c^2 \gg \tau$ this condition is

$$\frac{4\tau Y^2X}{c^2(1-X-Y^2)^2}\ll 1$$

and the two waves are given approximately by

$$\frac{k^2}{\omega^2}=\tau^{-1}(1-X-Y^2)$$

and

$$\frac{k^2}{\omega^2}=c^{-2}\left\{1-\frac{X(1-X)(1-\tau/c^2)}{(1-X)(1-\tau/c^2)-Y^2}\right\}.$$

The first is the P wave having velocity $(\tau/1-X-Y^2)^{1/2}$, provided this velocity is much less than c ; otherwise the full equation must be used. The second is the E wave and reduces, when $\tau=0$, to the well-known form (Booker 1934) of the original magneto-ionic theory. Thus electron pressure only changes the E wave appreciably when τ is comparable with c (temperatures of order 10^8 °K or more) in which case a relativistic treatment should be used ; or when the refractive index is nearly zero.

Doubt has been cast on the above results by Gross who compared the results of the transport treatment with his own derived from the Boltzmann equation. Under certain conditions his dispersion equation for the P wave differs considerably from that found above and assumes most unexpected forms. In particular the medium does not transmit any wave when $1/Y$ is an integer ; thus the transmitted spectrum has a series of narrow gaps at frequencies which are multiples of the gyro-frequency. Also Gross's dispersion equation takes a more complex form : in the case when $\tau k^2/\omega^2 \ll Y^2$ it has three different forms, as follows :

when $$X \gg Y^2 \quad k^2/\omega^2=8\tau^{-1}\,\frac{Y(1-X-Y^2)}{X^{1/2}},$$

$$X \simeq Y^2 \quad k^2/\omega^2=2\tau^{-1}(X+Y^2-1),$$

$$X \ll Y^2 \quad k^2/\omega^2=2\tau^{-1}\,\frac{Y^2(X+Y^2-1)}{X}.$$

The last two waves only propagate when $X+Y^2>1$, that is when, according to the equation derived above, the medium is overdense.

Gross remarks that " the same type of difference can be found if one does not restrict the discussion to the plasma-type solutions, but considers the strongly coupled waves when $ck/\omega \simeq Y$, $X^{1/2}$ " (that is, the E wave).

Whatever inaccuracies may eventually be found to result from the use of transport methods, their use seems justified in a preliminary survey of obliquely propagated waves. The use of Boltzmann's equations would appear to offer excessive mathematical difficulties.

§ 5. OBLIQUE PROPAGATION

In the general case, where propagation is neither along nor perpendicular to the magnetic field, eqn. (13) does not factorize and a full discussion becomes lengthy, beyond the scope of this paper. However, with the restriction that $\tau \ll c^2$ the waves may be separated by using our prior (approximate) knowledge of their characteristics.

Let us assume that the values of the refractive index (ck/ω) of the O and E waves are not substantially changed by electron pressure. In the regions of main interest ck/ω lies between zero and unity and so

$$\frac{\tau k^2}{\omega^2}=\frac{\tau}{c^2}\cdot\frac{c^2k^2}{\omega^2}\ll 1.$$

Replace $\tau k^2/\omega^2$ in eqn. (13) by a small constant (δ) ; the two roots corresponding to the O and E waves are then given by

$$\frac{c^2k^2}{\omega^2}=1-2X\left[2-\frac{Y_T{}^2}{1-X-\delta}\pm\left\{\left(\frac{Y_T{}^2}{1-X-\delta}\right)^2+4Y_L{}^2\right\}^{1/2}\right]^{-1}. \qquad (14)$$

This reduces to the well-known magneto-ionic equation (Booker 1934) when $\delta=0$ and, in general, is affected only slightly by the presence of δ. However, in regions of nearly zero or very high refractive index the value of ck/ω may be more critically dependent on δ. Also when $\tau \sim c^2$ it is evident that the effects of electron pressure may be of major importance. It may be noted that δ only affects the Y_T terms and so increases in importance as Y_T/Y_L increases.

To separate the P wave we assume its phase velocity is much less than c, that is $c^2k^2/\omega^2 \gg 1$, and also that X is of order unity or less. Equation (13) then reduces approximately to

$$\left(1-X-\frac{\tau k^2}{\omega^2}\right)(1-Y_L{}^2)-Y_T{}^2=0$$

which may be written

$$\frac{k^2}{\omega^2}=\tau^{-1}\left(1-X-\frac{Y_T{}^2}{1-Y_L{}^2}\right). \qquad . \quad . \quad . \quad . \qquad (15)$$

It may be noted that this equation does not hold in the interesting range where the term in brackets approaches zero, that is, near the natural plasma frequency. Here the phase velocity approaches and exceeds c and our simplifying assumption no longer holds. At yet higher phase velocities when $c^2k^2/\omega^2 \ll 1$ the dispersion equation takes the form

$$\frac{k^2}{\omega^2}=\tau^{-1}\left\{1-X-\frac{Y_T{}^2(1-X)}{(1-X)^2-Y_L{}^2}\right\}. \qquad . \quad . \quad . \qquad (16)$$

Some interesting properties of the P wave may be displayed by plotting $\mu^2 (\equiv c^2k^2/\omega^2$, the square of the complex refractive index) against X. This method was used by Ratcliffe (1933) to show the characteristics of the O and E waves. The curves are drawn for longitudinal propagation and transverse propagation; the region between the curves corresponds to the infinite number of oblique waves. One of Ratcliffe's curves is drawn in fig. 1 for the O and E waves; the full lines correspond to longitudinal propagation and the dashed lines to transverse propagation. The corresponding curves for the P wave are also shown and the two areas of oblique propagation are cross hatched. The equations used were those of § 4, using the *full* transverse equation. The value of $Y (\equiv (Y_L{}^2 + Y_T{}^2)^{1/2})$ chosen was 0·5 and real values of μ are seen to exist

Fig. 1

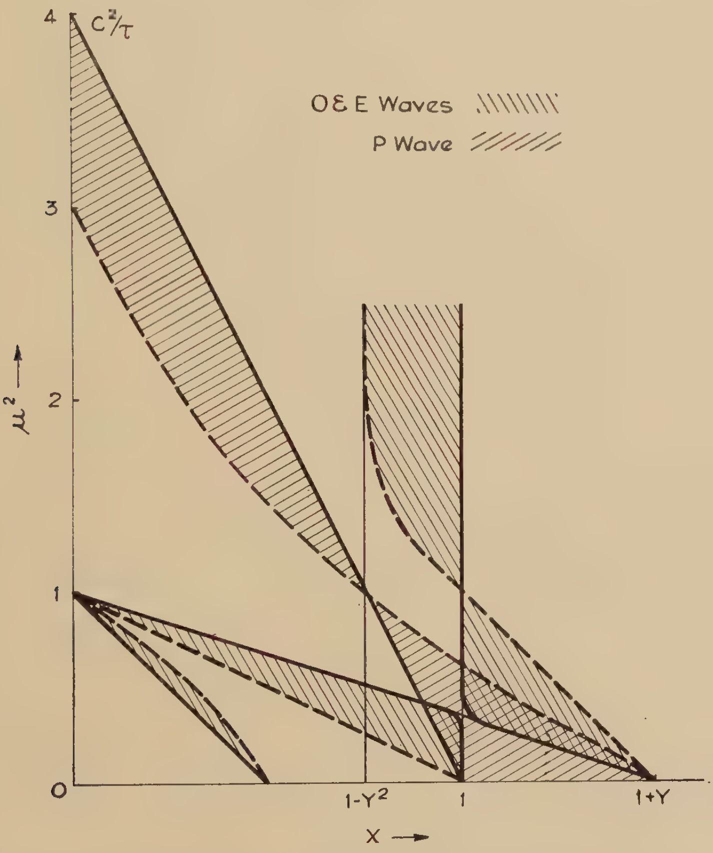

Areas on the μ^2—X diagram corresponding to the O and P waves. Full lines correspond to transmission along the magnetic field ($Y_T = 0$), dashed lines to propagation across the magnetic field ($Y_L = 0$). The hatched areas between these lines correspond to oblique propagation.

for values of X up to $1+Y$. The value of c^2/τ used was 4 which is very small, but was chosen to make the diagram a reasonable shape. It corresponds to an electron temperature of $\sim 1{\cdot}4\times 10^9$ °K.

The polarization of the P wave may now be determined, unfortunately only in the relatively uninteresting region away from the resonance frequency. Assuming $c^2k^2/\omega^2 \gg 1$ eqn. (12) yields, approximately,

$$\frac{E_z}{E_y} = -iY_L$$

and

$$\frac{E_x}{E_y} = \frac{-ic^2k^2}{\omega^2}\left(\frac{1-Y_L^2}{Y_T}\right).$$

Thus, provided Y_L is of order unity, E_y and E_z are of the same order but out of phase (elliptically polarized) and provided $1-Y_L^2/Y_T$ is of order unity, $E_x \gg E_y$ (or E_z). The greater part of the electric field associated with the wave is a potential field (see eqns. (3) and (10)) and lies in the direction of propagation.

The components of **H** may be found from eqn. (9)

$$H_y = -iY_L\frac{ck}{\omega}\cdot E_y$$

and

$$H_z = \frac{ck}{\omega}E_y$$

so that

$$\frac{H_y}{H_z} = -iY_L,$$

the waves showing elliptical polarization of the magnetic field with $H_y < H_z$.

The components of **v** are found from eqn. (11), remembering that $\frac{c^2k^2}{\omega^2} \gg 1$:

$$\frac{v_x}{v_y} = -i\left(\frac{1-Y_L^2}{Y_T}\right) \quad \text{and} \quad \frac{v_z}{v_y} = -iY_L.$$

Thus the electron velocity components tend in general to be of the same order of magnitude.

§ 6. PLASMA WAVES IN THE SOLAR ATMOSPHERE

Perhaps the region in which plasma waves may have the most interesting observable effects is the solar atmosphere. They may, for example, be a link in the mechanism of the non-thermal radio emission which requires ordered motion of the electrons (Piddington 1953). Magnetic fields exist throughout a large part of the solar atmosphere but particularly above sunspots where their distribution of strength and direction may be inferred with reasonable accuracy from visual observations. The characteristics of some possible plasma waves are given for such a region.

The phase velocity of the P wave is given by

$$V = \frac{\omega}{k} = \tau^{1/2} F(X, \mathbf{Y})$$

where F is given by eqns. (15) and (16) for the restricted conditions concerned but has not been determined for the interesting velocity range near c. It is likely that F has some roughly similar form within this range

Fig. 2

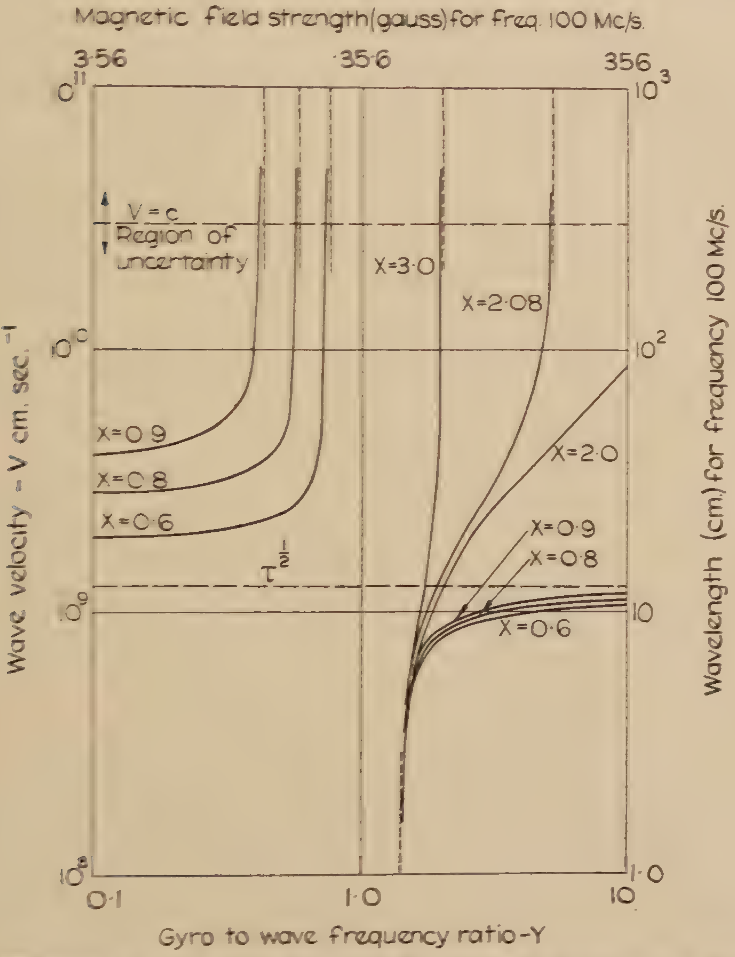

Plasma (P) wave velocities plotted against the ratio Y of electron gyro-frequency to the wave frequency for several different values of plasma frequency X. Also shown are the corresponding wavelengths and magnetic field strengths when the wave frequency is 100 Mc/s.

and so, for illustrative purposes, its value is taken from eqn. (15) and assumed to apply when $V \gtrsim c$. It is assumed that the actual values of V are in error when $V \sim c$ but that the general form of the velocity function so found is representative of the true function.

In fig. 2 the values of V are plotted for P waves in a gas at temperature 10^7 °K which corresponds to the 'hot regions' which occur normally above sunspots (Piddington and Minnett 1951). The waves move obliquely across the (uniform) magnetic field at an angle of $\pi/4$ and V is plotted for $Y(=\sqrt{2}Y_L=\sqrt{2}Y_T)$ ranging between 0·1 and 10. The corresponding values of magnetic field-strength when the wave frequency is 100 Mc/s are plotted, ranging from 3·56 gauss to 356 gauss. Five values of X are chosen ranging from 0·6 to 3·0; the electron density corresponding to $X=1$ for 100 Mc/s waves is approximately 10^8 cm^{-3}. The wavelength of 100 Mc/s waves is also plotted, ranging from 1·0 to 10^3 cm.

For values of $X<1\cdot0$ the V curves are discontinuous, being split into the ranges $Y>1$ and $Y<1$. The former has values of $V<\tau^{1/2}$, falling to zero when asymptotic to the line $Y=\sqrt{2}$. The latter has values of $V>\tau^{1/2}$, rising to infinity at a resonance value of Y. When $X>1$, each V curve is continuous and complete in the region $Y>1$. They are all asymptotic to the line $Y=\sqrt{2}$, at which value $V\rightarrow0$: they are also asymptotic to larger values of Y at which the plasma is resonant and $V\rightarrow\infty$. The curves for any other value of τ may be found by simply changing the vertical scale, remembering $V\propto\tau^{1/2}$.

The minimum wavelength of a plasma wave in the absence of a magnetic field is substantially greater than the Debye wavelength (Bohm and Gross 1949 a) which is $(\kappa T/4\pi ne^2)^{1/2}$. For the frequency 100 Mc/s and $n\sim10^8$ cm^{-3} (i.e. $X\sim1$) this is about 2·2 cm so that the waves having $V\gtrsim\tau^{1/2}$ cannot propagate. However, the presence of the magnetic field may assist propagation at lower values of V because of the restriction on electron motion. The electron gyro-radius when $H=40$ gauss is about 0·7 cm.

The curves of fig. 2 suggest interesting possibilities of wave growth and ion acceleration. However, in discussing these possibilities it should be borne in mind that in the region $V\gtrsim c$ the curves are at best inexact.

§ 7. GROWING P WAVES AND LINKED WAVES

Above sunspots there will be marked gradients in the strength and direction of the magnetic field and hence in V. The effects of gradients in X are likely to be smaller except when hydrodynamic shock waves are present, or P waves which are particularly sensitive to changes in X.

Gradients in V may lead to growth or decay of the P wave as shown by Bohm and Gross (1949 b) when a magnetic field is absent. Growth results when the wave velocity is decreasing and when a proportion of the ions present have velocities equal to the wave velocity. The same mechanism will operate in the presence of a steady magnetic field, but as the ions may have steady velocities only along the field, their velocity must now be $V\sec\psi$ where $\tan\psi=Y_T/Y_L$. The ions are decelerated by the component of the wave electrostatic field parallel to the steady magnetic field, that is to $E_x\sin\psi$ (for the wave velocity range discussed in § 5). This type of wave growth is likely to occur wherever $V<c$ and is decreasing away from the resonance region, owing to decrease in Y.

The wave will continue to grow at the expense of the fast ions which are retarded with the wave. This continues until $V \to \tau^{1/2}$ and the wave either disintegrates or decays, its energy resulting in local heating.

This mechanism, operating in reverse (with V increasing), may cause ion acceleration and could perhaps be responsible for solar cosmic rays. Provided V increases slowly enough the ions will be accelerated until $V \gtrsim c$ when they must leave the wave and start moving independently.

A numerical example of a growing P wave may be useful. Consider the wave corresponding to the $X=0{\cdot}8$, $Y<1$ curve of fig. 2. In moving away from its resonance boundary ($Y=0{\cdot}577$) it decelerates from $V=\infty$ through c down to $V=2{\cdot}8\times10^9$ when $Y=0{\cdot}1$. Suppose there are a few electrons having a component of velocity along $0x$ lying between $8{\cdot}1\times10^9$ and $1{\cdot}75\times10^{10}$ cm sec^{-1}. The wave decelerates through this range as Y falls from $0{\cdot}57$ to $0{\cdot}55$; over a medium sunspot such a change occurs in a distance of about 400 km for waves of frequency ~100 Mc/s (Piddington and Minnett 1951). The time of travel of a wave crest through this region is about 3×10^{-3} sec so that it would suffer negligible absorption due to electron collisions with heavy particles. If there were, say, 10 electrons per cm^{-3} having an average velocity of 10^{10} cm sec^{-1} and they lost half of their kinetic energy to the wave, the increase in energy would be about 2×10^{-7} erg cm^{-3}. If this energy is turned into energy of the electrostatic field of a P wave it corresponds to a peak value of about 1 volt cm^{-1}.

It is shown above that P waves may never emerge from the solar atmosphere and so cannot provide a direct explanation of the intense solar radio emission which reaches the earth. However, an indirect explanation may result in terms of coupling between the P wave and the O or E waves. The simple theory of weak waves shows no such coupling, but this theory only applies rigorously for infinitely weak disturbances. For finite disturbances and particularly for waves which have grown to considerable strength as indicated above, there is coupling between the waves. This coupling becomes effective in transferring and equalizing wave energies when the two waves have equal or nearly equal velocities and so remain in phase over many oscillations. We have seen that the P wave, within certain regions, has the same velocity as the O and E wave, so that strong coupling should result. The transfer of energy from the strong (P) to the weak (O or E) wave is inevitable since they comprise two systems resonating at the same frequency and linked by a common component of $\mathbf{H}$ or $\mathbf{E}$. The four magneto-ionic waves may be considered as mechanical oscillations of ions with which are associated electromagnetic fields, the latter providing the mechanical forces on the ions. When two such oscillations resonate, energy must be transferred from the stronger to the weaker because they will share, in general, a common part of the electromagnetic field.

A partial theory of intense solar radio noise is now clear. The P wave grows by one of the well-known mechanisms, and having become strong enough to introduce non-linear effects it transfers part of its energy to an

O or E wave having the same frequency and wavelength. The P wave then disintegrates, leaving the O or E wave to emerge from the solar atmosphere. The electric field calculated above and extending over a few hundred km would, when transferred to the O or E waves, be sufficient to explain solar radio bursts of moderate intensity.

§ 8. OTHER POSSIBLE MAGNETO-IONIC WAVES

The four magneto-ionic waves discussed in § 1 may occur in a highly ionized gas in which electrons and heavy ions predominate. In a lightly ionized gas, in which neutral atoms or molecules predominate, yet further types of waves may propagate. First consider the ions in this gas and assume that they suffer no collisions with neutral particles: they may then oscillate in the four modes already discussed. If a few collisions occur between ions and neutral particles these do not essentially alter the modes but cause dissipation of the waves by scattering. When collisions are sufficiently frequent, enough energy is transferred to cause the heavier and more sluggish mass of neutral particles to oscillate. Each neutral particle must suffer many collisions in a wave period which means that the frequency range of these oscillations is some orders of magnitude below that of the hydromagnetic waves in the ion plasma.

This process may be extended further by including other heavier particles (for example smoke) in a sufficiently tenuous gas which, in turn, is lightly ionized. It hardly seems desirable, however, to describe such waves as magneto-ionic waves of which either three (at radio frequencies) or four (over a wider frequency range) may be taken as fundamental.

ACKNOWLEDGMENT

The author is grateful to Mr. R. F. Mullaly for helpful discussion.

REFERENCES

APPLETON, E. V., 1932, *J. Inst. Elec. Eng.*, **71,** 642.
ASTRÖM, E., 1950, *Arkiv f. Fysik*, **2,** 443.
BAILEY, V. A., 1948, *Aust. J. Sci. Res.* A, **1,** 351.
BAKER, W. G., and GREEN, A. L., 1933, *Proc. Inst. Radio Engineers*, **21,** 1103.
BOHM, D., and GROSS, E. P., 1949 a, *Phys. Rev.*, **75,** 1851; 1949 b, *Ibid.*, **75,** 1864.
BOOKER, H. G., 1934, *Proc. Roy. Soc.* A, **147,** 352.
GROSS, E. P., 1951, *Phys. Rev.*, **82,** 232.
MARTYN, D. F., 1947, *Nature, Lond.*, **159,** 26.
PIDDINGTON, J. H., 1953, *Proc. Phys. Soc.* A, **66,** 97; 1955 a, "Hydromagnetic Waves in Ionized Gas", *Nature, Lond.* (communicated); 1955 b, "Growing Electromagnetic Waves", *Phys. Rev.* (communicated); 1955 c, "Hydromagnetic Waves in Ionized Gas", *Mon. Not. Roy. Astron. Soc.* (in press).
PIDDINGTON, J. H., and MINNETT, H. C., 1951, *Aust. J. Sci. Res.* A, **4,** 131.
RATCLIFFE, J. A., 1933, *Wireless Engineer*, **10,** 354.
THOMSON, J. J., and THOMSON, G. P., 1933, *Conduction of Electricity in Gases* (Cambridge: University Press), **2,** 353.
TONKS, L., and LANGMUIR, I., 1929, *Phys. Rev.*, **33,** 195.
WESTFOLD, K. C., 1949, *Aust. J. Sci. Res.*, **2,** 169.

CXIX. *A Study of Transparent, Highly Conducting Gold Films*

By E. J. Gillham, J. S. Preston and Betty E. Williams*

[Received June 14, 1955]

Abstract

Thin gold films deposited on a substrate of bismuth oxide or, better, between two films of bismuth oxide, are found to have exceptionally high electrical conductivity and optical transmission. Heating to several hundred degrees centigrade further enhances these properties, irreversibly. Typical results, for gold thickness 100 Å and heat-treatment at 450°c, are film-resistance $3\frac{1}{2}$ ohms 'per square' and white-light transmission 75% (or 82% using controlled interference effects).

The measured electrical and optical constants are remarkably close to those of gold in bulk. This appears to be due to a very fine-grain, continuous structure. Electron microscopy and diffraction show that even at 60 Å thickness no holes of resolvable size exist in the film, that the lateral dimension of the gold particles is some ten times the film thickness, and that the enclosing bismuth oxide films are amorphous, at least initially. The effect of the heating appears to include a considerable reduction in internal surface and also a marked reduction in surface-roughness. Surface reflection of conduction-electrons is found to change from fully diffuse to almost fully specular, as a result of the heating.

The function of the bismuth oxide seems to be to preserve, up to quite high temperatures, surface energy conditions controlling mobility of grains, and opposing increase in gold surface area. This would account for the absence of aggregation during deposition, and of grain-growth perpendicular to the surface during heating which would otherwise disrupt the films at much lower temperatures. In this respect, and possibly also in promoting a smooth gold surface, the oxide enclosure seems to simulate one of gold itself.

The films have a possible use as transparent conducting coatings, for the purpose of de-icing aircraft windows by direct electrical heating.

§ 1. Introduction

During work on transparent, electrically conducting film-coatings for glass, two of the authors (E. J. G. and J. S. P.) were asked to develop a coating suitable for de-icing aircraft windows by direct electrical heating. A power dissipation of about 1 w/cm^2 was envisaged. With a low voltage of about 100 volts, applied between bus-bars along the longer edges of the usual rectangular window, such a high dissipation is possible only with a low film resistance of about 10 ohms ‘ per square ’ (i.e. between line-contacts along opposite edges of a square specimen). At the same time, the light-transmission had to exceed 70%. As a coating-material, cadmium oxide (Preston 1950) in a thickness giving 10 ohms per square was found too yellow and absorbent. Stannic oxide (U.K. Patent Specifications Nos. 632, 227 and 632, 256), though very transparent, was found difficult to prepare with adequate surface uniformity. Other semiconductors appeared still less favourable.

---

*Communication from the National Physical Laboratory.

So, attention was turned to metal films—particularly gold films because of the high specific electrical conductivity and chemical stability of this metal. Simple calculation, from the accepted bulk-metal constants, gives a white-light transmission of over 70% and resistance well below 10 ohms per square, for an ideal lamina of gold of thickness 100 Å. These are much more favourable values than any experimental ones revealed in a search through the literature on gold films. However, the simple calculation neglects two factors. First, on the assumption that the surfaces of a conductor scatter or reflect conduction-electrons diffusely, the surfaces give rise to an excess component of resistance which, while generally entirely negligible, becomes practically significant in films whose boundary surfaces are closer together than, say, 100 or 200 Å (depending, of course, on the electronic mean-free-path for the material and temperature in question). At the start of the work, such an effect was taken to be inherent and unalterable. However, results were obtained later which indicate that electron scattering at the film-surfaces was in fact almost eliminated by the chosen modes of preparation and treatment of the films. The second point neglected in the simple calculation is the more or less granular structure of real gold films, contrasting with the ideal laminar model. This is a matter of common observation (Sennett and Scott 1950), and is held generally to be the chief reason why observed values of optical absorption and electrical resistance for thin gold films are excessive.

The present work started, then, with the object of finding a way to control granulation, and to hold the transmission and resistance of the resulting films consistently within satisfactory practical limits, close to those predicted by the simple calculation. The guiding principle was that the degree of granulation is controlled by the balance between the adhesive forces between the gold and its substrate (favouring ‘ wetting ’, and continuity of the film), and surface tension in the film (favouring disruption and granulation). Search was then made for a substrate-film material which could be relied on to exercize the desired influence on the structure of the superposed gold, would be itself highly transparent and, of course, would adhere well to glass. The search was successful, and preliminary observations have been published (Gillham and Preston 1952, article in *The Chemical Age*, July 5, 1952). Bismuth oxide was selected for the substrate material. This paper describes more fully the preparation of gold films upon it, and their distinctive electrical and optical properties.

The electrical conductivity of the bismuth oxide is entirely negligible compared with that of the gold, and so is left out of account.

§ 2. Preparation and General Description of Films

The films were all sputtered, in a plant and by a method already described (Preston 1950). The essential conditions were :—current-density at cathode 1·5 mA/cm^2, cathode dark-space 5 mm, specimen to be coated situated just outside the dark-space. For the gold films, a continuous flow of argon (99·8% commercial) at suitable pressure was used. For the bismuth oxide films, the cathode was of bismuth, and air was added to the inflowing argon in proportion just sufficient to ensure deposition of clear oxide films obviously free from excess metal. The exact composition of such films is not certain, but excess oxygen in their preparation is to be avoided. Both cathodes, of fine gold and of bismuth, were first etched by dummy sputtering-runs until clean of all foreign matter.

The thickness of bismuth oxide films so made was estimated by optical methods, high accuracy not being necessary. The rate of deposition was found to be 6·7 Å per second. For the gold films an accurate estimate of thickness was desired, also preferably in terms of sputtering-time since direct measurement of each sample would be neither easy nor convenient. By relative colorimetric estimation of colloidal gold, taken into solution from a series of films, it was shown that the mass of gold deposited was proportional to sputtering-time, between 0 and 20 seconds. Then, the absolute rate was found by weighing several 20-second specimens, and calculating thickness on the basis of the bulk-density of 19·3. The rate was found to be 11 ± 1 Å per second. All gold-thicknesses quoted hereafter are on this basis, which may not of course give the exact physical or optical thickness of films, in so far as their density might not be 19·3. It is, however, the only systematic basis for discussion. As an extra precaution, in making a series of gold films of different thicknesses, an additive method was used. For instance, specimens A and B were sputtered simultaneously for X seconds, then A and C simultaneously for X seconds, so that the thickness of A was accurately the sum of the thicknesses of B and C. This step-wise doubling of thickness afforded a check on, and correction for, slight variations in the rate of deposition over the whole series.

It was found that a 100 Å film of bismuth oxide was sufficient to obliterate all influence of the necessary glass supporting base. On this film, a 60 Å gold film had initial resistance 20 ohms per square, overall light transmission (tungsten 2700°K) 73%, and colour pale straw. Heat-treatment for a few minutes at 200°C was found to improve these properties, irreversibly, to 10 ohms per square and 75%. At higher temperatures the gold apparently disrupted, the film changing colour through the more familiar pale green to pale blue, with considerable decrease of conductivity and transmission. It seemed that up to 200°C increase in mobility of the gold permitted an increase in continuity or compactness of structure, under forces of adhesion, but that above 200° surface tension preponderated. To diminish still further the surface tension effect, therefore, specimens were prepared in which a second 100 Å bismuth oxide film was deposited on top of the gold. These were found to withstand heat-treatment or annealing* up to 350°C or more without disruption. In this way, with gold again of thickness 60 Å, a resistance of 7 ohms per square and transmission 76% were obtained.

The best overall technical performance was obtained with 100 Å gold sandwiched between two bismuth oxide films each of thickness about 450 Å, annealed for a few minutes at 350°C. Such a multiple coating is effectively a high-index half-wave layer, so that light-reflection is at a minimum. Also, because the relatively thin gold is situated approximately in the plane where the resultant electric vector of the interfering wave-trains is at a minimum, its optical absorption is at a minimum. In this way a combination of resistance 4 ohms per square and transmission 82% was achieved. The colour was then rather dependent on control of the thickness of the bismuth oxide, but for the correct thickness was like the slightly greenish colour of ordinary thick plate glass. Reproducibility of both types of sandwich film was found to be good, however, and it was also found that higher annealing temperatures than those quoted could be used safely, particularly for greater gold thicknesses. For instance, a 100 Å sandwich film can safely be annealed at 450°C. and then has a resistance of only $3\frac{1}{2}$ ohms per square.

To sum up, it was found that a substrate of bismuth oxide favoured consistent and low values of electrical resistance and optical absorption in the thin gold films. Also, there was the purely empirical observation that a final heat treatment was then possible and led to further improvement—which was very considerable in the case of gold films enclosed between two films of bismuth oxide, when the treatment could be carried up to a temperature of 350–450°C without break-up of the gold. The fact that in this way the resistance of a 100 Å gold film could be brought down to $3\frac{1}{2}$ ohms per square—not much more than the value of 2·45 deduced directly from the normal bulk-resistivity and the thickness—prompted a closer investigation into the resistive properties of such films, and measurements of their optical constants, in comparison with those of gold in bulk.

§ 3. EFFECTS OF ANNEALING, AND VARIATION OF ELECTRICAL RESISTIVITY WITH THICKNESS AND AMBIENT TEMPERATURE

For the electrical study a range of sandwich films was made, all with equal upper and lower bismuth oxide films 120 Å thick, but with gold thicknesses between 55 and 880 Å. They were made in triplicate according to the step-wise procedure already mentioned. From the measured resistances and linear dimensions of the specimens, the specific resistivities were calculated in ohm-cm. Then the mean value for the three specimens at each thickness was found. Before annealing, resistance measurements were made at ambient temperatures of 20°c and −183°c. After annealing at 350°c, measurements were made at 200°c, 20°c and −183°c. The mean values of specific resistivity so obtained are given in table 1.

---

* Hereafter the word annealing is used as the equivalent of heat-treatment in the broad sense, for brevity.

Table 1. Specific Resistivities of Gold Films in ohm cm $\times 10^{-6}$

Thickness of gold in Å	Unannealed films at		Annealed films at		
	20°c	−183°c	200°c	20°c	−183°c
55	$16{\cdot}8_5$	15·6	$6{\cdot}6_5$	4·8	$3{\cdot}1_5$
110	$11{\cdot}9_5$	10·5	$5{\cdot}6_5$	$4{\cdot}0_5$	2·3
220	$9{\cdot}5_5$	7·7	$5{\cdot}4_5$	3·9	2·1
440	7·8	$6{\cdot}1_5$	5·2	$3{\cdot}7_5$	$2{\cdot}0_5$
880	7·4	$5{\cdot}8_5$	$5{\cdot}1_5$	$3{\cdot}6_5$	$1{\cdot}9_5$

Fig. 1

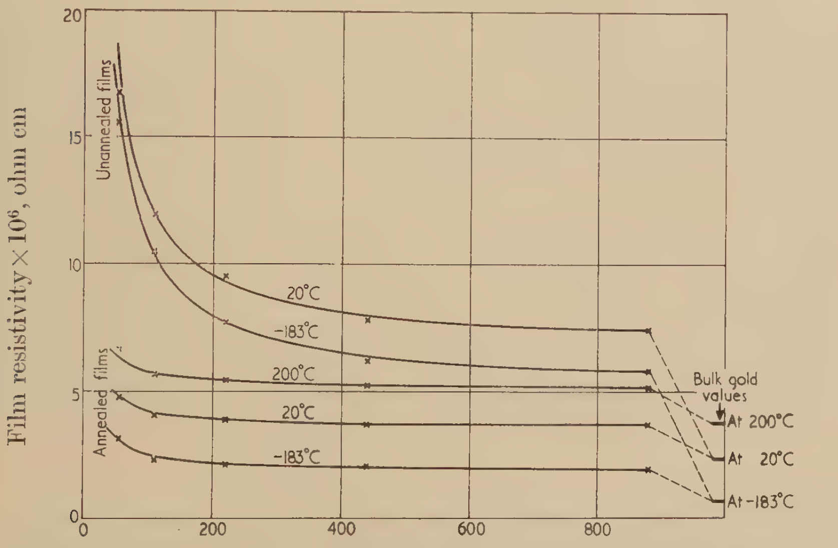

Variation of specific resistivity of gold films with thickness, annealing, and ambient temperature.

These results are plotted as crosses in fig. 1. At the right-hand edge of fig. 1 three short lines are also given, showing for comparison the accepted values for the specific resistivity of bulk gold at the three temperatures in question. Each column of resistivities can be fitted, within probable limits of error, to an equation of the form

$$\text{Film resistivity } \rho_F = \rho_B + k/t \qquad . \; . \; . \; . \; . \quad (1)$$

where ρ_B and k are constants, and t is the film thickness. Appropriate values of ρ_B and k are given in table 2.

The five full curves in fig. 1 are those for ρ_F obtained by inserting the five pairs of values from table 2 into eqn. (1). They are seen to represent the observations quite closely.

Table 2

State of Film	ρ_B in ohm cm $\times 10^{-6}$		k in ohm cm$^2 \times 10^{-12}$
		Diff.	
Unannealed, at 20°c	6·7	1·6	5·7
,, ,, −183°c	5·1		5·7
Annealed, at 200°c	5·1	1·5	0·66
,, ,, 20°c	3·6		0·66
,, ,, −183°c	1·85	1·75	0·66

Consider now the interpretation of the results, on the basis of this systematized representation. First, ρ_B is the value to which the film-resistivity tends for large values of thickness, i.e. it is the specific resistivity of the material of the films, in bulk. We see that this is markedly and irreversibly diminished by the annealing process. The reduction is like the one observed when bulk metal specimens are annealed, but is much larger. It may well be due to expulsion of occluded gas, as well as to elimination of dislocations, or even to some major change in structure from a more or less amorphous to a crystalline form (Kramer 1937). It can hardly be due to elimination of impurity in the ordinary chemical sense. It is interesting to note, however, that the values of ρ_B in table 2 conform well to Matthieson's rule, which often applies to metal specimens whose resistivity is excessive because of impurity or of dislocations in considerable number. According to this rule one would write

$$\rho_B = \rho_G + \rho_C$$

where ρ_G is the temperature-dependent specific resistivity of normal pure gold, while ρ_C is a temperature-invariant, 'residual', component due to the impurity or structural imperfection of the actual specimen. In such a case, the change in ρ_B produced by a change in ambient temperature would be found equal to the corresponding change in ρ_G. Now, the reference tables give $1{\cdot}69 \times 10^{-6}$ and $1{\cdot}46 \times 10^{-6}$ for the changes in ρ_G for the steps −183 to 20°c, and 20 to 200°c, respectively. The experimental changes in ρ_B (see table 2) are $1{\cdot}75 \times 10^{-6}$ and $1{\cdot}6 \times 10^{-6}$ for annealed and unannealed films, for the first step, and $1{\cdot}5 \times 10^{-6}$ for unannealed films for the second step. These show quite reasonable agreement with the accepted characteristics of ρ_G, in confirmation of the rule.

Thus, the film material behaves like pure bulk gold in a state of structural disorder, in respect of both the irreversible reduction of its bulk resistivity by annealing, and the size of the reversible changes in resistivity which accompany changes in ambient temperature, before as well as after annealing. This supports the view that low resistance has been reached in the present films by a process which secures an unusual degree of order or continuity of structure in so far, at any rate, as the *substance* of the gold in thin films is concerned.

Consider, now, surface effects. We may suppose the term k/t of eqn. (1) to represent the additional resistivity-component due to diffuse electron-reflection, or electron-scattering, at the film surfaces. Qualitatively, the observed values conform to this supposition, for from table 2 we see that k, or k/t for a given thickness, is not dependent on ambient temperature, so that k/t behaves as another residual-resistivity component, as one would expect for such an electron-scattering mechanism. Also, this residual component increases as thickness diminishes. This again would be expected, for as the thickness diminishes, the surface extent remains unchanged while the volume of film diminishes with thickness. Surface scattering thus becomes relatively more and more predominant, with a correspondingly increasing specific resistivity. It is not, of course, to be assumed that the surface component is represented *precisely* by a term varying as the reciprocal of thickness. This simple function is chosen as giving a satisfactory fit with measured values over the thickness-range covered in the experiments. The important point is that it is seen to be unaffected by changes in ambient temperature.

The really surprising feature of the figures given in table 2, however, is the very marked reduction in k produced by the annealing. The conclusion is inevitable that annealing produces some change in the surface topography of the films which results in a marked drop in diffuse electron reflection at the surfaces. It is worth examining this conclusion in terms of electron mean-free-path theory which Sondheimer (1952) has lately reviewed. It is sufficiently exact to use his approximate relationship for films having thicknesses greater than the mean-free-path. This can be written

$$\rho_F=\rho_B\left[1+\frac{3}{8}\cdot\frac{l}{t}(1-p)\right] \quad . \quad . \quad . \quad . \quad . \quad . \quad (2)$$

where l is mean-free-path, and p is the specular component of electron reflection at the film surfaces. If we compare eqns. (1) and (2) we find $l\,(1-p)=(8/3)(k/\rho_B)$. Using values of ρ_B (for 20°c) and k from table 2 this gives $l_1(1-p_1)=2{\cdot}27\times10^{-6}$ cm for unannealed films, and $l_2(1-p_2)=0{\cdot}49\times10^{\;6}$ cm for annealed films, at 20°c.

For the present purpose, we may assume that mean-free-path is inversely proportional to the basic specific resistivity ρ_B, so that $l_1/l_2=3{\cdot}6/6{\cdot}7$ and we find $(1-p_2)/(1-p_1)=0{\cdot}12$. Now $(1-p_1)$ cannot exceed unity, therefore $(1-p_2)$ cannot exceed $0{\cdot}12$, and p_2 must therefore be at least $0{\cdot}88$. The values $p_1=0$, and $p_2=0{\cdot}88$ are further confirmed because they lead to $l_1 = 227$ Å for the mean-free-path in unannealed films, and $l_2 = 408$ Å in annealed films, both quite reasonable values of mean-free-path in metal specimens having the resistivities just quoted.

There is room for some degree of inexactitude in the above treatment and assumptions, but there is clearly strong ground for concluding that electron reflection at the surfaces of the unannealed films is completely diffuse or almost so, while for annealed films the diffuse component is only about 0·1 and the specular component is about 0·9. This effect of annealing is of little practical importance in thick films. In films less than about 200 Å thick, however, it is more important than the drop in ρ_B, in lowering the actual resistance of the films. It is believed that this is the first investigation in which it has been possible to demonstrate the practical possibility of almost completely specular electron reflection at the boundary surfaces of a metal specimen.

The precise structural changes produced by annealing remain for speculation. Annealing might well expel occluded gas, and so diminish the extent of *internal* surface in the film and lead to closer packing. It would reduce the number of lattice imperfections and dislocations, perhaps transforming an almost amorphous layer into a microcrystalline one. As already mentioned these effects are quite consistent with the observed drop in ρ_B. They neither require nor suggest, however, an increase in surface smoothness of the films, while the sort of grain-growth which usually accompanies annealing would suggest, rather, a decrease in smoothness. In contrast, however, the change from zero to 0·9 for the specular electron reflection coefficient at the surfaces seems to require development of a very high degree of surface smoothness, with excrescences which are either only quite rare or else are of dimensions generally not exceeding the effective wavelength of the conduction electrons, viz. about 5 Å (see Müser 1954, on the diffraction of electrons by certain types of surface-structure). A possible structural change would be a preferred growth or extension of single-crystal domains along the run of the film but not perpendicular to it, perhaps also with a preferred orientation of certain crystal planes also parallel to the run of the film. Such a preferred growth or orientation need not be assumed to extend far from the surfaces into the body of a thick film. In a very thin film however, one would expect it to penetrate the whole thickness, and perhaps then be demonstrable by electron microscopy or diffraction.

Thus far, in using eqns. (1) and (2), we have followed the orthodox analysis. ρ_B is treated as the bulk-resistivity of the film-material, constant over a given set of films all in the same given condition (in practice, it may vary somewhat—but there is no experimental check on this). The variation of film-resistivity with thickness, over the set, is assigned quite separately to properties of the film surfaces. The assumption is that these properties are in no way related to, or determined by, the resistivity or structure of the body of the specimen. For a thick specimen, this seems reasonable. In really thin films however, or films built up like the present ones by continued deposition of similar material, one might expect to find some systematic relationship between surface properties and internal properties, dependent on some single parameter of the structure. For example, in wholly granular films, both surface roughness and extent of internal surface (or holes) would depend on grain size. Again, in the present films, annealing produces two simultaneous effects, namely a reduction in roughness and a decrease in ρ_c, the temperature-independent component of the bulk resistivity. These might both arise from a change in one single feature of the structure. We shall now look briefly at this kind of proposition, for what light it may throw on the physical nature of the films and of the annealing process.

Suppose a film to resemble, initially, a slice cut from sponge-rubber, full of holes and with surfaces which are rough because covered with sections through holes. Given a suitable hole-size, the surfaces will cause diffuse scattering of conduction-electrons, giving rise to a temperature-independent 'surface-resistivity' like the term k/t of eqn. (1). Inside the film the holes, being of size similar to that of the surface asperities, must also cause similar electron scattering, and give rise to another temperature-independent component of resistivity, which we may identify with ρ_c since it will not vary with t. If, then, annealing be supposed to reduce the number of holes in the bulk as well as in the surfaces, both these resistivity terms will decrease together, as in fact they are observed to do. This picture is not altered if we replace the concept of holes by one of grains, except that we must then suppose annealing to provoke a general coalescence of grains, and not a growth in the size of the grains at the expense of their number. We may, then, suppose our films to be initially granular, but with a smaller grain size than usual because of low mobility of gold over the bismuth oxide substrate. During annealing, we may suppose the oxide layers to preserve large surface tension forces tending to flatten the surfaces of the gold, and permitting the escape of 'bubbles' of gas, occluded in the inter-granular spaces, without permanent break-up of the gold surfaces. In this picture, the effect of annealing appears as a reduction in internal surface rather than in the number of dislocations, along with a reduction in the real extent of the external surface. It is probably as good an overall picture of the physical nature of the films, and of the effects of annealing, as can be drawn from the results of the electrical measurements.

In this picture, one envisages a grain size somewhere in the range between the electronic wavelength and the mean-free-path, in the films in their initial state, at least. It is not supposed that, in the unannealed films, collisions of the electrons with the film surfaces are in themselves inelastic, but rather that the redistribution of electron velocities caused by *specular* reflection at the individual grain facets results, effectively, in a reduction in the resultant drift velocity in the neighbourhood, and therefore in an excessive measured resistance. This seems to be the usual assumption in theoretical treatments of the subject, though it is often implicit rather than explicit. The grain size of about 40 Å revealed by the electron microscope examination described later does not conflict with this general picture.*

§ 4. METHOD OF MEASURING THE OPTICAL CONSTANTS

We turn next to an optical examination. The difference in colour and transmission, between unannealed and annealed films, was less striking than the differences in electrical properties, and an examination of both types of film did not seem likely to give any useful additional information on the structure. The optical measurements were therefore confined to annealed films, as contrasting with the greener films usually obtained on a glass base, and likely to give the closest comparison with the accepted constants for bulk gold.

Sandwich films were used, similar to those for the electrical measurements. There was a choice of methods, depending on what three quantities were selected from which to calculate the three unknowns, viz. the optically effective thickness, and the real and imaginary parts of the complex refractive index. Transmission, and back and front reflection factors are three such quantities, ideally. For very thin films, however, the relation between them is such that, unless measured with extreme accuracy, they amount in practice to only two independent quantities. Thickness, then, was taken as the third. Only that on the mass-per-unit-area basis was available, not necessarily exactly equal to the effective thickness. In addition, therefore, measurements of phase change on transmission and reflection were made. Phase change can be shown to be particularly sensitive to thickness (Ishiguro and Kuwahara 1951), and so these observations were used to check this, rather than to replace transmission and reflection factors as primary measured quantities. They were also of considerable use as a guide in certain methods of successive approximation used in the computations.

In the present case, the measurements of transmission and reflection factors were necessarily made on the whole composite film, situated on a glass base which could contribute an attenuation due to its own absorption and the reflection loss at its free surface. (Troublesome inter-reflections were avoided by using a wedge-shaped glass.) Corrections were thus necessary for the effects of the base. Further, to compute constants for the gold alone from the corrected measurements, certain optical data on the actual bismuth oxide present in the composite films were needed. The procedure was thus to examine the glass base plates first when uncoated. Then the whole area of the plates was coated with the bismuth oxide films, but the gold was confined, by masking, to a central strip. Thus the composite film was flanked on either side by areas having no gold, but an identical total thickness of oxide upon them. Then, by making measurements of transmission and reflection, on the two side areas as well as on the central strip, all the additional data required were obtained.

---

* But see also § 7, "Note added in proof".

Phase changes were measured with the aid of a Twyman–Green interferometer, combining the light reflected or transmitted by the films with that reflected from a suitable optical flat. Equal-thickness fringes, running at right angles to the lines dividing the gold sandwich from the adjacent clear oxide layers, were observed. Their shift, across these lines, was a measure of the phase change due to the gold. A necessary second-order correction for the actual thickness-step present was made, using the assumed thickness of gold as the height of the step.

All the measurements were made in collimated monochromatic light, incident practically normally. The form of the computations is given in § 8.

§ 5. OPTICAL RESULTS

Three specimens were made for optical examination, with gold of thicknesses 39, 71, and 103 Å, sandwiched between equal films of oxide each 100 Å thick. Annealing was limited to 300°C to avoid distorting the optically flat base plates. The electrical conductivities of the two thicker specimens were normal, for an annealing temperature of 300°C. That of the thinnest was low by a factor of two, and its structure must therefore be assumed to be in some way not quite typical. The results, namely ν and k, the real and imaginary parts of the refractive index of the gold, are given in table 3. In addition, as a matter of practical interest, T, R_1 and R_2, the transmission and front and back reflection factors, are also given. They are the measured values *after* elimination of attenuation due to absorption and free-surface reflection loss due to the glass support. Measured phase changes, not so interesting, ranged in angular measure up to $+25°$ for transmission, and between $-87°$ and $+182°$ for reflection.

Table 3. Optical Properties of three High-Conductivity Gold Films

Film thickness (mass/area basis)	Film resistivity ρ_F	Wavelength	Transmission and reflection factors			Optical constants	
(Å)	(ohm cm)	(mμ)	T	R_1	R_2	ν	k
39	$17{\cdot}2\times10^{-6}$	436	0·643	0·192	0·134	2·13	1·46
		481	0·705	0·155	0·099	1·78	1·55
		546	0·776	0·104	0·057	1·29	2·10
		636	0·803	0·075	0·021	0·93	3·01
71	$6{\cdot}7\times10^{-6}$	436	0·583	0·177	0·091	1·80	1·66
		481	0·663	0·138	0·060	1·44	1·70
		546	0·785	0·075	0·017	0·68	2·41
		636	0·829	0·062	0·014	0·43	3·06
103	$5{\cdot}6\times10^{-6}$	436	0·524	0·174	0·074	1·79	1·61
		481	0·617	0·133	0·039	1·42	1·58
		546	0·763	0·071	0·002	0·64	2·14
		636	0·770	0·113	0·060	0·30	3·38

The check-thicknesses derived solely from the optical measurements are not given.

They were about 20% greater than the assumed, tabulated thickness. This difference could not with certainty be regarded as significant, being just on the limit of the range corresponding to the estimated probable error of the phase measurements. It is, however, in the direction which might be expected.

Table 3 shows, for the 71 and 103 Å films, values of ν which agree almost within likely limits of error. At 39 Å ν is appreciably greater, by a factor which increases with wavelength. It is natural to associate this with the poorer conductivity of this film. The values of k have a moderate spread, but show no regular trend with thickness.

The general agreement of the values of ν and k for the two thicker films, coupled with the normal high conductivity, suggests that they are typical of the films here dealt with, in thickness of the order 100 Å. It is therefore of interest to compare them with recorded values for bulk gold on the one hand, and films deposited on glass on the other. For this purpose, the authors have chosen from the literature data which seem reliable, on internal evidence. The comparison is made in terms of the product νk, proportional to the optical absorption (Wolter 1937), and is shown in table 4.

Table 4. Values of the Product νk

Nature of gold	Authority	νk at wavelength ($m\mu$) :—			
		436	481	546	636
Bulk metal	Meier 1910 (interpolated)	2·20	1·93	1·67	1·16
High-conductivity film, *ca.* 100 Å	Present paper	2·88	2·24	1·37	1·01
100 Å film on glass	Goos 1937 (interpolated)	3·22	2·2	2·16	5·0

The present results are, overall, lower and more like the bulk metal values than Goos'. In particular, toward longer wavelengths, they show the steady downward trend characteristic of practically all published bulk values, and not a sharp upward tendency. This is consistent with the pale yellowish colour, as compared with the bluish-green reported by Goos and commonly seen. It supports the conclusion, from the electrical measurements, that the present films approach closely the ideal of a plane lamina having ‘ bulk ’ properties.

It seems possible, in fact, that the optical constants we have obtained for the present gold films are more nearly typical of bulk gold than any hitherto obtained by the use of thick or massive specimens. In a massive specimen, only a surface layer some 200 Å thick is involved in the measurements. The properties of this layer are known to be very dependent on the method of preparing and polishing the specimen, but they obviously cannot be checked by a direct d.c. measurement of resistivity, which is a sensitive test of normality. For thin films, such a measurement is possible and affords a check on the normality of the whole of the transparent, operative, metal layer. The surface-resistivity of massive specimens can indeed be measured approximately by high-frequency methods. Where these methods have been used on massive gold, they have usually given results indicating an appreciably higher resistivity than is observed for the present films (Reuter and Sondheimer 1948), so far confirming, in this respect, the superiority of the films as suitable specimens.

With regard to the trend of the product νk toward the longer wavelengths, an upward sweep is characteristic of much reported work on thin gold films on glass. Corresponding film-resistances are too seldom given, but the present authors have failed to produce greenish 100 Å film on glass, with less than about four times the resistance of the yellowish high-conductivity annealed films of the same thickness. In resistance, as well as in the product νk, the 39 Å film of table 3 lies (through some fault in preparation) about half way between the two types. A close relationship between optical properties and resistivity is thus confirmed, but not elucidated in detail.

§ 6. OBSERVATIONS BY ELECTRON MICROSCOPY AND DIFFRACTION

During the electrical and optical work, attempts were made to study the films by transmission in the electron microscope. It was not found possible to sputter the films on to formvar pellicles without destroying the pellicle, unless this was backed by a support. Wet-stripping of the already coated pellicle was thus necessary, for transfer to the specimen grids of the microscope. That this did not alter the properties of the film was confirmed by electrical measurements on a large sample before and after stripping. It was found very easy to overheat the films in the microscope, by bombardment with normal conditions. Therefore, the magnification, beam current, and exposure time were kept as low as possible. Moreover, only non-sandwich films (annealed only up to about 200°c) could be examined because of the large electron-scatter from the greater total mass of material in sandwich films. With these restrictions, it was unfortunately found that no distinction could be observed between films which had, and had not, been annealed before examination in the microscope. The photographs obtained were thus limited to the following formvar-based specimens :—Figure 2 (figs. 2, 3, Plate 20, fig. 4, Plate 21), Gold, thickness 60 Å, as sputtered ; fig. 3, Bismuth oxide, thickness 100 Å, as sputtered ; fig. 4, Bismuth oxide, 100 Å plus gold 60 Å, annealed at 200°c for 5 min; fig. 5 (fig. 5, Plate 21, fig. 6, Plate 22), Bismuth oxide, 100 Å plus gold 60 Å, heated just sufficiently to discolour it, and raise the resistance ; and fig. 6, the same specimen as in fig. 5 after severe electron bombardment in the microscope.

In all cases the magnification in the microscope was 3750, while that of the photographic reproductions is 10 000 overall.

Points to note are the similarity of fig. 2 to those for similar films obtained by other workers (Sennett and Scott 1950) ; the complete absence of observable structure in the bismuth oxide ; the shaded, rather than granular, appearance of the gold structure of the typical film in fig. 4 ; the change of this to something much more like fig. 2 after overheating ; and the final separation of the gold into quite large aggregates, fig. 6, due to severe heating.

Next, an attempt was made to study quantitatively the variation in gold thickness over the area of the gold+bismuth oxide film. Micrographs of this, and of the bismuth oxide alone, were taken under identical conditions of exposure and photographic processing, so as to permit of densitometric comparison of the photographs. The results showed conclusively the absence of any holes of resolvable size extending right through the gold layer. It was concluded, therefore, that the gold was continuous, but somewhat pitted or rough.

Finally, transmission–diffraction patterns were observed. For the bismuth oxide only two broad haloes indicative of amorphous structure were found. For the annealed gold on bismuth oxide, broadened rings for gold were seen, together with a few faint additional broad rings believed to result from slight crystallization of the bismuth oxide by the heat-treatment. Measurements of the half-breadths of the gold rings gave an approximate value of 40 Å for the dimension of the gold particles in the plane of the film. The relative intensities of the various $(h\ k\ l)$ reflections were not inconsistent with random orientation of the gold crystallites.

The chief information given by the microscope study is first that the yellowish high-conductivity films have definitely a more continuous structure than the bluish-green ones without oxide substrate. From the appearance of the photographs, this is thought to be due to a lesser degree of aggregation of the elementary particles or grains. Secondly, from the appearance of the overheated film, it may be concluded that a temperature above 200°c is required to produce aggregation of the same order as occurs naturally in films on a glass base at about room temperature. Thirdly, there is the observation that the gold crystallites are of size about 40 Å in the plane of the film and have no certain preferred orientation. This observation cannot be correlated closely with the inferences drawn from the electrical and optical properties. The particle size is, nevertheless, unusually small for gold films. However, the non-sandwich film annealed only to 200°c is not a very suitable type of specimen, being a necessary compromise. The technical difficulties in getting good electron micrographs of the gold in sandwich films, of avoiding bombardment heating so as to study the true unannealed state, and of preparing suitable pellicle-based specimens annealed at a temperature as high as 350 or 400°c are being studied, with the intention of further investigations by electron microscopy and diffraction.

Lastly, the observation that the bismuth oxide is amorphous may be a clue to its apparent ability to control the gold structure, though it seems to rule out simple epitaxial growth as the relevant mechanism. The microscope evidence does, however, lend considerable support to the basic idea of the whole investigation, namely, that the bismuth oxide in some way limits or imposes orderliness on the mobility of the gold, and so prevents the kind of free grain growth—especially perpendicular to the film—which must not proceed far if break-up is to be avoided, and continuity assured, in films as thin as 100 Å.

§ 7. SUMMARY AND CONCLUSIONS

It has been found, then, that sputtered films of gold as thin as 100 Å enclosed between sputtered films of bismuth oxide. have a consistent specific electrical conductivity about a quarter that of gold in bulk. Unlike unprotected films on glass, they withstand heat treatment at 400–500°c, after which their conductivity is three-quarters that of bulk gold. Their colour is pale yellowish. The optical transmission is raised by the heat treatment and is, throughout, higher than that of bluish-green films, on glass, of the same mass per unit area. The optical constants of the gold in the heat treated films are in good agreement with authoritative results of measurements on bulk specimens.

The chief interest lies in the unusually close approach, with films as thin as 100 Å or less, to the ideal of a plane lamina having the same constants as the bulk metal. Also of importance, however, are some of the conclusions we draw, in these circumstances, directly from observation. One is that electron reflection at the surfaces of the annealed films must be almost entirely elastic or specular, because effects related to the ratio of electronic mean-free-path to film thickness are only measurable with certainty in conditions when this ratio is upwards of about 20. Another is that the variation of specific conductivity with both thickness and temperature might find a simple alternative physical explanation in terms of granularity, affecting at one and the same time the surface roughness and the resistivity of the film material in bulk so that the electrical effects of these two factors, usually considered separately, might be related to a single variable, perhaps grain size. We note that the figure of 40 Å found by electron-diffraction for the grain size in the present films, is probably the smallest hitherto recorded for thin gold films. For gold on formvar, Sennett and Scott (1950) find a rather larger grain size, with good continuity only in films of thickness greater than about 180 Å.

Of almost equal interest are the means by which the close approach to bulk properties is obtained. It stands to reason that the films in the final state must be highly continuous, and this is confirmed in a general way by electron microscopy. The heat treatment seems to be annealing in the broadest metallurgical sense, that is to say, it probably expels occluded gaseous impurity, reduces lattice dislocations, and increases the areas of ordered structure in the gold. The function of the bismuth oxide seems to be to preserve, up to usefully high annealing temperatures, conditions in which increase in the area of the gold would be accompanied by an increase, rather than a decrease of potential energy—conditions disfavouring the break-up of the gold into agglomerates of ' droplets ', both during deposition and during the later annealing (Cabrera and Terrien 1949). There seems here to be a field of study to which further work with thin films could make its own unique contribution of fundamental value.

NOTE ADDED IN PROOF

Since this paper was prepared, electron microscope observations have been successfully made on a gold film 100 Å thick, between two bismuth oxide films and supported on a carbon pellicle, after annealing for half an hour at 450°C. A micrograph is shown in fig. 7 (Plate 22) for comparison with fig. 4 (Plate 21). A rather similar, but larger-scale, structure is evident. Electron diffraction clearly indicated that the size of the gold particles in the plane of the film is about 1000 Å, and that there is some preferred orientation. The bismuth oxide is no longer entirely structureless, but still exhibits only a comparatively small crystallite size.

Thus, in a typical fully annealed high-conductivity film, the gold is probably composed of a continuous sheet of monocrystalline lamellae, each of lateral dimensions some 10 times the mean thickness of the film, connected possibly by smaller regions in which the gold is in a greater state of disorder. The type of structural growth suggested in § 3 is thus largely confirmed.

By the contrast it affords, the present work throws a little more light, perhaps, on the significance of the abnormal conductivity and optical constants of the more familiar green gold films, in terms of resistance and film-structure, but makes no serious contribution to existing theories (for example, Garnett 1904). It does however raise the question whether, particularly if the technique described could be extended to other metals, high-conductivity films might not be as good a medium for the study of the optical properties of metals as the surface layers of bulk specimens, seeing that the conductivity and structure of the former are open to direct observation while those of the latter, throughout the relevant depth of about 200 Å or so, are much less easy to examine for ' normality '.

§ 8. APPENDIX ON OPTICAL CALCULATIONS

Mainly algebraic calculation was used to derive the refractive index of the gold from the observed optical results, using the matrix notation of 4-terminal network theory (Herpin 1947). Complex E_1 and H_1 representing the electric and magnetic fields to the left of the optical system are related to those on the right by the square matrix A

$$\begin{bmatrix} E_1 \\ H_1 \end{bmatrix} = A \begin{bmatrix} E_2 \\ H_2 \end{bmatrix}.$$

For a uniform slab, of refractive index n (possibly complex, $n=\nu-ik$) and optical thickness $\theta=2\pi nl/\lambda$

$$A=\begin{bmatrix} \cos\theta & \dfrac{i\sin\theta}{n} \\ in\sin\theta & \cos\theta \end{bmatrix}. \qquad (1)$$

provided the units of E and H are chosen so that, for a forward travelling wave in the medium, $H=nE$.

Denoting by A_b the A-matrix for each oxide layer, and by A_g that for the gold film, we have for the whole system

$$A_t=A_bA_gA_b. \qquad (2)$$

To determine A_t, and thence A_g, from the experimental results, it is convenient to introduce the amplitude transmission factor $t=\sqrt{T}\exp[i\phi(T)]$, where T is the measured factor and $\phi(T)$ the corresponding measured phase change, and similar amplitude reflection factors r_1 and r_2. The matrix E which relates the amplitudes (actually electric amplitudes multiplied by the square root of the appropriate refractive index) of the forward and backward travelling waves on the left of the optical system to those on the right may then be written

$$E=\begin{bmatrix} 1/t & -r_2/t \\ r_1/t & t-r_1r_2/t \end{bmatrix}.$$

As might be expected, the relation between E and A_t involves the refractive indices n_1 and n_2 of the media to the left and right of the system, thus

$$A_t=\tfrac{1}{2}\sqrt{\frac{n_2}{n_1}}\begin{bmatrix} 1 & 1 \\ n_1 & -n_1 \end{bmatrix}E\begin{bmatrix} 1 & 1/n_2 \\ 1 & -1/n_2 \end{bmatrix}. \qquad (3)$$

Combining (2) and (3) we obtain

$$A_g=A_b^{-1}\tfrac{1}{2}\sqrt{\frac{n_2}{n_1}}\begin{bmatrix} 1 & 1 \\ n_1 & -n_1 \end{bmatrix}E\begin{bmatrix} 1 & 1/n_2 \\ 1 & -1/n_2 \end{bmatrix}A_b^{-1}. \qquad (4)$$

A_b is known from the measured thickness and index of the oxide layers, $n_1=1$, and n_2 is the known index of the glass base, so that A_g, which describes completely the optical properties of the gold film, may be calculated from (4) in terms of measured t, r_1 and r_2. If the gold film is in fact homogeneous, A_g will be of the form given by (1) and it will be possible to calculate from its elements the index n of the gold, the optical thickness θ, and thence the geometric thickness l.

The dependence of index on thickness in (4) is only in implicit form. Hence, to calculate index from thickness and intensity ratios, a process of successive approximation was used. In this, $\phi(T)$, the argument of complex t, was used as an adjustable parameter. The arguments of r_1 and r_2 may be obtained graphically in terms of any selected $\phi(T)$ from the following equation, which holds for a symmetrical system on a glass base of index n_2.

$$r_2-r_1=\frac{n_2-1}{n_2+1}(1+t^2-r_1r_2). \qquad (5)$$

A trial value of $\phi(T)$, together with $\phi(R_1)$ and $\phi(R_2)$ found from (5), and also the measured intensity ratios, were inserted in (4), giving a calculated thickness. This was then brought into sufficiently close agreement with the assumed (mass per unit area) thickness by step-by-step adjustment of $\phi(T)$ and repetition of the calculations. In this way, values of r and k for the gold were derived from (4) in conformity with the measured transmission and reflection factors and the assumed thickness.

Finally, the observed factors and phases were inserted directly into (4) to derive a thickness based solely on the optical measurements, providing the cross-check on thickness for which the phase measurements were mainly intended.

ACKNOWLEDGEMENTS

The authors acknowledge the cooperation of Mr. A. E. L. Tate and Mr. H. G. Short, of the Metallurgy Division, N.P.L., who respectively supplied cathodes for the sputtering plant, and made the colorimetric estimations of gold samples ; and also of Mr. F. H. Burch of the Metrology Division, N.P.L. who made the weighings. Much of the tedious work of preparing and measuring specimens was done by Mr. G. W. Gordon-Smith of the Light Division, N.P.L. The authors are also grateful to Dr. E. H. Sondheimer of Queen Mary College, London, for valuable criticism during the preparation of this account of their work.

The work described above has been carried out in the Light and Metallurgy Divisions of the National Physical Laboratory and this paper is published by permission of the Director of the Laboratory.

REFERENCES

CABRERA, N., and TERRIEN, J., 1949, *Rev. Opt.*, **28,** 635.
GARNETT, J. C. M., 1904, *Phil. Trans.* A, **203,** 385.
GILLHAM, E. J., and PRESTON, J. S., 1952, *Proc. Phys. Soc.* B, **65,** 649.
GOOS, F., 1937, *Z. Phys.*, **106,** 606.
HERPIN, A., 1947, *C. R. Acad. Sci.*, **226,** 1872.
ISHIGURO, I., and KUWAHARA, G., 1951, *J. Phys. Soc. Japan*, **6,** 71.
KRAMER, J., 1937. *Z. Phys. Lpz.*, **106,** 675.
MEIER, W., 1910, *Ann. Phys. Lpz.*, **31,** 1017.
MÜSER, H. A., 1954, *Phil. Mag.*, **45,** 1237.
REUTER, G. E. H., and SONDHEIMER, E. H., 1948, *Proc. Roy. Soc.* A, **195,** 336.
PRESTON, J. S., 1950, *Proc. Roy. Soc.* A, **202,** 449.
SENNETT, R. S., and SCOTT, G. D., 1950, *Journ. Opt. Soc. Amer.*, **40,** 203.
SONDHEIMER, E. H., 1952, *Advances in Physics*, **1,** 1.
WOLTER, H., 1937, *Z. Phys. Lpz.*, **105,** 269.

CXX. *Measurement of the Elasticity of Solid Argon with an Ultrasonic Interferometer*

By J. R. Barker* and E. R. Dobbs
Department of Physics, Queen Mary College, University of London †

[Received May 13, 1955]

Abstract

The adiabatic compressibility and adiabatic Poisson's ratio for solid argon have been measured by determining the velocities of longitudinal and transverse ultrasonic waves in fine-grained polycrystalline specimens between 65° and 80°K. The cryostat, the ultrasonic interferometer and the preparation of the specimens are described. The compressibility is estimated to rise from 0·42 to $0{\cdot}62\times10^{-10}$ cm^2/dyn between 0°K and the melting-point; Poisson's ratio is 0·30. Existing data are used to estimate the expansivity at various temperatures. The compressibilities are compared with other measurements and with various theoretical estimates. The results are consistent with a Gruneisen parameter $\gamma=\alpha V/\kappa_s C_p=1{\cdot}2$.

§ 1. Introduction

The inert gases have spherically symmetrical interatomic forces and crystallize in close-packed structures. They have therefore been the subject of many theoretical investigations on the solid state which ideally require a knowledge of the specific heat, expansivity and compressibility as functions of temperature and pressure to verify their predictions. Such information has been obtained by Dugdale and Simon (1953) for solid helium, but in this case the large influence of zero point energy makes helium unsuitable for checking theories based on a simple interatomic potential function (see, for example, Dugdale and MacDonald 1954). The heavier inert gases (argon, krypton, xenon) are much less influenced by zero point energy and, of these, argon is available to a high degree of purity at small cost, whereas krypton and xenon are much rarer and expensive. Argon is therefore, in many ways, a suitable substance for a detailed investigation of the properties of the solid state.

The specific heat has already been measured and, as will be shown, an estimate of the thermal expansion can be made from existing data. This paper describes the measurement of the velocities of longitudinal and transverse ultrasonic waves in solid argon in the temperature range 65° to 80°K. A knowledge of these velocities, together with the appropriate densities, enables the adiabatic compressibility, and adiabatic Poisson's ratio, at zero pressure to be directly calculated. These elastic coefficients can then be used with the other data on solid argon, to check the deductions that have been made from various models of the solid state.

---

* Now at Department of Electrical Engineering, Imperial College, London.

† Communicated by Professor G. O. Jones.

§ 2. GENERAL EXPERIMENTAL METHOD

Elasticity measurements, particularly of metals, have shown that only measurements with strain-free, homogeneous specimens yield results that are characteristic of the substance rather than its crystalline state. Ideally, for solid argon, as with other cubic crystals, the three independent elastic constants (c_{11}, c_{12}, c_{44}) should be measured using suitable single crystals. Because of the difficulty of producing and handling such crystals at low temperatures, we have made our measurements on fine-grained, polycrystalline specimens which are elastically isotropic.

The usual static methods of measuring elasticity are not easily adapted to low temperatures and, in the case of the low boiling point elements which have very small elastic limits, are limited in sensitivity by the necessity of avoiding plastic deformation. For argon, Stansfield (1954) has found that the tensile strength is about 50 g wt/mm^2 for coarse-grained, polycrystalline specimens at 75°K (cf. 20 kg wt/mm^2 for copper at room temperature). An ultrasonic method that does not involve large elastic displacements is therefore desirable. The composite resonator and pulse methods have both been extensively used with single crystals at low temperatures, but are only suitable for polycrystalline material when the grain-size can be made very small compared with the wavelength of the sound.

A preliminary investigation (Barker, Dobbs and Jones 1953) showed that a compact, transparent, polycrystalline solid of grain-size of the order of 0·1 mm (as estimated from x-ray diffraction photographs) could be formed by depositing the solid from the vapour on to a cooled surface at a rate of growth of about 0·1 mm/min. The velocity of longitudinal waves in such a specimen was found to be 1300 m/s at 78°K, so that the desired acoustic wavelength (λ) of 1 mm or more would only be produced by sound at frequencies below 1·3 Mc/s. This is too low a frequency for accurate measurements by the pulse method in solid argon and so we have adapted the quartz crystal acoustic interferometer, commonly used for gases and liquids, to be suitable for the low boiling-point elements in the solid state.

Essentially, a plane wave of sound (the active area of the transmitting crystal is about 20 λ) is propagated through an aggregate of argon crystals about 0·1 λ in diameter. This sound is reflected at a prepared, flat, solid–vapour interface producing the usual resonance when stationary waves are set up in the solid argon for each $\lambda/2$ increase in thickness.

The velocity of sound is thus found from the known frequency of the quartz oscillations and the measured thicknesses of the specimen at each resonance.

§ 3. The Apparatus

A general outline of the apparatus, which is a development of that used in the earlier work, is shown in fig. 1. The solid argon is formed in the cylindrical Perspex cell a mounted between the liquid oxygen reservoir d and the quartz crystal transducer q, shown in detail in the inset figure.

Fig. 1

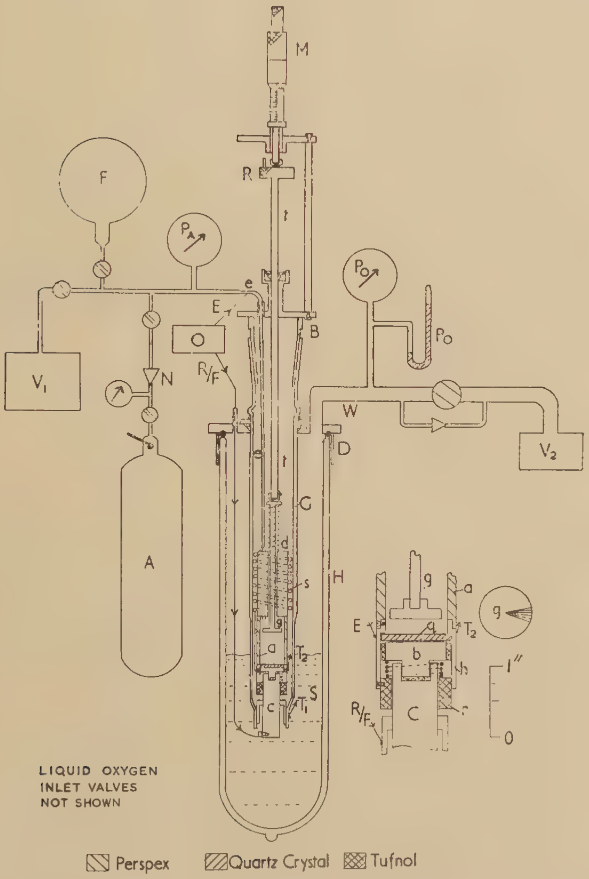

Cryostat and ultrasonic interferometer
(inset: quartz crystal transducer in its Perspex cell).

The quartz crystals used were thick discs, 1·000±0·001 in. diameter, and operated in thickness vibration at their resonant frequency. They were manufactured and gold-plated by the Quartz Crystal Co. on all faces, except for an annular ring ($\frac{3}{4}$ in. int. dia.) on the back face (fig. 2). This back face was mounted on a ground brass block b (fig. 1), surrounded by an insulating Tufnol ring. The front face was pressed at its rim against the square shoulder of a brass tube h by a steel spring held between the lower Tufnol ring r and the brass block b, both of which could slide along the brass rod c. In this way electrical connections were made to the upper face through the tube h, and to the lower face through the rod c, a phosphor bronze spring and the ground block b. At the same time the contact between b and the quartz was sufficiently rough to prevent the sound being transmitted downwards. The springs not only maintained these contacts at the low temperatures of the experiments, but also enabled crystals of thicknesses from ½ to 6 mm to be used in the same holder.

Fig. 2

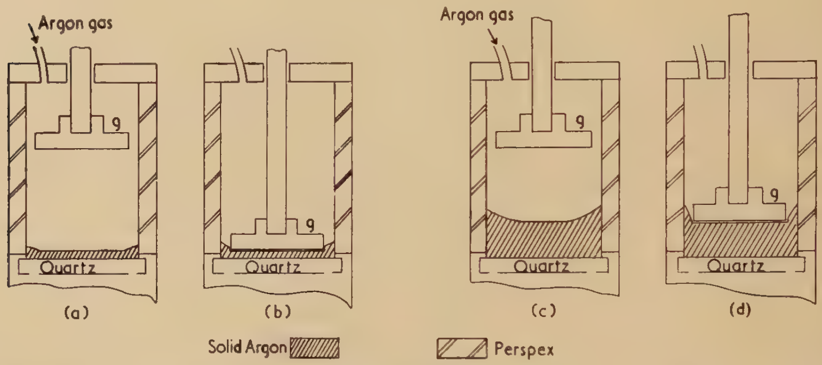

Flattening of solid argon: (*a*) and (*b*) at second minimum; (*c*) and (*d*) at eighth.

The crystal holder was rigidly connected by the Perspex tube a to the brass cylinder d through which passed a ground brass rod, ending in the flat steel disc g. In this way this disc could be displaced along an axis perpendicular to the quartz crystal, by the micrometer M (at room temperature) acting through the thin stainless steel tube t. Connections were made using ball-bearings so that the coupling was flexible. The tube t, and hence the disc g, could also be rotated about a vertical axis, using the head R. The lower side of the disc g was acoustically flat, but was covered with fine radial grooves for cutting a flat face on the solid argon. For reflection of the sound, the flatness and parallelism of the sides of the argon block should be within $\lambda/4$ (see, for example, Gold 1951), which in our case is about 0·25 mm—they were, in fact, true to better than 0·1 mm as checked with an optical flat.

The complete interferometer was mounted in a vacuum enclosure formed by the brass cone B, the Pyrex tube G and the glass-to-metal seal S. It could be evacuated through the tube e by the high vacuum system V_1. The Pyrex tube G was sealed with an O-ring into the brass top-plate D mounted similarly on the glass Dewar vessel H, which had two ½ in. wide vertical slits left on opposite sides in its silvering as observation windows. The connections from the tuned circuit O were an earth lead E via the tube e to the tube h, and an R/F input lead through a pin seal in D to the rod c. Also going through D were the inlet tubes for the liquid oxygen valve, its control rod, and the wide tube W through which the Dewar vessel could be evacuated by the high-speed pumping system V_2 at a controlled rate.

§ 4. EXPERIMENTAL PROCEDURE

Starting at room temperature, the high vacuum system V_1 was used to exhaust to below 10^{-4} mm mercury the 3 l. flask F, the argon inlet tubes up to the needle valve N, and the vacuum enclosure BGS. An Avo signal generator, loosely coupled to the tuned circuit O, was then adjusted to resonance at the frequency of the quartz crystal, as indicated by an anode-bend detector joined to the tuned circuit O. (Typical circuit diagrams are given by Vigoureux, 1950.) The Dewar vessel D was then half-filled with liquid oxygen and the pumping system V_2 used, together with the liquid oxygen inlet valve, to attain the temperature required for the experiment.

This was roughly indicated by the vacuum gauges p_0 and/or P_0 acting as oxygen vapour pressure thermometers and was measured by the thermocouples T_1 and T_2. These thermocouples were made from specially selected 33 s.w.g. eureka/40 s.w.g. copper wires supplied by the London Electric Wire Co. and were calibrated against a standard oxygen vapour pressure thermometer (Scott 1941) in the temperature range 60°–90°K to an absolute accuracy of 0·1°K. The thermocouple T_2 showed that this simple cryostat took up to 1 hr. to attain equilibrium and then maintained its temperature within 0·2°K at the quartz crystal during the definitive runs of about 6 hr., while the liquid oxygen level was kept within $\frac{1}{8}$ in. of that shown in fig. 1 by a trickle from the inlet valve.

Before admitting the argon gas, the reservoir d was filled with liquid oxygen (the tubes for this also attached d to the brass cone B and are omitted from fig. 1 for clarity). The interferometer was then isolated from V_1 and argon gas from the cylinder A admitted through a two-stage regulator and the needle valve N at a very slow rate. The gas filled the flask F and the interferometer at a pressure, indicated by the vacuum gauge P_A, that rose until it was a little above the vapour pressure of argon at the temperature of the experiment, but below the triple point pressure (52 cm mercury). Under these conditions solid argon sublimed from the supersaturated vapour on the colder parts of the interferometer, but not on the tool g, nor in the copper inlet spiral s, since both were at 90°K, i.e. above the triple-point (83·8°K). After a few minutes, a transparent layer of solid argon could be seen on the quartz crystal. It was formed from the cooled argon gas (the reservoir d was kept full of liquid oxygen) and its thickness increased by about 0·1 mm/min.

As the argon covered the quartz crystal it damped its voltage resonance, shown by a minimum in the anode current of the detector as read on a backed-off microammeter. The growth of the argon could be observed through slits in the Dewar and its surface remained flat enough to show maxima and minima on the microammeter for each $\lambda/4$ increase in thickness. It was allowed to grow until the second minimum had just been passed (fig. 2 (*a*)), when the argon supply and the flask F (fig. 1) were disconnected from the interferometer, leaving only the vacuum gauge P_A and the narrow tube e connected to Perspex cell. The argon quickly reached equilibrium, as shown by the gauge P_A (acting as a vapour pressure thermometer) and the microammeter.

The tool g was then lowered, using the micrometer M, until it reached the solid argon when it was alternately rotated and further depressed into the solid argon, subliming away first part of the ridge at its edge and then cutting out a cylinder $\frac{3}{4}$ in. diameter in the block (fig. 2 (*b*)). Initially, the stainless steel tool was at about 90°K, but its lower surface was rapidly cooled in the sublimation process to be only a little warmer than the solid argon. When the surface was seen from the appearance of the turning marks of the tool to be flat, the readings of the microammeter and of micrometer became consistent and were recorded.

Fig. 3 Fig. 4

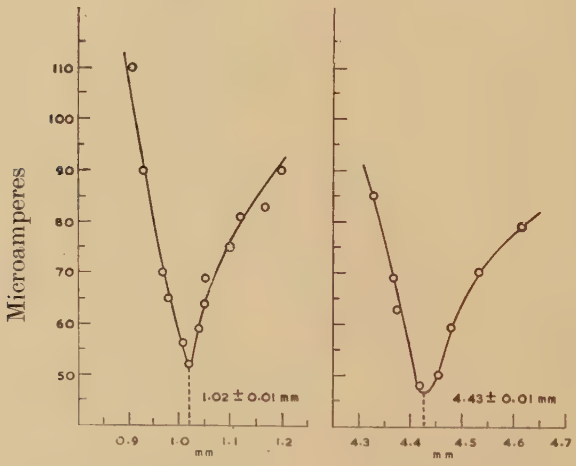

A second minimum. An eighth minimum.

Resonance in solid argon.

As the tool slowly cut into the argon, the ultrasound, radiated as a plane wave from an active area of $\frac{3}{4}$ in. in diameter of the quartz crystal, was reflected at the moving solid argon–vapour interface. The microammeter readings, plotted against the position of this surface from an arbitrary zero (fig. 3), showed a pronounced minimum when the thickness of the block was one ultrasonic wavelength. During these readings the frequency of the signal generator was kept within 100 c/s of the resonant frequency of the quartz crystal, as detected by a standard frequency meter.

Having followed through the resonance curve corresponding to a thickness of λ (the second minimum), the tool g was removed from the vicinity of the solid argon and argon gas was again slowly admitted to the interferometer. The microammeter showed the solid argon growing through the second minimum and then on until the third minimum had just been passed, when the process of subliming away the surplus argon and observing the resonance curve on the microammeter and micrometer was repeated. A number of minima were detected in this way, figs. 2 (*c*) and (*d*) showing the appearance of the block before and after cutting through the eighth minimum. The resonance curves became less pronounced as the attenuation of the ultrasound increased in the thicker argon blocks : for example fig. 4 shows a resonance curve corresponding to the eighth minimum of a run with a 1 Mc/s X-cut quartz crystal at 67°K.

This attenuation was mainly due to the scattering of the ultrasound at the grain-boundaries and was kept as small as possible by choosing a quartz crystal that produced a wavelength of 1 mm or more in the solid argon. It was found, however, that above 75°K the attenuation rapidly increased with thickness and prevented more than four consecutive minima being accurately observed, whereas up to ten could be recorded at lower temperatures. This increase of attenuation can probably be accounted for by recrystallization and grain-growth of the solid argon, for this type of attenuation is very sensitive to the size of the grains—as shown, for example, by Mason (1954).

§ 5. RESULTS OF MEASUREMENTS

(i) *Ultrasonic Velocities*

The interferometer was used as an absolute instrument, the velocities being given by the product of the frequency of the oscillations and their mean wavelength in the solid argon. As a check, however, it was used to find the longitudinal velocity in two liquids (ether and carbon tetrachloride) having similar velocities at room temperature to those observed in the argon. In each case the measurements agreed with the published values to within 1%.

The argon gas was supplied by the British Oxygen Company and was stated to be at least 99·8% argon by volume ; the main impurity was nitrogen with less than 2 in 10^5 of other gases. The solid argon formed from it was found to melt sharply, however, at the triple point, showing that the impurity level in the solid was very low.

The accuracy of the velocity measurements in solid argon was essentially limited by the grain-size attenuation, which prevented a large number of minima being observed at the high temperatures. The wavelength was given by the mean of successive half-wavelength measurements from an arbitrary zero, thus eliminating any errors due to end-effects or thermal contractions of the various links between the micrometer and the argon surface. The longitudinal velocities (v_l), measured with a 1 Mc/s X-cut crystal, had probable errors ranging from $\frac{1}{2}\%$ at 67°K to 2% at 79°K. The transverse velocities (v_t) measured with a 600 kc/s Y-cut crystal, were associated with greater grain-size attenuation and had probable errors of 3% at 67°K and 4% at 74°K.

Fig. 5

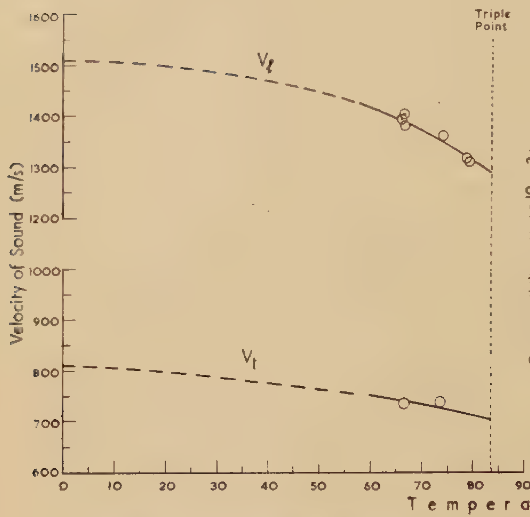

Ultrasonic velocities in solid argon.

Fig. 6

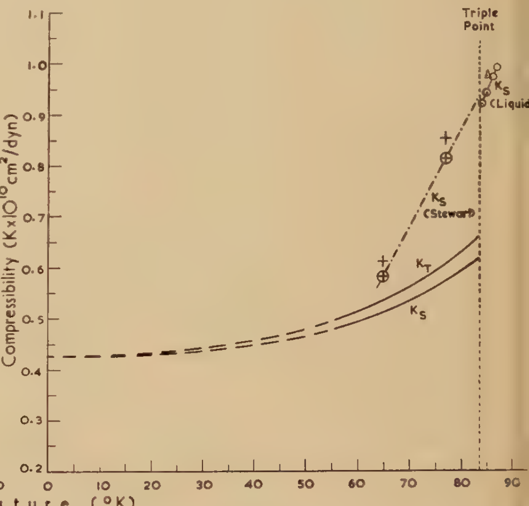

Compressibilities of solid and liquid argon. (+ Stewart, κ_T; ⊕ Stewart, κ_s; ○ Itterbeek and Verhaegen, κ_s; △ Galt, κ_s.)

Both velocities are shown plotted against temperature in fig. 5, with a reasonable extrapolation to the absolute zero in each case. Smoothed values taken from the graphs are given in table 1.

Table 1

temp. (°K)	0	30	60	70	80	84
v_l (m/s)	1510	1485	1420	1375	1320	1290
v_t (m/s)	810	785	750	735	715	705
v_t/v_l :	0·54	0·53	0·53	0·53	0·54	0·55

(ii) *Elastic Coefficients*

The elasticity of an isotropic medium can be specified in terms of any two elastic coefficients; those most suitable for our purpose are the adiabatic compressibility (κ_s) and adiabatic Poisson's ratio (σ_s). In our case, they are given by $\kappa_s = 1/\rho(v_l^2 - \frac{4}{3}v_t^2)$ and $\sigma_s = (\frac{1}{2}v_l^2 - v_t^2)/(v_l^2 - v_t^2)$, where ρ is the density of the solid argon.

The density of solid argon has been found, using x-rays, to be $1{\cdot}68 \pm 0{\cdot}06$ g/cm³ at 20°K by de Smedt and Keesom (1925) and to be $1{\cdot}65 \pm 0{\cdot}02$ at 40°K by Simon and von Simson (1924). At the triple point the density of liquid argon is 1·42±0·01 (Baly and Donnan 1902) and the expansion on melting (cm³/mole) has been found to be 2·96 (Simon, Ruhemann and Edwards 1930), 3·15 (Bridgman 1934) and 3·53 (Clusius and Weigand 1940). These give a mean density at the triple point of 1·608±0·015. Using the fact that the expansivity is zero at 0°K, a smooth curve of density against temperature was drawn from which the three experimental points differed by less than 0·01 g/cm³. Values of the density and expansivity (α) from this curve are given in table 2.

Table 2

temp. (°K)	ρ (g/cm³)	$10^{10}\,\kappa_s$ (cm²/dyn)	σ_s	$10^4\alpha$ (/°C)	$10^7 C_p$ (*)	$10^{10}\,\kappa_T$ (cm²/dyn)	σ_T	γ
0	1·677	0·42	0·30	0	0	0·42	0·30	—
30	1·664	0·44	0·31	4·3	18·4	0·44	0·31	1·27
60	1·636	0·49	0·30	6·8	26·8	0·51	0·30	1·26
70	1·625	0·53	0·30	7·5	29·3	0·56	0·29	1·19
80	1·612	0·59	0·29	8·1	32·2	0·63	0·28	1·06
84	1·607	0·62	0·29	8·4	35·5	0·67	0·27	1·00
	Liquid argon							
84	1·415	0·92	—	45	41·6	2·00	—	—

* (erg/mole/°C)

Using the smoothed values of the velocities and density, a graph of compressibility (κ_s) and temperature has been drawn (fig. 6). This compressibility and the adiabatic Poisson's ratio (σ_s) are given for several temperatures in table 2; their experimental error does not exceed 10%. The specific heat (C_p) has been measured from 10°K to 80°K by Clusius (1936) and can be used to calculate the isothermal compressibility, $\kappa_T=\kappa_s+\alpha^2T/\rho C_p$ and the isothermal Poisson's ratio,

$$\sigma_T=\sigma_s-[(1-2\sigma)(1+\sigma)(\alpha^2T)]/(3\kappa\rho C_p).$$

These results are listed in table 2 and κ_T is plotted on fig. 6.

§ 6. DISCUSSION

In comparing our measurements of the compressibilities with those of other workers, it is important to remember that we have measured directly only the ultrasonic velocities and in calculating the compressibilities have used data on the density (for κ_s) and specific heat (for κ_T) that have been measured independently. The experimental error in these data is about 1%, but since the measurements have been made on solid specimens formed in rather different ways, they may differ from specimen to specimen in an unknown way. Measurements of the density and specific heat on essentially similar specimens to those used in the present work are, however, in progress at Queen Mary College and may lead to a revision of the following conclusions on solid argon.

With these reservations, our results for κ_s and κ_T are accurate to about 10% and may be compared (fig. 6) with the measurements of κ_T made by Stewart (1955) using the piston-displacement method. His condensed argon was a loosely packed aggregate of crystals in a cylindrical steel cavity of 0·8 cm^3, which he compacted irreversibly at the temperature of condensation by rapidly applying his maximum pressure, 4000 kg/cm^2. His curves of piston-displacement *versus* pressure then became reproducible and by fitting a curve to these measurements of $\Delta V/V$ he was able to calculate κ_T as a function of the applied pressure. As shown in fig. 6, his zero-pressure values of κ_T are about 40% higher than our measurements. Moreover, when his values are converted to adiabatic compressibilities (κ_s), they are seen to lie in a line which coincides with κ_s for the liquid at the melting-point, as measured ultrasonically by Itterbeek and Verhaegen (1949) and Galt (1948). It therefore seems possible that his maximum pressure did not completely compact the solid, but left it less dense than a normal polycrystalline specimen. No measurements of the compressibility at different compacting pressures nor any values of the density are given in his paper. We checked our density at 65°K, using a volumenometer similar to that used by Baly and Donnan (1902) for liquid argon, and obtained $1{\cdot}61 \pm 0{\cdot}05$ compared with 1·63 from the x-ray data (table 2). Our values of κ_s do indeed show an increase of 50% on melting, which is not unreasonable when compared with the other increases on melting of 15% in volume and 25% in specific heat.

In a previous paper (Barker *et al.* 1953) we showed that our preliminary estimates of the compressibility lay within the range covered by the theoretical estimates of Kane (1939) and Rice (1946). Since then, Barron and Domb (1954) and Salter (1954 a) have extended the dynamical theory of the face-centred cubic lattice so that a more direct comparison can be made with theory. Barron and Domb show that for polycrystalline material where the intermolecular forces are of the Lennard–Jones type, Poisson's ratio is 0·27 and v_t/v_l is 0·56, independent of the force constant when only nearest-neighbour interactions are considered. These values are substantially in agreement with the values of Poisson's ratio (table 2) of 0·30 and v_t/v_l of 0·54 (table 1) derived from our measurements. Using an interatomic potential of the form $\phi(r)=4\epsilon[(\sigma/r)^{12}-(\sigma/r)^6]$, and values of ϵ, σ derived from the second virial coefficient of argon gas, Barron and Domb obtain values at 0°K of $v_l=1470$ m/s and $\kappa=0{\cdot}38\times10^{-10}$ cm^2/dyn, which they expect to be increased to about 1620 m/s and $0{\cdot}42\times10^{-10}$ cm^2/dyn when distant neighbour interactions and zero-point energy are taken into account. We obtain 1510 m/s and $0{\cdot}42\times10^{-10}$ cm^2/dyn from our measurements of v_l and κ when they are extrapolated to 0°K.

Salter (1954 a), allowing for distant neighbour interactions in his static energy and also incorporating an approximate expression for the zero-point energy, has calculated expressions for the elastic constants in terms of de Boer's reduced coordinates. We have evaluated the compressibility of solid argon at 0°K from Salter's equations and obtain $0{\cdot}52\times10^{-10}$ cm²/dyn, assuming that $\rho=1{\cdot}68$ (table 2). Since Salter's equations involve differences between terms of the order ρ^5 and ρ^3, they are very sensitive to the value of ρ adopted and the agreement between theory and experiment must be considered satisfactory until more accurate density data are available.

Our measurements enable Gruneisen's parameter, $\gamma=\alpha V/\kappa_s C_p$, to be calculated, yielding the values shown in the last column of table 2. It will be seen that γ is falling slightly as the melting-point is approached. The total change is, however, hardly outside our experimental error. It is of interest to note that the compressibility data of Stewart, although very different from ours, also lead to a γ falling (from 1·07 at 65°K to 0·77 at 77°K) near the melting-point. Previous estimates of γ for argon are those of Simon and Kippert (1928), who obtained 4·5, and Rice (1946) who used 4·3 in his calculations. But Simon has said (quoted by Salter 1954 b) that he considers $\gamma=4{\cdot}5$ is suspect as being too high. Certainly our value of $\gamma=1{\cdot}2$ is much nearer the values for, say, the alkali metals (1·17 to 1·48) or the alkali halides (1·25 to 2·00).

Our measurements are continuing and are being extended to lower temperatures. A detailed comparison with theory will be made later.

Acknowledgements

We are grateful to Professor G. O. Jones for his help in the early stages of this research and for his constant encouragement. We also acknowledge with thanks the loan of apparatus by the Central Research Fund of the University of London and the technical assistance of Mr. W. Baldock, who constructed much of the apparatus.

References

Baly, E. C. C., and Donnan, F. G., 1902, *J. Chem. Soc.*, **81,** 914.
Barker, J. R., Dobbs, E. R., and Jones, G. O., 1953, *Phil. Mag.*, **44,** 1182.
Barron, T. H. K., and Domb, C., 1954, *Phil. Mag.*, **45,** 654.
Bridgman, P. W., 1934, *Phys. Rev.*, **46,** 930.
Clusius, K., 1936, *Z. Phys. Chem.* B, **31,** 459.
Clusius, K., and Weigand, K., 1940, *Z. Phys. Chem.* B, **46,** 1.
Dugdale, J. S., and MacDonald, D. K. C., 1954, *Phil. Mag.*, **45,** 811.
Dugdale, J. S., and Simon, F. E., 1953, *Proc. Roy. Soc.* A, **218,** 291.
Galt, J. K., 1948, *J. Chem. Phys.*, **16,** 505.
Gold, T., 1951, *Phil. Mag.*, **42,** 787.
Itterbeek, A. van, and Verhaegen, L., 1949, *Proc. Phys. Soc.* B, **62,** 800.
Kane, G., 1939, *J. Chem. Phys.*, **7,** 603.
Mason, W. P., 1954, *Piezoelectric Crystals and their Application to Transducers* (New York : Van Nostrand), Chap. 15.
Rice, O. K., 1946, *J. Chem. Phys.*, **14,** 321.
Salter, L., 1954 a, *Phil. Mag.*, **45,** 360 ; 1954 b, *Ibid.*, **45,** 369.

Scott, R. B., 1941, *Temperature: Its Measurement and Control in Science and Industry* (New York: Reinhold), p. 215.

Simon, F. E., and Kippert, F., 1928, *Z. Phys. Chem.*, **135,** 113.

Simon, F. E., Ruhemann, M., and Edwards, W. A. M., 1930, *Z. Phys. Chem.* B, **6,** 331.

Simon, F. E., and Simson, C. von, 1924, *Z. Phys.*, **25,** 160.

Smedt, J. de, and Keesom, W. H., 1925, *Leiden Commun.*, **178***b*.

Stansfield, D., 1954, *Thesis,* Bristol University.

Stewart, J. W., 1955, *Phys. Rev.*, **97,** 578.

Vigoureux, P., 1950, *Ultasonics* (London: Chapman and Hall), p. 50.

CXXI. *The Electrical Properties of Electroluminescent Phosphors*

By A. N. INCE and C. W. OATLEY
Engineering Laboratory, University of Cambridge*

[Received March 30, 1955; revised May 25, 1955]

SUMMARY

Measurements have been made of the dielectric properties of a number of electroluminescent phosphors in the form of powders and polycrystalline lumps. There appear to be two quite separate mechanisms giving rise to dispersion: one which is present in the dark and the other which is stimulated by irradiating the phosphor with ultra-violet light. The latter is very similar to the dispersion found in ordinary non-electroluminescent powders and has not been studied further. The former, which seems to be characteristic of electroluminescent phosphors, produces dispersion at very low frequencies and has been investigated in detail. Measurements have also been made of the variation of dielectric properties with voltage and with temperature.

To explain the effects observed it is assumed that electronic barriers are formed in the specimen and that motion of some of the ions in the barrier region takes place. On the basis of this model it is found possible to account in a semi-quantitative manner for the experimental results. Values are deduced for the height of the barrier and for the number and diffusion coefficient of the mobile ions.

§ 1. INTRODUCTION

SINCE Destriau (1936, 1947) first showed that certain phosphors emit light when placed in a sufficiently strong alternating electric field many investigators have studied this phenomenon, but it must be admitted that the underlying mechanism of electroluminescence is still somewhat obscure. A number of authors have drawn attention to the interesting electrical properties of these phosphors. Thus, in papers by Roberts (1952, 1953), Zalm, Diemer and Klasens (1954), and by Butler and Waymouth (1954), attention has been drawn to the fact that the d.c. conductivity varies greatly with the applied voltage and curves have been given showing how the permittivity and power-factor depend on the applied alternating voltage at various frequencies. Some of these authors also noticed that the electrical characteristics of a specimen were different when the phosphor was kept in the dark from what they were when it was irradiated with visible or ultra-violet light.

---

* Communicated by the Authors.

Many of the effects reported in these papers had been observed in this laboratory also, and it was therefore decided to make a more detailed study of the electrical behaviour of some electroluminescent phosphors. The results which have been obtained are reported below in two separate groups. The first of these is concerned with the variation of the dielectric properties of the phosphor with frequency and with temperature while, in the second, the variation with applied voltage is described.

§ 2. MATERIALS AND APPARATUS

Most of the measurements reported below have been carried out on an electroluminescent polycrystalline lump of copper-activated zinc sulphide (sample A). X-ray examination suggested that the total number of crystallites in this specimen was of the order of 10^4. For the d.c. measurements, which required a different arrangement of electrodes, a similar polycrystalline piece (sample B) was used. The deeper colour of sample A suggested that it contained a higher proportion of activator than sample B. Some a.c. measurements also were made on sample B, which showed the same general behaviour as sample A. The rough dimensions of these samples were $0{\cdot}4 \times 0{\cdot}5 \times 0{\cdot}14$ cm.

A few measurements were made on a single crystal of electroluminescent copper-activated zinc sulphide of much smaller dimensions ($0{\cdot}2 \times 0{\cdot}2 \times 0{\cdot}05$ cm), but this was difficult to handle and was fractured before it could be thoroughly investigated.

Measurements have also been made on a number of electroluminescent powder phosphors. These were of the zinc sulphide type with suitable activators to produce light of blue, green or yellow colour in the different cases. The exact composition of these commercial phosphors was not known.

When powders were used, a known quantity of the phosphor was suspended in a solution of polystyrene in benzene and allowed to settle on a metal electrode about 4 cm^2 in area. When the mixture had dried a second electrode was added. For most purposes this was of tin or aluminium foil which was stuck to the surface of the phosphor mixture with a little of the polystyrene solution or with silicone oil. When it was desired to make measurements with the phosphor illuminated, the second electrode was of glass rendered conducting with a film of tin oxide. The thicknesses of dielectric films prepared in this way ranged from about 0·01 cm upwards and were measured with an accuracy of about 0·0005 cm by means of a dial gauge. These thin films were particularly useful for measurements at high field-strengths.

For the measurement of the capacitance C and equivalent parallel resistance R of the condenser formed by the specimen and its two electrodes a bridge of the type shown in fig. 1 was used. Such bridges have been discussed by Clark and Vanderlyn (1949) and have the great advantage that they are virtually unaffected by stray capacitances to earth, so that no Wagner earthing device is needed. With the notation of the figure, the balance conditions are :

$$\frac{n_1}{n_2}=\frac{C}{C_1}=\frac{R_1R_2+R_1R_3+R_2R_3+RR_1}{RR_2}. \quad . \; . \; . \quad (1)$$

The coils n_1 and n_2 are wound on a high-permeability core and it has been shown by Oatley and Yates (1954) that high accuracy can be achieved with the bridge even when the turns ratio is 100 or more. Thus the capacitance and power factor of a very small condenser can readily be measured. The numbers of turns n_1 and n_2 were chosen to suit the range of frequencies required and, with two or three pairs of coils, it was found possible to cover the range from 10 c/s to 50 kc/s, though relatively few measurements were made below 30 c/s. The balance detector consisted of a sharply tuned amplifier and an oscilloscope, so that no trouble was caused by harmonics of the input voltage.

Fig. 1

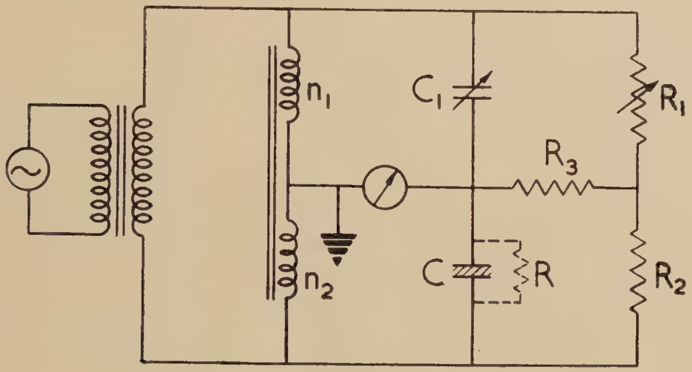

Bridge circuit.

For measurements in the frequency range from 50 kc/s to 10 Mc/s a standard Q-meter was used.

With either method of measurement the voltage applied to the specimen did not normally exceed 3 v so that there was no appreciable variation of dielectric properties throughout the cycle. When the non-linearity of the dielectric was being investigated, the voltage across the specimen could be increased to 500 v.

It has previously been suggested that non-linearity of the phosphor dielectric is caused by traces of moisture, but we have not been able to confirm this. In general our specimens were kept in a vessel containing a little phosphorus pentoxide, while measurements were being made on them. Some measurements were made, however, after the specimens had been heated to 200°c in a vacuum and kept there for several hours. The results obtained under these conditions were practically the same as in air ; in particular, the non-linearity was as marked as ever.

§ 3. General Survey of Results on Dielectric Dispersion

It is convenient to express the results of measurements of the permittivity and power factor of the dielectric in terms of the components ϵ_1 and ϵ_2 of the complex permittivity $\epsilon_1 - j\epsilon_2$, and fig. 2 shows the variation of these quantities with frequency for specimen A when irradiated with ultra-violet light. In the curve for ϵ_2 the large values at very low frequencies followed by a fall and then a peak at about 15 kc/s suggest that two quite separate mechanisms are operating simultaneously, and this is confirmed by the two points of inflexion in the curve for ϵ_1.

Fig. 2

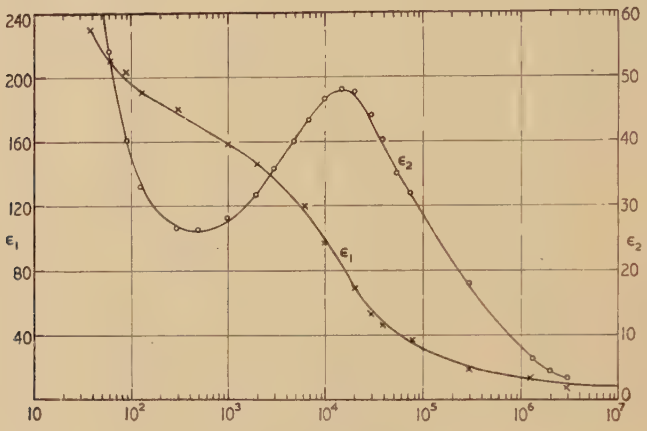

Frequency (c/s)

Dispersion curves for sample A irradiated with ultra-violet light.

When the measurements were repeated with the specimen in the dark, the curves of fig. 3 were obtained and there is now no sign of any anomaly at 15 kc/s. If we assume that the two mechanisms postulated above operate independently of each other, and that the one centred on 15 kc/s is caused by irradiation with ultra-violet light, it is legitimate to subtract the values of fig. 3 from those of fig. 2 to give the curves shown in fig. 4, which are now characteristic of the single mechanism caused by irradiation.

Returning to the curves of fig. 3, it is clearly of interest to know what behaviour would be encountered at still lower frequencies. With the present form of apparatus and with the relatively low capacitances (<100 pF) which were to be measured, it was not found possible to work at frequencies below 10 c/s. However, if the dispersion is of the Debye type, there should be a peak in the curve for ϵ_2 and the frequency at which this peak occurs should be greater at high temperatures than at low. Some measurements were therefore made on sample B and on an electroluminescent phosphor in powder form at a temperature of 300°c, but even at this temperature the values of ϵ_1 and ϵ_2 were rising steadily at the lowest frequencies at which measurements could be made.

Fig. 3

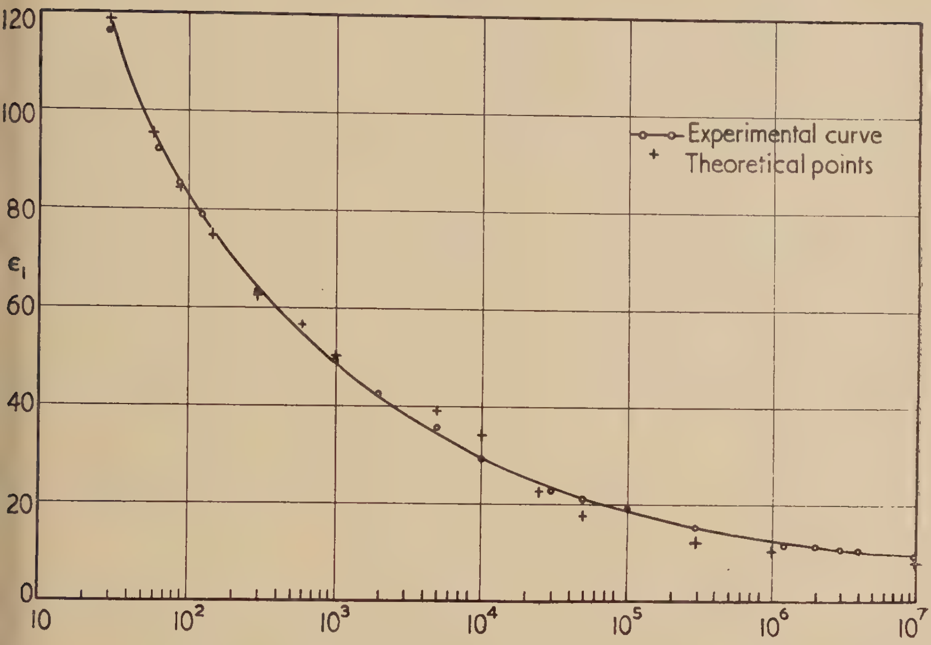

(*a*)

Frequency (c/s)

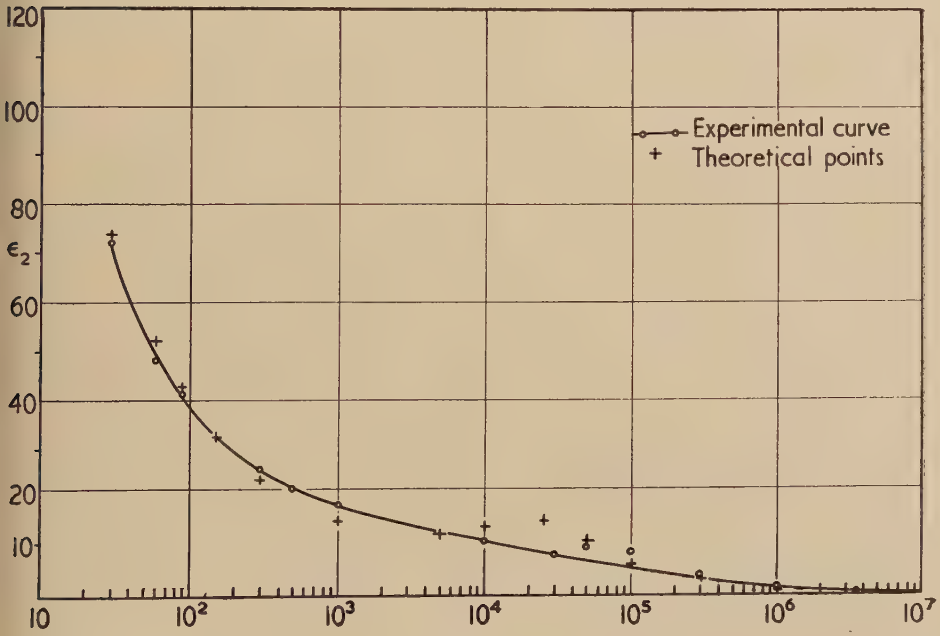

(*b*)

Frequency (c/s)

Dispersion curves for sample A in the dark.

§ 4. Discussion of Results on Dispersion

The curves shown in fig. 4 are clearly of the general type that can be represented by the Debye equations (Fröhlich 1949). If the dispersion could be ascribed to a process governed by a single relaxation time, the maximum value of ϵ_2 should be given by $(\epsilon_s - \epsilon_\infty)/2$, where ϵ_s and ϵ_∞ are the values of ϵ_1 at zero frequency and infinite frequency respectively. In fact the maximum value of ϵ_2 is rather less than this, which suggests that there is a small spread of relaxation times. A more detailed analysis by means of a Cole–Cole plot (Cole and Cole 1941) confirms this suggestion.

Fig. 4

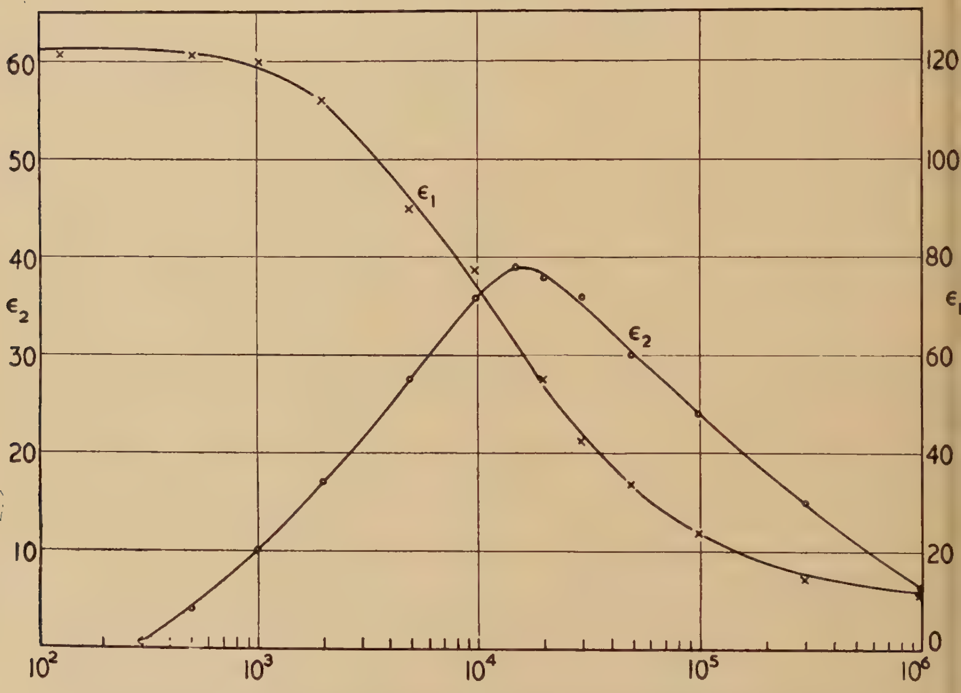

Results obtained by subtracting the values of fig. 3 from those of fig. 2.

Results of the type shown in fig. 4 are well known for ordinary non-electroluminescent phosphors when stimulated with ultra-violet light (Garlick and Gibson 1947) but in such cases the relaxation times have usually been an order of magnitude smaller than the mean value of 10^{-5} sec found from fig. 4. These results will not be considered further since they do not appear to be connected with the phenomenon of electroluminescence. On the other hand ordinary phosphors do not exhibit any marked dispersion when they are not stimulated by radiation. Thus the remainder of this paper will be concerned principally with results obtained under these conditions.

Turning now to the curves of fig. 3, since no peak value has been found for ϵ_2 in the range of frequencies investigated it is not immediately obvious whether the results can or cannot be represented by the Debye equations. To test this point, use was made of the equations

$$\epsilon_2{}^2=(\epsilon_s-\epsilon_1)(\epsilon_1-\epsilon_\infty), \quad . \quad . \quad . \quad . \quad . \quad . \quad (2)$$

$$(\omega\tau)^2=(\epsilon_s-\epsilon_1)/(\epsilon_1-\epsilon_\infty) \quad . \quad . \quad . \quad . \quad . \quad . \quad . \quad (3)$$

where τ is the relaxation time and the values of ϵ_1 and ϵ_2 correspond to angular frequency ω. These equations should hold for any substance to which the Debye theory applies and for which there is a single relaxation time (Fröhlich 1949). Taking values from fig. 3, putting $\epsilon_\infty=10$ and using eqn. (2), ϵ_s was calculated for frequencies of 1 kc/s, 100 c/s and 30 c/s. These values of ϵ_s were then substituted in eqn. (3) to give values of τ. The results are shown in the table and it is clear that there is no consistency in the values of either ϵ_s or τ. Furthermore, the values of τ are incorrect since they would correspond to a peak of ϵ_2 in the range of frequencies covered by fig. 3. It is safe to conclude therefore that Debye theory with a single relaxation time cannot account for the experimental results. It is less easy to be certain that agreement between theory and experiment could not be reached by postulating a suitable spread of relaxation times, but such an explanation does not seem particularly plausible.

f	ϵ_s	τ
1 kc/s	88	$3{\cdot}4\times10^{-4}$ sec
100 c/s	137	$2{\cdot}1\times10^{-3}$ sec
30 c/s	307	$5{\cdot}6\times10^{-3}$ sec

Many authors have attempted to explain the dielectric properties of inhomogeneous materials in terms of a system containing particles which behave as capacitances separated by material of high, but not infinite, resistivity. It is easy to show that a simple system of this type containing only one capacitance in series with one resistance gives rise to dispersion which can be represented by the Debye equations, so the comments made in the foregoing paragraph apply to this model also. To explain the curves of fig. 3 it would be necessary to postulate a very complex system in which a wide spread of relaxation times was operative. If, however, the capacitances are assumed to vary with frequency, it is possible to construct a much simpler model and this, in effect, is what is done below, the capacitances being ascribed to the existence of barriers either between crystallites or at the surfaces of the specimen adjacent to the electrodes.

Whenever barriers are formed in this way and an alternating electric field is applied to a specimen which has appreciable conductivity the local accumulation of charge can contribute to the measured capacitance and power loss of the specimen and may swamp all other factors.

Conditions in the barrier region will be determined by the numbers of the different types of carrier, by their mobilities and rates of formation and recombination, by the ease with which they can pass to the electrodes and by many other factors. Progress towards a general solution of the problem has been made by Jaffé (1933, 1952) and by Macdonald (1953) but their formulae are very complex and involve assumptions which may or may not be valid in the present experiments. In the first instance, therefore, our experimental results will be compared with those predicted by a simplified treatment due to Volger, Stevels and van Amerongen (1953). These authors assume that only one type of conducting carrier is present in the specimen and that carriers of this type cannot pass from the specimen to the electrodes. Under these conditions the type of barrier formed will depend on the ratio of the conductivity σ to the angular frequency of the applied electric field. If $\omega \ll 4\pi\sigma/\epsilon$ where ϵ is the permittivity of the medium itself when no barriers are formed, the build-up of charge near the electrodes will be governed almost entirely by space-charge and the barrier will be of the well known Schottky type. Such barriers lead to a surface capacitance which is independent of frequency and cannot therefore account for our experimental results.

If, on the other hand $\omega \gg 4\pi\sigma/\epsilon$ the quantity of charge which can build up near an electrode during the half-cycle before the direction of the applied field is reversed, is so small that space charge is negligible. The accumulation of charge is then opposed only by diffusion which is brought into play by the concentration gradient. If x is the distance from the electrode in a one-dimensional system and n the concentration of charge carriers, the relevant equation is

$$\frac{\partial n}{\partial t}=D\frac{\partial^2 n}{\partial x^2} \qquad . \quad . \quad . \quad . \quad . \quad . \quad . \quad . \quad . \quad (4)$$

where D is the diffusion coefficient. At the electrode the total current is by hypothesis, zero, so

$$\sigma E=eD\left(\frac{\partial n}{\partial x}\right)_{x=0} \qquad . \quad . \quad . \quad . \quad . \quad . \quad . \quad . \quad . \quad (5)$$

Solving (4) and inserting the boundary condition (5) we find that, when the applied electric field is given by $E=E_0 \sin \omega t$, the steady-state value of n is

$$n=n_0+\frac{\sigma E_0}{e\sqrt{D\omega}}\exp\left[-x\sqrt{\left(\frac{\omega}{2D}\right)}\right]\sin\left[\omega t-\frac{\pi}{4}-x\sqrt{\left(\frac{\omega}{2D}\right)}\right] \quad . \quad (6)$$

where n_0 is the carrier concentration when there is no field.

Volger, Stevels and Amerongen then show that, in addition to the normal capacitance C and equivalent parallel resistance R of the specimen, there is now a barrier capacitance C_b and parallel resistance R_b such that

$$C_b=\sqrt{\left(\frac{2}{\omega D}\right)}\sigma, \qquad . \quad . \quad . \quad . \quad . \quad . \quad . \quad . \quad (7)$$

$$R_b=\sqrt{\left(\frac{D}{2\omega}\right)}\Big/\sigma=\delta/\sigma \qquad . \quad . \quad . \quad . \quad . \quad . \quad (8)$$

where $\delta=\sqrt{(D/2\omega)}$ may be taken as a measure of the thickness of the barrier.

Since a barrier of this type will be formed at each electrode, the equivalent circuit for the complete specimen will be as shown in fig. 5. Both C_b and R_b tend towards zero as ω gets very large, so C and R can be determined from measurements at high frequencies, and C_b and R_b can then be calculated at any other frequency when the total impedance of the specimen is known.

A comparison of this equivalent circuit with the experimental results shows that the model gives a good qualitative picture of the variation of ϵ_1 and ϵ_2 with frequency but is wrong in certain particulars. For example, at very low frequencies, eqns. (7) and (8) taken with the complete equivalent circuit suggest that ϵ_2 should be greater than ϵ_1 whereas it is actually only about half as great as ϵ_1. Furthermore, as will now be shown, when numerical values are inserted into the equations, it becomes clear that the model so far considered is too simple.

Fig. 5

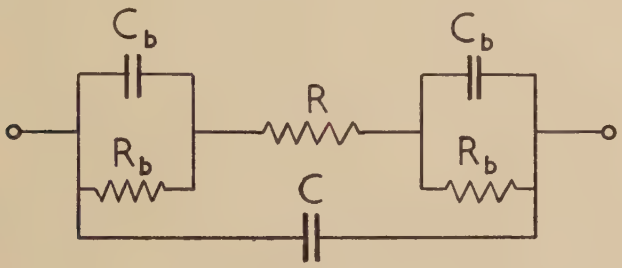

Simple equivalent circuit of specimen.

The variation of ϵ_1 and ϵ_2 with frequency (fig. 3) indicates that the barrier must be of the type in which space-charge is negligible and the variation of charge is governed by diffusion. But this implies that $4\pi\sigma/\epsilon \ll \omega$ even at the lowest frequency of measurement which was 10 c/s. Putting ϵ equal to 10, this means that σ must be less than 10 e.s.u. or, converting to practical units, that the resistivity of the material must exceed 10^{11} ohm cm. Such a value is several orders of magnitude greater than the value (about 10^6 ohm cm) which can be deduced from the equivalent parallel resistance of the specimen at frequencies above 100 kc/s. The high-frequency value of the equivalent parallel resistance might, of course, be influenced by other sources of dielectric loss and in that case it would bear no relation to the resistivity of the material. However, if the resistivity really were as great at 10^{11} ohm cm, the bulk resistance of the specimen would be so great (R in the equivalent circuit of fig. 5) that it would be quite impossible to account for the measured values of impedance by any barrier effects.

Consider next the possibility that a thin layer of the specimen adjacent to each electrode (or at the surface of each crystallite) has a resistivity of the order of 10^{11} ohm cm, but that the bulk resistivity is about 10^6 ohm cm. The equivalent circuit would then be as shown in fig. 6 (*a*) where C_b and R_b are the barrier constants as before, while C_a and R_a are the normal capacitance and resistance of the high-resistance layer.

Fig. 6

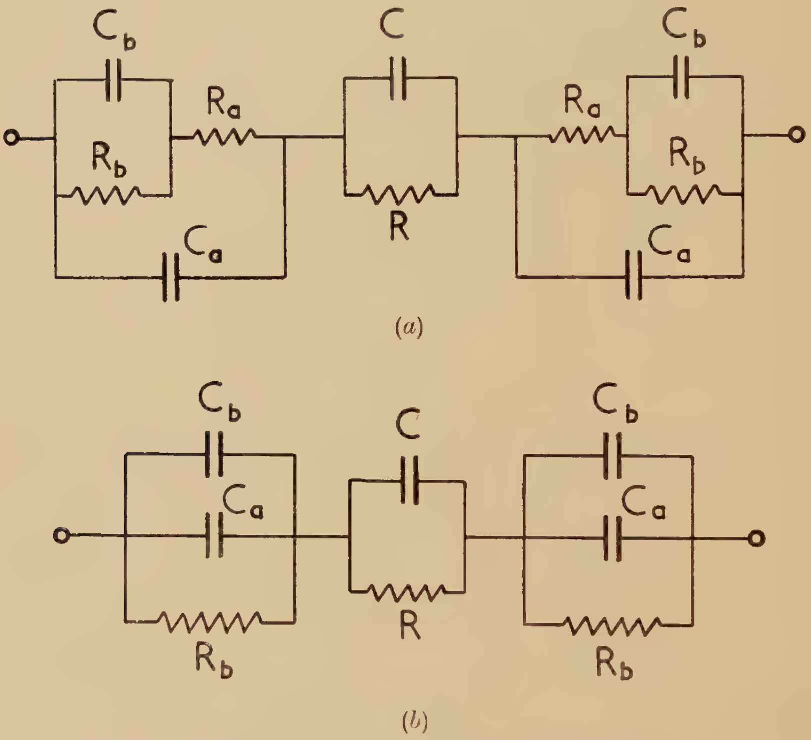

(*a*)

(*b*)

$$C_b=\frac{\sigma}{\sqrt{D/2}\sqrt{\omega}},\quad C_a=50\ \ \mathrm{pF/cm^2},\quad R_b=\frac{\sqrt{D/2}}{\sigma\sqrt{\omega}}$$

$$=\frac{630}{\sqrt{f}}\,\mathrm{pF/cm^2}\qquad\qquad =\frac{282}{\sqrt{f}}\times10^6\ \Omega/\mathrm{cm^2}$$

Improved equivalent circuit of specimen.

This is a much more promising model which represents the experimental results very satisfactorily provided R_a makes a negligible contribution to the total impedance. Assuming for the moment that this is the case, the equivalent circuit is as shown in fig. 6 (*b*).

As before, the values of C and R can be obtained from measurements at frequencies above 100 kc/s. Furthermore, if we assume the resistance of R_b to be equal to the reactance of C_b and each to be equal to $\sqrt{(2D/\omega)}/\sigma$ as theory indicates, the values of $\sqrt{(2D)}/\sigma$ and C_a can be found from measurements of ϵ_1 and ϵ_2 at one other frequency, which may conveniently be low enough for the reactance of C to be very large in comparison with R. Then, assuming C_a to be independent of frequency, the magnitudes of C_b and R_b at any other frequency, and hence the overall values of ϵ_1 and ϵ_2 can be calculated. In figs. 3 (*a*) and 3 (*b*) a number of values of ϵ_1 and ϵ_2 calculated in this way are plotted. The values of $\sqrt{(2D)}/\sigma$ and C_a used were chosen to give the best overall agreement with the experimental curves, and are indicated in fig. 6 (*b*).

The assumption that R_a is negligibly small raises a difficulty which has not been completely resolved and which must now be discussed. Consider first the case where the high-resistance layer consists of homogeneous material of composition different from that of the bulk. Since our specimens were activated by the diffusion of copper inwards from the surface, it would not be surprising if the resistivity of the surface region were different from that of the bulk of the material. However, with resistivity ρ and thickness d, the resistance of such a layer of unit cross section would be $d \,.\, \rho$, while its capacitance would be $\epsilon/4\pi d$. It then follows that, at all relevant frequencies, the reactance of this capacitance would be small compared with the resistance of the layer. In terms of the equivalent circuit of fig. 6 (*a*) this means that, if R_a is negligibly small in comparison with R_b, the impedance of R_b and C_b will be effectively short-circuited by the reactance of C_a and this is contrary to the experimental results.

Fig. 7

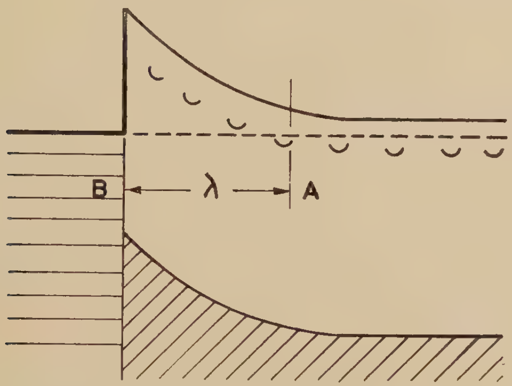

Schematic representation of barrier.

Following Jaffé (1933, 1952) it may be assumed that both positive ions and electrons (or, alternatively, negative ions and holes) are present in the material but that, in the vicinity of an electrode, a rectifying barrier is set up. Using the conventional representation of such a barrier, as in fig. 7, there will be a region of the material of width λ from which free electrons have been largely drained and this region can thus constitute the high-resistance layer which has previously been postulated.

As is well known, the capacitance of this barrier layer corresponds to a thickness λ of dielectric but, when calculating its resistance, allowance must be made for the fact that the resistivity increases rapidly from A to B. This occurs because electrons from the bulk of the material can diffuse into the barrier region, but the concentration of such electrons decreases very rapidly with distance to the left of A. Assuming the conductivity at any point to be proportional to the electron concentration, a rough calculation suggests that the resistance of the layer would be about $0{\cdot}05\rho_{\mathrm{B}}\lambda$ per cm^2, where ρ_{B} is the resistivity at the electrode. The ratio of resistance to capacitive reactance is less by a factor of twenty, therefore, than in the case of a homogeneous barrier previously considered. This factor is still inadequate to make R_a (fig. 6 (*b*)) negligible; nevertheless it seems probable that the picture presented by Jaffé's theory is essentially correct. In view of the inhomogeneous nature of the specimen, it would not be difficult to introduce further plausible assumptions which would have the effect of reducing R_a to a sufficiently low value. In particular, one might postulate a non-uniform distribution of immobile ionized donors which would concentrate a large part of the voltage drop into the immediate vicinity of the electrode without altering the width of the layer from which free electrons had been drained. This would have the effect of reducing R_a without appreciably changing C_a. However, the present measurements throw no light on the mechanism which makes R_a negligibly small, so further speculation is unprofitable.

The representation of the behaviour of the specimen by means of an equivalent circuit cannot, of course, be more than a crude approximation to the truth. At the same time it does provide a rough physical picture of what is taking place and the separation of the various effects, which is inherent in it, makes comparison of theory and experiment much simpler than it otherwise would be. The measured values of the components of the equivalent circuit, which are tabulated in fig. 6 (*b*), will now be used to calculate various properties relating to the charge carriers. In view of the approximation introduced by the use of an equivalent circuit, the results will probably not be very accurate, but they should be correct as to order of magnitude.

§ 5. CALCULATION OF CONSTANTS

It has so far been assumed that only two barrier regions exist in the material but, with a polycrystalline specimen, this may not be the case. Let us assume that there are S pairs in series. Then the true magnitudes of C_a and C_b will be S times as large as the values given in fig. 6 (*b*), while the value given there for R_b will have to be divided by S. However, with these new constants, the overall variation of ϵ_1 and ϵ_2 with frequency will be the same as before.

From the magnitude of C_a and taking the permittivity of the material to be 10, the value of λ the width of the layer from which electrons have been drained is found to be $10^{-2}/S$ cm. This region will be referred to as the electron barrier. Within it, at any rate near the electrode, the ionic conductivity must be less than 10^{-11} (ohm cm)$^{-1}$ if diffusion of ions is to produce an additional impedance with the correct frequency variation. Furthermore, electronic conductivity in this region must be still lower if it is not to short-circuit the effects produced by the ions.

Substitution of this maximum value of the ionic conductivity and the measured value of C_b into eqn. (7) gives for the diffusion coefficient

$$D \leqslant 10^{-4}/S^2 \text{ cm}^2/\text{sec.} \qquad (9)$$

Similarly, from eqn. (8), the maximum value of δ, the width of the region where variation of ion density is appreciable, is found to be $3\times10^{-4}/S$ cm at 100 c/s and $3\times10^{-5}/S$ cm at 10 kc/s. This region will be referred to as the ion barrier and it is to be noted that it occupies only a small fraction of the width of the electron barrier. This fact, together with the original assumption that variation of ion density does not produce appreciable space-charge, provides justification for the separation of the effects due to ions and electrons respectively and their representation by components in an equivalent circuit.

If the ions in question were normal constituents of the crystal moving by way of lattice defects, it has been shown by Mott and Gurney (1940) that the ratio σ/D should be of the order of 3×10^4, whereas our measurements give a value of about 10^{-6}. It therefore seems more likely that we are concerned with the diffusion of interstitial ions. For these the Einstein relation

$$v/D = e/\kappa T \qquad (10)$$

where v is the mobility, should hold and this leads to a maximum value of $4\times10^{-3}/S^2$ cm/sec per v/cm for v. Finally if n_0 is the concentration of interstitial ions

$$\sigma = n_0 e v \qquad (11)$$

and this gives

$$n_0 \geqslant 3\times10^{10} S^2/\text{cm}^3. \qquad (12)$$

These values of D, v and n_0 are all reasonable for interstitial ions if S lies between 1 and 100. For a single crystal S would presumably be unity, but with polycrystalline specimens such as were used in the present measurements it is not improbable that sufficient of the activator copper would diffuse along the grain boundaries to set up barriers there. A rough determination of the crystallite size by means of x-rays showed that, in samples A and B, the number of grain boundaries in series between the electrodes was of the order of 10.

§ 6. D.C. Measurements and the Variation of Electrical Properties with Temperature

The d.c. resistances of the polycrystalline specimens were so high that reliable measurements of them could not be made without the use of guard-ring electrodes. It was found possible to deposit suitable silver electrodes on sample B by vacuum evaporation and the results of d.c. measurements at room temperature are shown in fig. 8. The corresponding resistance per unit area for small applied voltages is about 2×10^{11} ohms, which is consistent with the upper limit for electronic conductivity deduced above.

Fig. 8

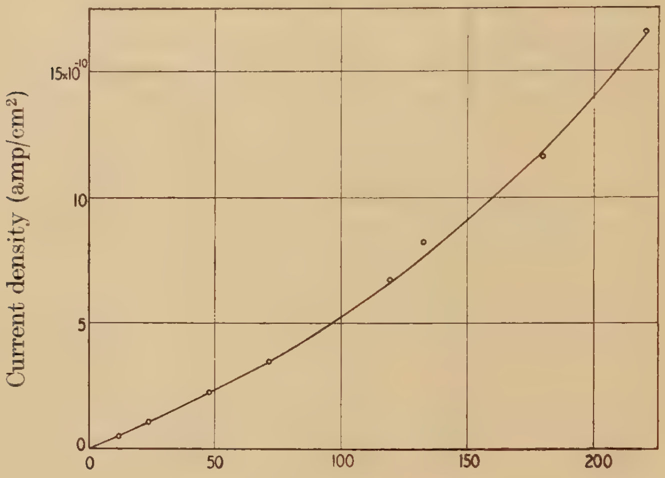

d.c. volt

Dark current/voltage curve for sample B.

Measurements were also made of the variation of the low-voltage d.c. resistivity ρ with temperature and a semi-log plot of the results is shown in fig. 9. From this it appears that the change of d.c. resistance is to be associated with an activation energy of about 0·5 ev, and it is reasonable to identify this with the height of the rectifying electronic barrier.

This height, V_D, is connected with the concentration n_1 of ionized donors within the electronic barrier and the width λ of the barrier, by the well known expression

$$\lambda=[V_D\epsilon/2\pi n_1 e]^{1/2}. \qquad (13)$$

Taking for λ the value $10^{-2}/S$ cm found previously, this gives

$$n_1 \doteqdot 2\times10^{11}S^2/\text{cm}^3. \qquad (14)$$

Comparison of eqns. (12) and (14) shows that it would not be inconsistent to identify the ionized donors with the mobile interstitial ions. However, there is no reason why n_0 and n_1 should be equal, since some of the donors may be immobile. Furthermore, if the distribution of donors is not uniform, their concentration in the ionic barrier may differ from the mean value throughout the electronic barrier.

Since the electronic barrier region occupies an appreciable part of the total volume of the specimen, it is reasonable to take n_1 as the concentration of free electrons in the bulk of the material. The bulk conductivity σ_∞ will then be given by

$$\sigma_\infty = n_1 e u \quad . \quad . \quad . \quad . \quad . \quad . \quad . \quad . \quad . \quad . \quad . \quad (15)$$

where u is the electronic mobility. Taking 10^{-6} (ohm cm)$^{-1}$ for σ_∞, this gives

$$u = 30/S^2 \text{ cm/sec per v/cm.} \quad . \quad . \quad . \quad . \quad . \quad . \quad . \quad . \quad (16)$$

This is a reasonable value if S is equal to unity, but rather low if S is of the order of 10.

Fig. 9

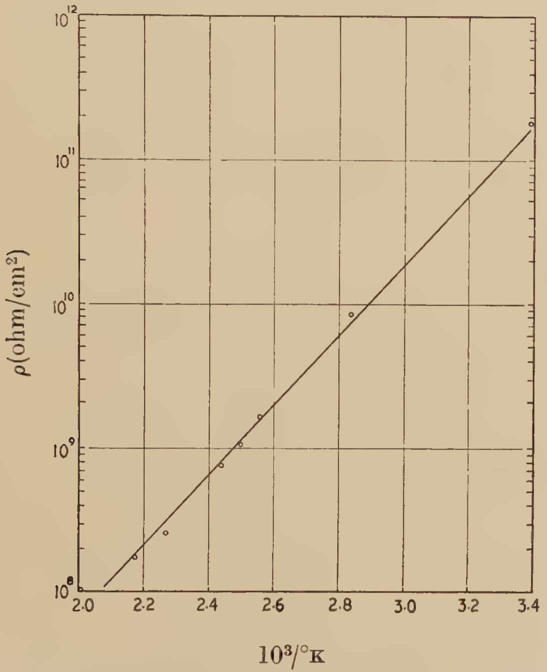

Temperature variation of d.c. resistance for sample B.

From the diffusion theory of rectification at an electronic barrier, the limiting value ρ_∞ for the resistance per unit area in the reverse direction with large applied voltage should be given by

$$1/\rho_\infty = (n_1 e u/\lambda) \exp(-e V_D/\kappa T). \quad . \quad . \quad . \quad . \quad . \quad . \quad (17)$$

Inserting the values already found for u, n_1, λ and V_D, this gives

$$\rho_\infty = 10^{13} \Omega/\text{cm}^2. \quad . \quad . \quad . \quad . \quad . \quad . \quad . \quad . \quad . \quad (18)$$

This is about one hundred times as great as the measured value, but such discrepancies are commonly found in investigations on rectifiers and have been attributed to field-emission of electrons from the metal into the semiconductor. In any case, bearing in mind the approximate nature of our calculations, the discrepancy is not serious.

Measurements have also been made of the variation of a.c. impedance with temperature for sample A and from these, using the equivalent circuit of fig. 7, the variation of C_b with temperature has been calculated. This time the semi-log plot, shown in fig. 10, leads to an effective activation energy of 0·15 ev. According to eqn. (7) C_b is proportional to $\sigma/\sqrt{D}$ and both σ and D may be expected to vary with temperature. If the number of interstitial carriers is assumed to be constant, σ will change only because the mobility v changes and, since v is proportional to D, (eqn. 10), C_b should then be proportional to $\sqrt{D}$. In this case the activation energy found from fig. 10 will be half the height of the potential hill to be surmounted by an interstitial ion in going from one position to an adjacent one, viz. 0·30 ev. If d is the distance between these two positions and ν the frequency with which the ion can vibrate, D should be given as to order of magnitude (Mott and Gurney 1940) by

Fig. 10

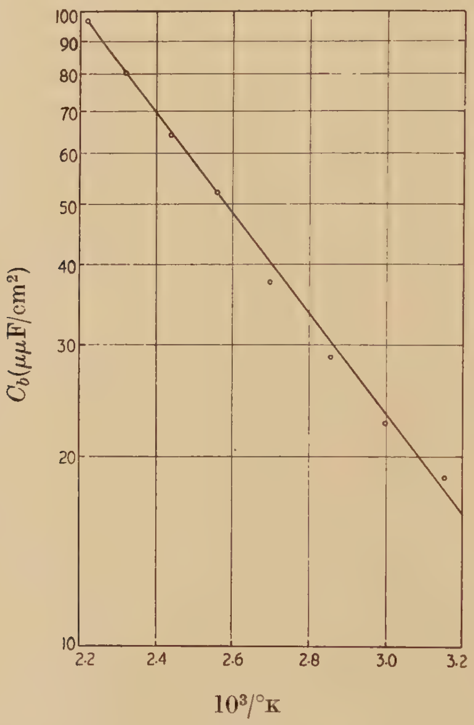

Temperature dependence of barrier capacity (sample A).

$$D = d^2\nu \exp(-U/\kappa T) \quad . \quad . \quad . \quad . \quad . \quad . \quad . \quad . \quad (19)$$

where U is the height of the potential hill. Putting $\nu = 10^{13}$ and $d^2 = 10^{-15}$ cm², we find for the order of magnitude of D the value 10^{-7} cm²/sec, which is consistent with the value given by eqn. (9).

Fig. 11

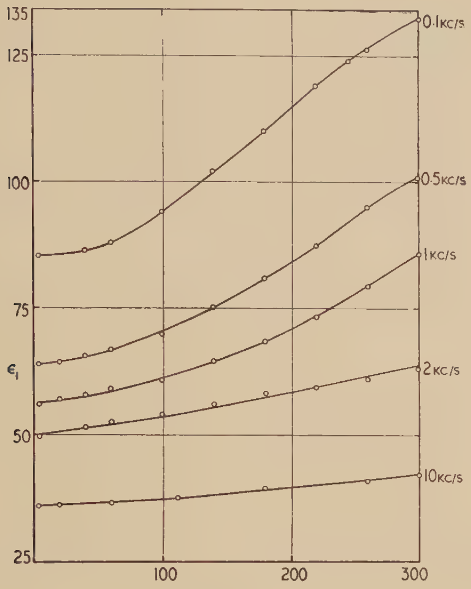

(*a*)

a.c. volt

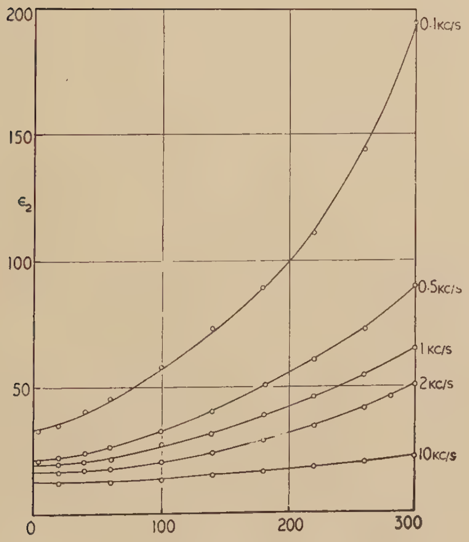

(*b*)

a.c. volt

Dependence of complex permittivity on applied voltage. (Sample A in the dark.)

§ 7. Non-Linear Effects

It has previously been reported that the electrical behaviour of an electroluminescent powder is a function of the strength of the electric field applied to it and, in the present experiments, an investigation of these non-linear effects was carried out. As before the results were found to depend on whether the specimen was kept in the dark or irradiated with ultra-violet light, and in figs. 11 (*a*), 11 (*b*) and 12 are curves showing the variation of ϵ_1 and ϵ_2 in the two cases for sample A. Since it has already been shown that two quite separate mechanisms are involved, it is legitimate to subtract the ‘ dark ’ from the ‘ light ’ values to give the curves of fig. 13 for the mechanism which depends on stimulation by ultra-violet light.

Fig. 12

- - - in dark —— with u.v. excitation, frequency=1000 c/s

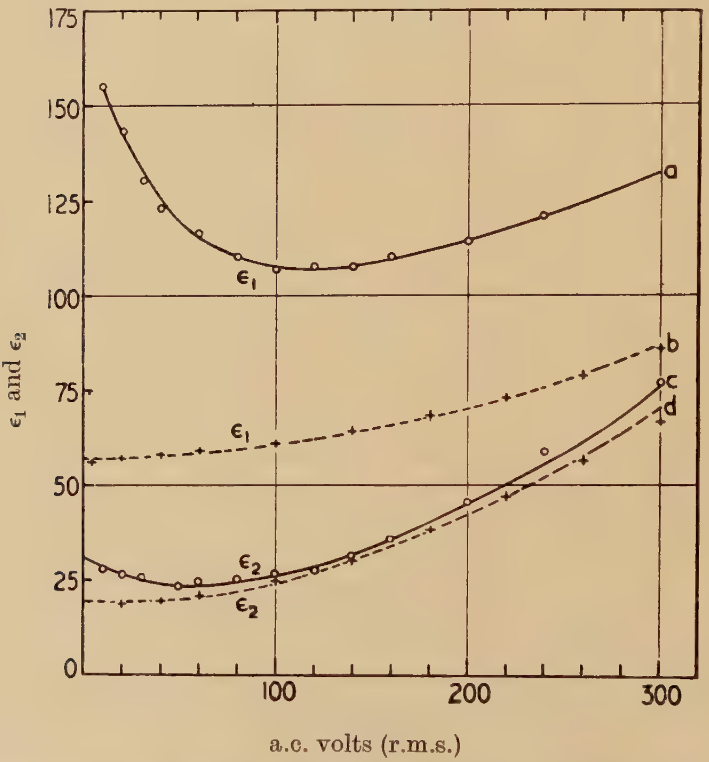

Variation of complex permittivity with applied voltage (sample A).

Curves very similar to those of fig. 13 have been obtained with certain ordinary phosphors, which are not electroluminescent, when these were irradiated with ultra-violet light. There is no reason to suppose, therefore, that this part of the non-linearity is connected with electroluminescence and it will only be discussed briefly in the present paper.

It has been shown in § 4 that the mechanism brought into play by light-stimulation conforms to the Debye equations. A model which is often invoked in such cases is one in which dipoles (or single charges) in the solid have two or more positions of equilibrium separated by potential hills. The discussion of this model (Fröhlich 1949) usually assumes that $E\mu \ll \kappa T$, where μ is the dipole moment and E the applied field, but if this is not the case it can be shown that, to a second approximation,

$$\epsilon_1=\epsilon_\infty+\frac{\epsilon_s-\epsilon_\infty}{1+\tau^2\omega^2}\left(1+\frac{\mu^2E^2}{4\kappa^2T^2}\frac{\tau^2\omega^2-1}{\tau^2\omega^2+1}\right), \quad \ldots \quad (20)$$

$$\epsilon_2=\frac{(\epsilon_s-\epsilon_\infty)\tau\omega}{1+\tau^2\omega^2}\left(1+\frac{\mu^2E^2}{4\kappa^2T^2}\frac{\tau^2\omega^2-3}{\tau^2\omega^2+1}\right). \quad \ldots \quad (21)$$

If $E\mu$ is comparable with κT, still higher terms will become important.

Fig. 13

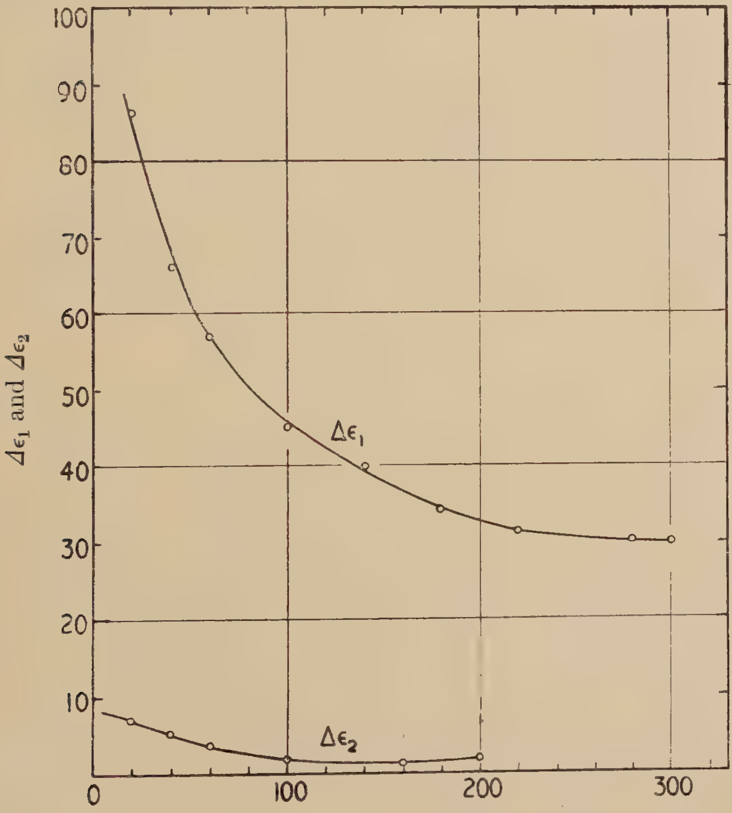

a.c. volt (r.m.s.)

Result of subtracting the ' dark ' from the ' light ' values in fig. 12.

The curves of fig. 13 were taken at a frequency of 1 kc/s, for which $\omega\tau \ll 1$, so eqns. (20) and (21) predict that both ϵ_1 and ϵ_2 should decrease with increasing field-strength, in agreement with the experimental results.

A more stringent test of the equations would be to see whether the non-linearity changes sign at sufficiently high frequencies. This was not possible with the existing apparatus since the Q-meter with which the high-frequency measurements were made did not provide a sufficiently high field-strength. The matter is therefore left for further investigation at a later date.

Returning now to the curves of figs. 11 (*a*) and (*b*), consider the effect of applying relatively large alternating voltages to the specimen in the light of the mechanism which has been invoked to explain the low-frequency dispersion in the dark. In the theory leading up to eqn. (6) it was assumed that the conductivity σ of the high-resistance layer is a constant. However, this will no longer be true if the change in concentration of carriers in the barrier region, brought about by the alternating field, is an appreciable fraction of the initial concentration n_0. Thus, with sufficiently strong fields, σ in eqn. (6) will vary throughout the cycle and the barrier impedance will become non-linear. An analytical solution in this case would be extremely complicated and will not be attempted. It is to be noted, however, that changes in σ are in step with changes in n so that we might expect the variations of n to be larger than they would have been if σ had remained constant. This implies that C_b should increase with increasing applied voltage while R_b should decrease, as is found to be the case. In this context C_b and R_b are mean values averaged throughout the cycle. Furthermore, eqn. (6) shows that the variations of n are inversely proportional to $\sqrt{\omega}$ so it might be expected that the non-linearity of C_b and R_b (measured by changes from the small-signal values) would vary with frequency in

Fig. 14

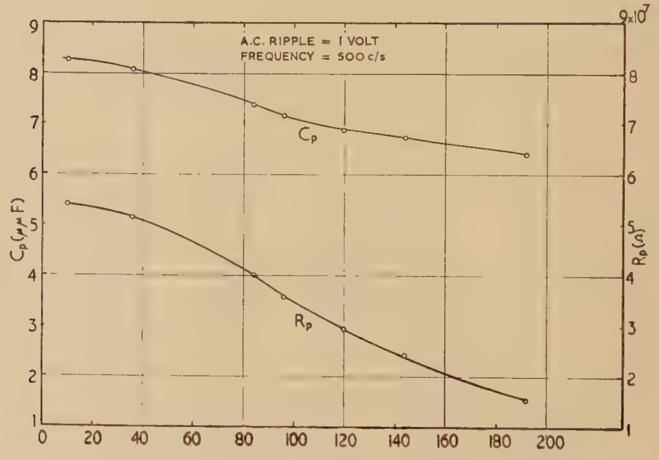

d.c. bias (volt)

Variation of equivalent parallel resistance and capacitance with d.c. bias. (Sample A in the dark.)

roughly the same manner. The experimental curves of fig. 11 show that this is the case.

Substituting in eqn. (6) the value of $\sigma/\sqrt{D}$ previously deduced, it is easy to show that the variation of ionic concentration throughout the cycle at, say, 100 c/s will be comparable with the mean concentration when the voltage applied to specimen A is a few tens of volts. Under these conditions non-linearity would be expected and is, in fact, observed.

So far, only variations of C_b and R_b have been considered, but C_a also will depend on the applied voltage. The width of the electronic barrier is governed by space charge, so λ will increase and C_a will decrease with increase in applied voltage. The changes in C_a will thus be in the opposite direction to those in C_b and to those observed experimentally. It must be assumed therefore that changes in C_b predominate. The fact that electronic barriers alone would lead to a variation of capacitance with applied voltage of the wrong sign, provides additional evidence for the existence of effects caused by mobile ions.

Measurements have been made of the impedance of sample A using a small alternating voltage of about 1 v superimposed upon a d.c. bias which could be varied over a wide range. Some results of such measurements are shown in fig. 14, but this case has proved very intractable from a theoretical point of view. It can easily be shown that when sufficient bias is applied to produce an appreciable change of impedance, ionic space-charge must be of great importance. Under these circumstances eqn. (6) is no longer valid.

§ 8. CONCLUSIONS

A great many measurements have been made on electroluminescent powders of various kinds and in all cases the results were qualitatively similar to those described above. In general the powders exhibited less marked dispersion than the polycrystalline specimens, but the two separate regions of dispersion were nevertheless present. It has been shown that the high-frequency dispersion is very similar to that which occurs in phosphors which are not electroluminescent (Garlick 1949), though the relaxation time is usually about one-tenth as long in these latter cases. This difference may or may not be significant.

The low-frequency dispersion has not been reported in phosphors which are not electroluminescent and it is therefore natural to attempt to correlate it with the phenomenon of electroluminescence. To explain this phenomenon other investigators have invoked the presence of rectifying electronic barriers (Zalm *et al.* 1954, Piper and William 1954) and such barriers form an essential feature of the model which has been put forward to account for the present results. By themselves, however, they cannot readily be used to explain the observed low-frequency dispersion and we have therefore been led to postulate the existence of mobile ions which cannot pass to the electrodes. The resulting model is selfconsistent and provides a satisfactory explanation of a variety of experimental results.

Since electroluminescence is not quenched when a specimen is placed in a magnetic field of the order of 10^5 gauss (Ince 1954), it seems necessary to assume that electric fields present in certain parts of the phosphors are much greater than would be expected from the applied voltage and the thickness of the specimen. It is possible that the necessary inhomogeneity of field is brought about solely by the presence of electronic rectifying barriers. The width of these barriers has already been discussed and the voltage drop across them at any frequency can be calculated from the equivalent circuit of fig. 6 (*b*). It appears that the field within the barrier might be large enough to account for electroluminescence.

This leaves unanswered the question whether ionic mobility plays an important part in the phenomenon of electroluminescence. Evidence for the presence of mobile ions in electroluminescent phosphors has been given, but the effects ascribed to these ions would probably not have been observed if electronic barriers had not also been present to reduce the electronic conductivity to a very small value. For this reason ionic mobility may have escaped observation in phosphors which are not electroluminescent. Nevertheless, experiments such as those of Waymouth and Bitter (1954) in which an electroluminescent phosphor was subjected to pulsed fields, suggest that ionic mobility might provide an explanation of the very slow build-up and decay of light output which were there observed.

Acknowledgments

We are greatly indebted to the following organizations who were good enough to send us samples of electroluminescent phosphors: The G.E.C. Research Laboratories, Thorn Electrical Industries Ltd., Sylvania Electric Products Inc., and the General Electric Research Laboratory, Schenectady.

We wish to thank Miss P. J. Brown of the Crystallographic Department of the Cavendish Laboratory, who kindly carried out an x-ray examination of two of our samples.

We are also grateful to the Admiralty for a grant to cover the cost of equipment.

References

Butler, K. H., and Waymouth, J. F., 1954, *Brit. Jour. App. Phys.*, Supplement No. 4, 33.

Clark, H. A. M., and Vanderlyn, P. D., 1949, *Proc. Instn. Elec. Engrs.*, **96**, Pt. II, 365.

Cole, K. S., and Cole, R. H., 1941, *Jour. Chem. Phys.*, **9**, 341.

Destriau, G., 1936, *J. Chim. Phys.*, **33**, 587; 1947, *Phil. Mag.*, **38**, 700.

Fröhlich, H., 1949, *Theory of Dielectrics* (Oxford: University Press).

Garlick, G. F. J., 1949, *Luminescent Materials* (Oxford: University Press). p. 143.

Garlick, G. F. J., and Gibson, A. F., 1947, *Proc. Roy. Soc.* A, **188**, 485.

Ince, A. N., 1954, *Proc. Phys. Soc.* B, **67**, 870.

Jaffé, G., 1933, *Ann. Phys.*, **16,** 217 ; 1952, *Phys. Rev.*, **85,** 354.
Macdonald, R., 1953, *Phys. Rev.*, **92,** 4.
Mott, N. F., and Gurney, R. W., 1949, *Electronic Processes in Ionic Crystals* (Oxford : University Press), p. 33 and p. 51.
Oatley, C. W., and Yates, J. G., 1954, *Proc. Instn. Elec. Engrs.*, **101,** Pt. III, 91.
Piper, W. W., and William, F. E., 1954, *Brit. Jour. App. Phys.*, Supplement No. 4, p. 39.
Roberts, S., 1952, *J. Opt. Soc. Amer.*, **42,** 850 ; 1953, *Ibid.*, **43,** 590.
Volger, J., Stevels, J. M., and van Amerongen, C., 1953, *Philips Res. Rep.*, **8,** 452.
Waymouth, J. F., and Bitter, F., 1954, *Phys. Rev.*, **95,** 941.
Zalm, P., Diemer, G., and Klasens, H. A., 1954, *Philips Res. Rep.*, **9,** 81.

CXXII. *Ultrasonic Attenuation in Metals*

By A. B. PIPPARD
The Royal Society Mond Laboratory, Cambridge*

[Received June 6, 1955]

ABSTRACT

The attenuation of ultrasonic waves by conduction electrons is analysed in terms of the free-electron model of a metal. At such low frequencies that the electronic free path is smaller than the wavelength, the result obtained agrees with that found by other authors using simpler concepts, but this agreement breaks down when the free path becomes comparable with or larger than the wavelength. At very high frequencies the attenuation of longitudinal waves increases in proportion to the frequency without limit, while that of transverse waves tends to a constant value. The drop in attenuation observed when a metal becomes superconducting is shown to present quite serious problems of interpretation, and tentative suggestions are made as to possible explanations.

§ 1. INTRODUCTION

RECENT experiments by Bömmel (1954) and Mackinnon (1955) have revealed that ultrasonic waves propagated through pure metals suffer an attenuation which increases at the lowest temperatures towards a maximum at the absolute zero. If the metal becomes superconducting the attenuation falls sharply, but apparently not discontinuously, below the transition temperature. The effect in normal metals has been discussed along similar lines by Mason (1955), Morse (1955) and Kittel (1955), the first two in particular giving a numerical analysis of Bömmel's results for lead and tin which shows that the explanation advanced by these authors is substantially correct. If the electrons in the metal are regarded as a degenerate Fermi gas enclosed in a box which is subjected to periodic distortion, then in the absence of collisions the Fermi surface will be adiabatically distorted, a spherical surface for example becoming ellipsoidal. Collisions of the electrons with the ionic lattice tend to restore the surface to its spherical shape, but the process is never complete, particularly if the relaxation time is long. In consequence the total electronic energy is on the average somewhat greater than its equilibrium value, and there is a steady dissipation of mechanical energy as heat through the influence of collisions. The rise of attenuation with lowering

---

* Communicated by the Author.

temperature is then readily interpreted as due to an increase of relaxation time, as is directly indicated by the behaviour of the electrical resistance.

This view of the process, though it leads to the correct answer at sufficiently low frequencies, is nevertheless deficient in some respects. In the first place it suggests that the attenuation should vary quadratically with frequency up to such frequencies that $\omega\tau$ is comparable with unity, ω being the angular frequency and τ the relaxation time of the electrons. However, as was pointed out to the author by Dr. Morse in conversation, on account of the Fermi velocity being much greater (by a factor of about 300 in most metals) than the velocity of sound, long before $\omega\tau$ reaches unity, the electronic free path has become comparable with the wavelength of the sound wave, and it is then no longer permissible to isolate for consideration a portion of the metal small in comparison with the wavelength. Secondly, the assumption that deformation of the ionic lattice leads automatically to a change in the distribution function of the electrons, as if they were enclosed in a box, does not accord with the true situation. In reality it is the combined effect of collisions and electric fields which brings about this change. The principal object of this paper is to give a solution of the problem which takes these points into account, for the ideal case when the electrons form a free degenerate gas with spherical Fermi surface. It will then be possible to see more clearly what problems are raised by the behaviour of superconductors, and suggestions will be made as to the nature of the new mechanisms operating under these circumstances.

§ 2. LONGITUDINAL WAVES

Consider an infinite block of metal carrying a plane longitudinal wave in the z-direction, of frequency ω and wavenumber k. All variables associated with the wave may then be understood to be multiplied by $\exp\{i(\omega t-kz)\}$, so that the differential operators take the form $\partial/\partial x=\partial/\partial y=0$, $\partial/\partial z=-ik$, $\partial/\partial t=i\omega$. The wave velocity v_s is of course ω/k. In the undistorted metal let there be N free electrons per unit volume, occupying all velocity states up to v_0, the Fermi velocity. During the passage of the wave, which may be characterized by a particle velocity u, the density of electrons will not necessarily remain constant but will have a periodic increment n. If the densities of electrons and ions do not keep exactly in step there will be space charges leading to a periodic electric field $\mathscr{E}$ in the z-direction. We now calculate what distortions the Fermi surface suffers as a consequence of the combined effects of $\mathscr{E}$ and of collisions. For this purpose we adopt the simple kinetic device of following a single electron having velocity v_0 through the lattice; as a result of $\mathscr{E}$ and collisions it acquires an additional velocity v_0' in the direction of its motion, and this value of v_0' is taken to give the displacement of the Fermi surface in this particular direction.

An electron moving with velocity v_0 at an angle θ to the z-direction experiences an electric field which oscillates at a frequency $\omega(1-v_0\cos\theta/v_s)$, and since in a field $\mathscr{E}$ its change of velocity is given by the equation $dv_0'/dt=e\mathscr{E}\cos\theta/m$, it follows that due to $\mathscr{E}$ alone, collisions being neglected,

$$i\omega[v_0']_{\mathscr{E}}(1-v_0\cos\theta/v_s)=e\mathscr{E}\cos\theta/m. \quad . \quad . \quad . \quad . \quad . \quad . \qquad (1)$$

To take account of collisions we assume that v_0' is continuously relaxing, with relaxation time τ, towards the value which it would have if the electron gas were locally in equilibrium. This equilibrium value of v_0' is not zero for two reasons: first because the local electronic density is $N+n$, not N, and secondly because the lattice is in motion with velocity u. The velocity distribution in local equilibrium thus corresponds to a Fermi sphere of radius $v_0(1+\frac{1}{3}n/N)$ onto which is superposed a uniform velocity u. And the local equilibrium value of v_0' is thus given by the equation

$$v_0'{}_{\mathrm{eq}}=\tfrac{1}{3}nv_0/N+u\cos\theta. \quad . \quad . \quad . \quad . \quad . \quad . \quad . \quad . \qquad (2)$$

We may therefore introduce the effect of collisions by writing

$$[dv_0'/dt]_{\mathrm{coll}}=i\omega[v_0']_{\mathrm{coll}}(1-v_0\cos\theta/v_s)=(\tfrac{1}{3}nv_0/N+u\cos\theta-v_0')/\tau. \quad . \qquad (3)$$

Hence, combining (1) and (3)

$$v_0'=[v_0']_{\mathscr{E}}+[v_0']_{\mathrm{coll}}=\frac{(e\mathscr{E}\tau/m+u)\cos\theta+\frac{1}{3}nv_0/N}{1+i\omega\tau-ikl\cos\theta} \quad . \quad . \quad . \qquad (4)$$

where l is the electronic mean free path, defined as $v_0\tau$.

From (4) which gives the displaced form of the Fermi surface, the electronic current density J_e may be immediately calculated, since

$$J_e=\tfrac{3}{2}Ne\int_0^{\pi}v_0'\sin\theta\cos\theta\,d\theta=\frac{3Nef}{akl}(e\mathscr{E}\tau/m+u)-\frac{nev_0f}{ikl} \quad . \quad . \qquad (5)$$

where a is written for $kl/(1+i\omega\tau)$ and

$$f=1-\tfrac{1}{2}\int_{-1}^{1}\frac{dx}{1-iax}. \quad . \quad . \quad . \quad . \quad . \quad . \quad . \quad . \quad . \qquad (6)$$

Now from J_e the value of n may be found, since according to the equation of continuity $J_e=nev_s$. Hence from (5) and (4)

$$J_e=\frac{3Nef}{akl}\,\frac{e\mathscr{E}\tau/m+u}{1+f/(i\omega\tau)}, \quad . \quad . \quad . \quad . \quad . \quad . \quad . \quad . \qquad (7)$$

and

$$v_0'=(e\mathscr{E}\tau/m+u)\frac{\cos\theta-f/[a(\omega\tau-if)]}{1+i\omega\tau-ikl\cos\theta}. \quad . \quad . \quad . \quad . \quad . \qquad (8)$$

For the purpose of calculating dissipative effects we are interested not so much in v_0' as in the difference, $\Delta v_0'$, between v_0' and the value $v_0'{}_{\mathrm{eq}}$ given by (2):

$$\Delta v_0'=(e\mathscr{E}\tau/m+u)\frac{(1-f)\cos\theta-if/a}{(1+i\omega\tau-ikl\cos\theta)[1+f/(i\omega\tau)]}-u\cos\theta. \quad . \qquad (9)$$

Thus the departure of the Fermi surface from local equilibrium is determined apart from the value of $\mathscr{E}$. Provided the frequency is much lower than the plasma frequency $\omega_p(=[4\pi Ne^2c^2/(m\epsilon)]^{1/2})$ the space charge needed to develop the required value of $\mathscr{E}$ is so small that no serious error results from assuming no space charge, i.e., putting $J_e = Neu$ ($-Neu$ is the lattice current density). Then $\mathscr{E}$ is found from (7), and (9) takes the form

$$\Delta v_0' = u\left\{\frac{a^2\cos\theta}{3f(1-ia\cos\theta)} - \tfrac{1}{3}ia - \cos\theta\right\}. \quad . \quad . \quad . \quad (10)$$

In general, however, if we do not assume $J_e = Neu$, but instead write the total current density as $J_e - Neu$ and relate it to $\mathscr{E}$ by means of the equation (in electromagnetic units)

$$J_e - Neu = -\frac{i\omega\epsilon}{4\pi c^2}.\mathscr{E},$$

then $\Delta v_0'$ takes the more complicated form

$$\Delta v_0' = u\left\{\frac{(i\omega\tau - \omega^2/\omega_p{}^2)[(1-f)\cos\theta - if/a]}{\{(3ifv_s/av_0) - \omega^2/\omega_p{}^2[1+(f/i\omega\tau)]\}(1+i\omega\tau - ikl\cos\theta)} - \cos\theta\right\}. \quad . \quad . \quad . \quad (11)$$

The simpler form (10) is recovered by neglecting the terms in (11) which contain $\omega^2/\omega_p{}^2$, and which are, in all practical applications to metals, many orders of magnitude smaller than the other terms. It is of interest to note, however, that the plasma terms appear in such a form as seems to allow no conditions under which they could contribute any marked effects, even if, as is perhaps possible in semiconductors, ω becomes comparable with ω_p. The discussion which follows will be based on (10).

Because of the departure from equilibrium represented by $\Delta v_0'$ in (10), there will be a continuous irreversible conversion of electronic energy into heat by collisions with the lattice. If the mean energy excess over that corresponding to local equilibrium is ΔE per unit volume, the rate of production of heat will be $2\Delta E/\tau$ per unit volume, the factor 2 arising from the definition of τ as the relaxation time for the velocity, while the energy excess is proportional to $|\Delta v_0'|^2$. In fact if u represents the peak amplitude of the particle velocity in the wave, at any part of the Fermi surface the displacement oscillates between $\pm|\Delta v_0'|$. If we consider an element dS of the Fermi surface, at the moment when the displacement is $+|\Delta v_0'|$, there are $3NdS|\Delta v_0'|/(4\pi v_0{}^3)$ electrons displaced above the equilibrium level, each with an average excess energy $\frac{1}{2}mv_0|\Delta v_0'|$, so that the excess energy of this group of electrons oscillates between zero and $3NmdS|\Delta v_0'|^2/(8\pi v_0{}^2)$, with a mean value $3NmdS|\Delta v_0'|^2/(16\pi v_0{}^2)$. Hence for the whole Fermi surface

$$\Delta E = \frac{3Nm}{16\pi v_0{}^2}\int_S |\Delta v_0'|^2\,dS = \frac{3Nm}{8}\int_0^\pi |\Delta v_0'|^2 \sin\theta\,d\theta,$$

and the mean rate of heat production per unit volume

$$Q = \frac{3Nm}{4\tau}\int_0^\pi |\Delta v_0'|^2 \sin\theta\,d\theta. \quad . \quad . \quad . \quad . \quad . \quad . \quad . \quad (12)$$

In general a and f are complex, and the evaluation of $|\Delta v_0'|^2$ from (10) is very tedious. But in the interesting range of frequencies for which a

is not too much greater than unity, so that $\omega\tau$ is still much less than unity, it is sufficiently accurate to take a as equal to kl, when f becomes real and equal to $1-\tan^{-1}a/a$. Then after some reduction (12) takes the form

$$Q=\frac{Nmu^2}{2\tau}\left(\frac{1}{3}\frac{k^2l^2\tan^{-1}kl}{kl-\tan^{-1}kl}-1\right). \quad . \quad . \quad . \quad . \quad . \quad . \quad (13)$$

A more searching analysis of $|\Delta v_0'|^2$ shows in fact that (13) is a very good approximation even when $\omega\tau$ is not negligible, and may be taken to apply at all frequencies.

The attenuation constant of the wave may now be written down immediately, since α, the attenuation of energy per unit length, is given by $2\,Q/(v_s\rho u^2)$, ρ being the density of the metal.

Thus

$$\alpha=\frac{Nm}{\rho v_s\tau}\left(\frac{1}{3}\frac{k^2l^2\tan^{-1}kl}{kl-\tan^{-1}kl}-1\right). \quad . \quad . \quad . \quad . \quad . \quad . \quad (14)$$

At low frequencies, for which the mean free path is much smaller than the wavelength, that is $kl\ll 1$,

$$\alpha=\frac{4Nmv_0^2\omega\tau}{15\rho v_s^3}\left(1-\frac{9}{35}(kl)^2+\frac{23}{175}(kl)^4-\ldots\right). \quad . \quad . \quad (15)$$

As the frequency is raised so that kl exceeds unity, the law of attenuation approaches the limiting form

$$\alpha\approx\frac{\pi Nmv_0\omega}{6\rho v_s^2}. \quad . \quad . \quad . \quad . \quad . \quad . \quad . \quad . \quad . \quad . \quad (16)$$

The leading term of (15) is the same as is obtained by the simple treatments of Mason and Morse, which neglect free path effects. Morse's analysis suggests that the attenuation continues to rise as ω^2 until such a frequency as makes $\omega\tau$ comparable with unity, when it flattens off to the constant value of $4Nmv_0^2\,(15\rho v_s^3\tau)$. The present analysis shows however that at the much lower frequency at which $kl\doteqdot 1$ the attenuation becomes proportional to ω and independent of τ. It is perhaps worth remarking that this behaviour is reminiscent of the anomalous skin effect (Pippard 1947, Reuter and Sondheimer 1948) which also becomes independent of τ when the mean free path is very long. Moreover, just as in the latter phenomenon most of the current is carried by a small group of electrons, so here, in ultrasonic propagation, when l is very long the deformation of the Fermi surface is mainly confined to the small region occupied by those electrons whose velocity component along the direction of wave propagation is equal to the velocity of sound.

§ 3. TRANSVERSE WAVES

In transverse waves there are no density changes and hence no electric fields resulting from space charge. On the other hand it is possible that the lattice and electronic currents may not cancel one another, in which case magnetic fields will be generated, and from these electric fields by induction. If the transverse wave is propagated in the z-direction, with a particle velocity u in the y-direction, the magnetic field will lie along the x-direction and the electric field along the y-direction. If the electronic current (in the y-direction) is J_e, then according to Maxwell's equations

$$\partial^2\mathscr{E}/\partial z^2 = -k^2\mathscr{E} = 4\pi i\omega J = 4\pi i\omega(J_e - Neu). \quad . \quad . \quad . \quad . \quad (17)$$

The analysis of the deformation of the Fermi surface proceeds exactly as before, leading to the result that for an electron moving at an angle θ to the z-direction and at an azimuthal angle ϕ,

$$v_0' = \frac{e\mathscr{E}\tau/m + u}{1 + i\omega\tau - ikl\cos\theta}\sin\theta\cos\phi. \quad . \quad . \quad . \quad . \quad (18)$$

The value of v_0' corresponding to local equilibrium, that is, a uniform translation with velocity u, is $u\sin\theta\cos\phi$. The electronic current density is found from (18) by integration over the Fermi sphere,

$$J_e = Neg(e\mathscr{E}\tau/m + u), \text{ where } g = \tfrac{3}{2}(1 - f/a^2 - f), \quad . \quad . \quad (19)$$

and f and a have the same significance as before. Hence from (17), (18) and (19)

$$v_0' = \frac{(k_0^2 + k^2)/(gk_0^2 + k^2)u\sin\theta\cos\phi}{1 + i\omega\tau - ikl\cos\theta}, \quad . \quad . \quad . \quad . \quad (20)$$

and
$$\Delta v_0' = \left\{\frac{k_0^2 + k^2}{(gk_0^2 + k^2)(1 + i\omega\tau - ikl\cos\theta)} - 1\right\} u\sin\theta\cos\phi, \quad . \quad (21)$$

in which $k_0^2 = 4\pi i\omega Ne^2\tau/m = 4\pi i\omega\sigma$, σ being the conductivity.

The detailed behaviour of $\Delta v_0'$ is seen to depend on the relative magnitudes of k and k_0, that is of the sound wavelength and the classical skin depth of electromagnetic waves of frequency ω. We shall not discuss all the cases that can arise, but confine our attention to that of most interest, in which l is long enough for kl to reach and exceed unity while k^2 is still much less than k_0^2. Then so long as k^2 is also much less than gk_0^2 we may write for $\Delta v_0'$

$$\Delta v_0' \doteq \left(\frac{1/g}{1 - ikl\cos\theta} - 1\right) u\sin\theta\cos\phi,$$

and, since g may be taken as real until such high frequencies that $\omega\tau \sim 1$,

$$|\Delta v_0'|^2 \doteq \frac{(1/g - 1)^2 + k^2l^2\cos^2\theta}{1 + k^2l^2\cos^2\theta} u^2\sin^2\theta\cos^2\phi. \quad . \quad . \quad (22)$$

The attenuation constant is now calculated exactly as before, yielding the result

$$\alpha = \frac{Nm}{\rho v_s'\tau} \cdot \frac{1 - g}{g}, \quad . \quad . \quad . \quad . \quad . \quad . \quad . \quad . \quad (23)$$

where $g = 3/(2k^2l^2)[(k^2l^2 + 1)/(kl)\tan^{-1}(kl) - 1]$ and v_s' is the velocity of transverse waves. When $kl \ll 1$, α may be expanded as a series,

$$\alpha = \frac{Nmv_0^2\omega^2\tau}{5\rho v_s'^3}\left(1 - \frac{8}{35}(kl)^2 + \frac{22}{175}(kl)^4 - \ldots\right). \quad . \quad . \quad (24)$$

As with longitudinal waves, the leading term in α is just what would be obtained by the simple relaxation theory, and comparison of (15) and (24) shows that the free path effect gives rise to very similar initial departures from this theory.

As kl attains values greater than unity, while $\omega\tau$ is still very small, g tends to the value $3\pi/(4kl)$, and α to the form

$$\alpha \approx \frac{4Nmv_0\omega}{3\pi\rho v_s'^2} \quad . \; . \; . \; . \; . \; . \; . \; . \; . \quad (25)$$

which is similar in form to the corresponding result (16) for longitudinal waves. However, as kl increases further it begins to be invalid to neglect k^2 in comparison with gk_0^2 in (21). The critical frequency at which $|gk_0^2|$ equals k^2 is given by $(3\pi^2 v_s'^3 \sigma/l)^{1/2}$, which is independent of the value of τ and equal to about 10^9 c/s for most metals. At about this frequency α begins to fall and eventually becomes independent of frequency. This last stage occurs either when k_0^2 becomes much smaller than k^2, so that the skin depth exceeds the wavelength, or when $\omega\tau$ becomes much greater than unity. Under either circumstance the electric field falls to a low value and the electrons are not appreciably affected by the passage of the wave, except for a small group, having $v_0 \cos\theta = v_s'$, which move with the wave and acquire a drift velocity u in the y-direction. This group, however, in contradistinction to its importance at lower frequencies and in longitudinal waves, now plays a quite negligible role. The limiting form of α at the highest frequencies is given by the expression

$$\alpha = \frac{Nm}{\rho v_s' \tau} \quad . \; . \; . \; . \; . \; . \; . \; . \; . \quad (26)$$

being independent of frequency and inversely proportional to the relaxation time.

§ 4. APPLICATION TO REAL METALS

There is no need to repeat here the comparison which Mason and Morse have made between their theories and Bömmel's experimental results, since the experiments refer to a regime in which kl is somewhat less than unity, and there is no significant difference between the results of the simpler theories and those obtained here. The satisfactory nature of the agreement obtained shows that the free-electron model gives a good semi-quantitative account of the real situation. If the electron gas is not free, but has band structure, the analysis given here corresponds, as Kittel's (1955) analysis shows, to transfer of electrons from one part to another of the same Brillouin zone. It should be remembered, however, that if the electrons occupy more than one zone, the energy levels in two zones may be differently affected by uniform compression, and in the passage of longitudinal waves there may occur a periodic transfer of electrons between zones, with a relaxation time perhaps quite different from that used here. This effect would not occur with transverse waves, so that studies of the attenuation of both types of wave in the same specimen would enable it to be detected. From a formal point of view this effect may be described as a second viscosity of the electron gas, leading to an imaginary term in the bulk modulus. The possibility of second viscosity is considered by Mason, who concludes from Bömmel's measurements that it is much smaller than the first viscosity, the effect which we have analysed at length here.

It is of interest to consider the attenuation to be expected at very high frequencies, of the order of 10^{11} c/s or more, such as occur in the thermal excitations of the ionic lattice. Transverse waves will not be highly attenuated, since the conditions will be such that (26) applies, but the attenuation of longitudinal waves will be considerable, as described by (16). There seems to be no reason why $1/\alpha$ should not be regarded as defining a mean free path for phonons, provided the phonon wavelength is large enough for the model used to be valid. Putting in reasonable values of the parameters, and taking ω equal to 5×10^{11} (corresponding to a temperature $\hbar\omega/k$ equal to 3°K), we find that the effective free path $1/\alpha$ is about 2×10^{-3} cm. This is of the same order of magnitude as the free path calculated by the quantum theory of electron-phonon interactions, and indeed what we have analysed here is the classical analogue of one of the principal scattering mechanisms, the interaction between electrons and the periodic potential associated with a longitudinal phonon.

The magnitude of this potential may be simply derived from the electric field, since $ik\phi=\mathscr{E}$, and from (7) we have, putting $J_e=Neu$,

$$e\phi=\frac{mu}{ik\tau}\left\{\frac{akl}{3f}\left(1+\frac{f}{i\omega\tau}\right)-1\right\}. \qquad (27)$$

Now the equilibrium value of the Fermi velocity, and hence of the kinetic energy at the Fermi level, varies periodically with the wave, and so does the potential energy $e\phi$. The total energy varies with an amplitude $e\phi+mv_0^2u/(3v_s)$, which from (27) may be written in the form

$$\Delta E_{\text{tot}}=\frac{mv_0^2u}{3v_s}\cdot i\omega\tau\left\{\frac{1-1/f}{1+i\omega\tau}+\frac{3}{k^2l^2}\right\}. \qquad (28)$$

It may be seen from this expression that at all frequencies ΔE_{tot} is very much smaller than the kinetic energy variation $mv_0^2u/(3v_s)$; the field is always able to adjust itself to maintain the Fermi level practically constant.

§ 5. SUPERCONDUCTORS

Bömmel's and Mackinnon's observations that the attenuation falls rapidly as the temperature is lowered through the superconducting transition raises a number of interesting points. It might at first be regarded as a matter for some surprise that the behaviour is the same for both longitudinal and transverse waves, for in the former the acceleration of normal electrons is accomplished mainly by electric fields, while in the latter collisions are nearly sufficient to produce the required motion. If one is accustomed to think of a superconductor as a metal which cannot support an electric field it is not obvious that the transition to superconductivity should affect both wave types similarly. This difficulty is, however, readily resolved. It is true enough that in a uniform superconductor an electric field gives rise to a steadily increasing electric current, but in a non-uniform superconductor it is not simply the electric field which is the accelerating force, but the gradient of the chemical potential μ, of which the electrical potential is only one part. This may be seen by considering a thermoelectric circuit consisting of two different superconductors ; the known absence of a thermoelectric potential difference leads immediately to the consequence that μ is constant over all parts of a superconductor in which current is not changing, even if it is not at a uniform temperature. Now, as has just been shown in § 4, the effect of the electric field in a longitudinal wave is to maintain the Fermi level, and hence μ, practically constant, so that there will be no tendency for any 'superconducting electrons' present to move in such a way as to eliminate the field. There is thus no significant difference between longitudinal and transverse waves in this respect, and the following discussion may conveniently be confined to the latter.

If the two-fluid model of a superconductor be accepted it is understandable that on passing the transition temperature the attenuation due to normal electrons should drop, since these become less in number as the superconducting electrons increase. Whether or not the latter give rise to additional attenuation is a question that cannot be resolved without a more detailed model, but if they do not, the most elementary view suggests that the observed drop in attenuation merely reflects the decrease in the number of normal electrons. Yet the rate of drop is very rapid, far more rapid than would be predicted by any existing model of the superconducting state (e.g., Gorter and Casimir 1934), from which a decrease roughly as T^4 might be expected. For this reason Morse (1955) suggested that the normal electrons are more tightly coupled to the lattice in the superconducting state, that is, there is a decrease in free path as the temperature is lowered past the transition. This explanation, however, cannot be accepted without question, since there is other evidence which appears to contradict it. For example, the thermal conductivity in tin does not begin to fall rapidly when the superconducting state is reached, as it would if there were a decrease in the free path ; indeed, in order to explain the temperature variation of thermal conductivity Heisenberg (1948) was led to suppose that the free path of normal electrons was actually greater in the superconducting than in the normal state. It seems necessary therefore to discover a mechanism which decreases the free path concerned in the attenuation of ultrasonics without decreasing that concerned in the conduction of heat. One can only speculate about what this mechanism may be, but at least it does not seem an impossible task if the additional coupling between the normal electrons and the ionic lattice is effected through the intermediary of the superconducting electrons.

Let us consider, for example, a probably unrealistic model of the superconducting state, in which the superconducting electrons, amounting to a fraction $(1-x)$ of the total number, occupy a sphere of about the same radius as the Fermi sphere, while the remaining fraction, x, of normal electrons occupy a similar sphere, so that the total density of states remains constant. Let us suppose the model has the following properties :

(*a*) The superconducting assembly, unlike the normal assembly, is incapable of thermal excitation. This is consistent with the absence of thermoelectric effects in superconductors.

(*b*) The superconducting assembly is tightly coupled with the lattice, so that when a transverse wave passes the sphere remains spherical, but acquires the local lattice velocity.

(*c*) The normal assembly interacts with the lattice in the same way, and with the same free path, as do the electrons in the normal state of the metal.

(*d*) The two assemblies interact strongly with one another. It is not unreasonable to postulate this since it is known (e.g., Pippard 1951) that the width of the transition region between normal and superconducting phases may be much smaller than the free path.

First let us neglect the interaction (*d*). Then at not too high ultrasonic frequencies both normal and superconducting assemblies will drift with the transverse displacements so that only a very small net current is set up by the wave. But while the superconducting assembly remains spherical, the normal assembly will be deformed in a manner similar to that expressed by eqn. (21). This will lead to a similar dissipation of energy as heat in the same way as in the normal metal, but reduced by a factor x. There will, however, be a second consequence—at different parts of the Fermi surface there will be a different energy gap between the ‘ Fermi levels ’ of the two assemblies. Since the magnitude of this gap is determined by the processes leading to the superconducting condensation and is not arbitrary, it seems likely that the interaction (*d*) will lead to a sharing of momentum between the two assemblies so that to a good approximation the gap stays constant at all points, and each surface has the same deformation from spherical form. In order that momentum may be locally conserved at all points of the Fermi surface, the effect of the interaction will be to reduce the deformation of the normal assembly by a factor x. Since therefore the attenuation of the sound wave is proportional to the number of normal electrons and to the square of the deformation we may expect α to vary as x^3 ; according to the Gorter–Casimir theory x varies as T^4, so that α may vary as T^{12}. This rapid variation is roughly what is needed to account for the observations, although the data published are not sufficiently detailed for any precise exponent to be fitted to them.

It should be noted that the interaction between the normal and superconducting assemblies need not alter in any way the thermal excitation of the former, since the latter is assumed incapable of excitation. Thus this process does not lead to a diminution of the free path which is applicable to problems of thermal conduction. It need hardly be remarked that the model developed above is not intended as a serious contribution towards a theory of superconductivity. It is introduced simply to point out the sort of problem raised by the experimental observations and to suggest the lines along which a solution might be possible. There may be other solutions along quite other lines, but it seems that the behaviour of ultrasonic attenuation in superconductors is not a trivial matter by any means, and that these new observations may contribute valuable evidence leading to a better understanding of superconductivity in general.

ACKNOWLEDGMENTS

I should like to express my gratitude to Prof. R. W. Morse and Dr. J. M. Ziman for valuable discussions.

REFERENCES

BÖMMEL, H. E., 1954, *Phys. Rev.*, **96,** 220.
GORTER, C. J., and CASIMIR, H. B. G., 1934, *Phys. Z.*, **35,** 963.
HEISENBERG, W., 1948, *Two Lectures* (Cambridge : University Press).
KITTEL, C., 1955, *Acta Metall.*, **3,** 295.
MACKINNON, L., 1955, *Phys. Rev.*, **98,** 1181.
MASON, W. P., 1955, *Phys. Rev.*, **97,** 557.
MORSE, R. W., 1955, *Phys. Rev.*, **97,** 1716.
PIPPARD, A. B., 1947, *Proc. Roy. Soc.* A, **191,** 385; 1951, *Proc. Camb. Phil. Soc.*, **47,** 617.
REUTER, G. E. H., and SONDHEIMER, E. H., 1948, *Proc. Roy. Soc.* A, **195,** 336.

CXXIII. *Thermodynamics of a Sheared Superconductor*

By A. B. Pippard
The Royal Society Mond Laboratory, Cambridge*

[Received June 6, 1955]

Recent measurements by Olsen (1955) have shown that the rigidity modulus n differs in the normal and superconducting states of tin by an amount which varies with temperature approximately as $(1-T^4/T_c^{\,4})$, without a discontinuity at the transition temperature, T_c. This work was carried out by torsion measurements on polycrystalline samples, while Landauer (1955), working with single crystals of tin, found evidence for a discontinuity at T_c; otherwise the temperature variation was similar to that found by Olsen. In this note we give a simple thermodynamic treatment of the problem which provides an explanation of Olsen's result and reveals a difficulty in reconciling it with that of Landauer.

Let us consider unit volume of a single crystal specimen in the form of a rectangular or nearly rectangular parallelepiped, and take the edges of the specimen to be the xyz-axes. Let it be subjected to a uniform shear stress Σ applied along those faces which contain the z-axis, and let the corresponding shear strain be θ. Then it is readily shown by an extension of the usual thermodynamic treatment of the phase transition in superconductors that the critical magnetic field H_c is determined by the equation

$$H_c^2/(8\pi)=G_n-G_s \quad . \quad . \quad . \quad . \quad . \quad . \quad . \quad . \quad . \quad (1)$$

in which G_n and G_s are the values in zero field, for the normal and superconducting states respectively, of the potential $U-TS-\Sigma\theta$ which has the property that $(\partial G/\partial \Sigma)_T=-\theta$. Hence, from (1),

$$\Delta\theta\equiv\theta_s-\theta_n=\frac{H_c}{4\pi}\left(\frac{\partial H_c}{\partial \Sigma}\right)_T . \quad . \quad . \quad . \quad . \quad . \quad . \quad . \quad (2)$$

The significance of this result is readily apparent. For a cubic crystal, or a crystal of lower symmetry cut so that the x- and y-axes are axes of crystal symmetry, positive and negative values of Σ are equivalent, so that $(\partial H_c/\partial \Sigma)_T=0$ and correspondingly $\theta_s=\theta_n$. But in general $(\partial H_c/\partial \Sigma)_T$ need not vanish, and the non-vanishing value of $\theta_s-\theta_n$ corresponds to a spontaneous shearing of the crystal at the phase transition, even in the absence of a shear stress. There is no need to assume a change in crystal symmetry; for example a spontaneous shearing could occur in a tetragonal crystal such as tin if the axial ratio were different in the superconducting and normal states. It is necessary in this case, however, that the tetrad axis shall not lie along any axis of the specimen, for then the specimen will only change the ratio of its sides without deformation of its angles.

---

* Communicated by the Author.

Differentiating (2) with respect to Σ we obtain an expression for the change in isothermal rigidity modulus $n(\equiv(\partial\Sigma/\partial\theta)_T)$ when the phase transition is initiated by a magnetic field,

$$\Delta n \equiv n_s - n_n \doteqdot -n^2\Delta\left(\frac{1}{n}\right) = -\frac{n^2}{4\pi}\left\{\left(\frac{\partial H_c}{\partial\Sigma}\right)^2_T + H_c\left(\frac{\partial^2 H_c}{\partial\Sigma^2}\right)_T\right\}. \quad . \quad (3)$$

It is here assumed, as is borne out in practice, that $\Delta n \ll n$. Under such conditions as those considered above, when $\Delta\theta=0$ for $\Sigma=0$, Δn takes the form $-(n^2H_c/4\pi)(\partial^2H_c/\partial\Sigma^2)_T$, and clearly vanishes at the transition temperature since there $H_c=0$. On the basis of simple assumptions Olsen's result may now be derived from this expression. These assumptions are that H_c varies parabolically with temperature and that the electronic specific heat is not appreciably altered by shearing. Then H_c takes the form $H_0(1-T^2/T_c^2)$ and H_0/T_c is independent of Σ. It follows from (3) that, since we are assuming $dH_0/d\Sigma=0$,

$$\Delta n = -\frac{n^2H_0}{4\pi}\frac{d^2H_0}{d\Sigma^2}(1-T^4/T_c^4), \quad . \quad . \quad . \quad . \quad . \quad (4)$$

in agreement with Olsen's results.

If, on the other hand, we do not assume $\Delta\theta$ to vanish when $\Sigma=0$, the first term in (3) also contributes to Δn. In particular as the transition temperature is approached Δn tends, not to zero, but to the value

$$(\Delta n)_{T_c} = \lim_{T\to T_c}\left\{-4\pi n^2\left(\frac{\Delta\theta}{H_c}\right)^2\right\}. \quad . \quad . \quad . \quad . \quad . \quad (5)$$

Consequently if $\Delta\theta$ rises, like H_c, linearly from zero as the temperature is reduced below T_c, there will be a discontinuity in Δn at the transition.

It might seem, at first sight, as if the explanation of the discrepancy between Landauer's and Olsen's measurements might be resolved by the use of these results, but in fact no such easy solution seems possible. For according to (5) $(\Delta n)_{T_c}$ is essentially negative, that is, the rigidity cannot increase when a metal becomes superconducting; if then there are any crystal orientations for which $(\Delta n)_{T_c}$ does not vanish these will show up when a polycrystalline sample is used, as in Olsen's experiments. The fact that Olsen observed no discontinuity in rigidity implies therefore that there are no orientations for which the discontinuity is very great, in other words the axial ratio in tin does not suffer significant change between the superconducting and normal states at any temperature. It is important to note that one cannot argue from the effective isotropy of a polycrystalline sample that $\Delta\theta$ in (2) vanishes and in consequence $(\Delta n)_{T_c}$ must also vanish; for it is invalid to apply the arguments given above to any but a monocrystalline specimen. This may be made clear by considering the composite specimen shown in the figure, consisting of two crystallites with their tetrad axes symmetrically disposed. Each crystallite may suffer a spontaneous deformation $\Delta\theta$ when the phase transition occurs in a field H_c, so that according to (5) there may be a discontinuity in n at the transition temperature. But the application of the same argument to the specimen as a whole would lead to the conclusion that $\Delta\theta$ was necessarily zero, and hence also $(\Delta n)_{T_c}$. The flaw in the latter argument lies in the assumption of a homogeneous sample. The composite specimen becomes thermodynamically inhomogeneous as soon as a stress is applied, since the stress tends to increase the value of H_c in one crystallite and decrease it in the other; thus no critical field is definable in the presence of a stress, and the thermodynamical treatment breaks down. The polycrystalline specimen is merely a more elaborate example of the same type of system, and one can see that the discontinuity in n must be calculated as the mean over all crystallites, and not found by applying a spurious thermodynamical argument to the specimen as a whole.

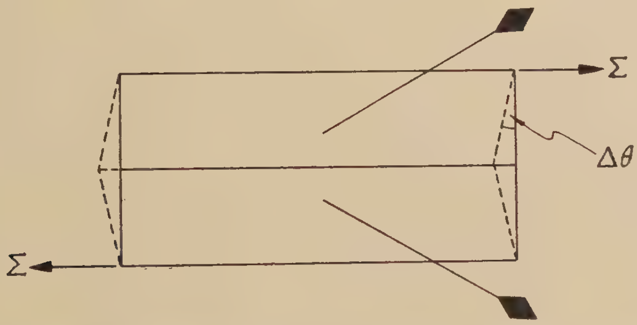

Composite specimen containing two crystallites, with tetrad axes along the directions indicated by the lozenges. The dotted lines show the effect of a spontaneous shearing at the phase transition.

For the same reason care must be exercized in considering a monocrystalline wire subjected to a torsional couple Γ and suffering thereby a twist ϕ. If Σ and θ in the above argument were replaced by Γ and ϕ it would immediately follow, if the argument were sound, that no discontinuity in the torsion constant could occur at the transition temperature, since at no temperature, when $\Gamma=0$, would the wire spontaneously twist when the phase transition was initiated by a magnetic field. The fallacy in such an argument is again that a twisted monocrystal is in general inhomogeneous, the critical field being raised on one side and lowered on the other exactly as in the example shown in the figure. By consideration of each element of the wire separately, however, it follows that $(\Delta n)_{T_c}$ does not necessarily vanish and that therefore a discontinuity in torsion constant may occur at the transition temperature, provided the crystal is not so oriented as to preclude a discontinuity in n for reasons of symmetry. Now in fact Landauer's experiments were performed with a crystal of tin having the tetrad axis very nearly perpendicular to the axis of the wire.

and this is one of the special orientations for which $(\Delta n)_{T_c}$ should vanish. This is because the shear stresses produced by twisting lie in planes which contain the tetrad axis. In order that a discontinuity in n shall be observed it is necessary to choose a crystal orientation such that the wire may spontaneously shear at the phase transition and not merely change its cross section, as with the orientation used by Landauer. It is, of course, possible that Landauer's observation of a discontinuity in n at T_c is due to the fact that the tetrad axis lay a few degrees off the normal to the wire axis. But if this is so it is to be expected that there are other orientations for which $(\Delta n)_{T_c}$ is even higher than that observed by Landauer, and it is then remarkable that Olsen found no discontinuity with a polycrystalline specimen. It seems more likely that Olsen's result is to be believed, that $(\Delta n)_{T_c}$ is small for all orientations of tin, and that Landauer's result arises from some instrumental error associated with the phase transition.

ACKNOWLEDGMENT

I should like to express my gratitude to Dr. D. Shoenberg, F.R.S., for several valuable discussions.

REFERENCES

GRASSMAN, P., and OLSEN, J. L., 1955, *Helv. Phys. Acta*, **28**, 24.
LANDAUER, J. K., 1954, *Phys. Rev.*, **96**, 296.
OLSEN, J. L., 1955, *Nature, Lond.*, **175**, 37.

CXXIV. *Formation of Etch Pits on Slip Lines in Aluminium*

By G. Wyon and J. M. Marchin
Centre de Recherches Metallurgiques de l'Ecole des Mines de Paris*

[Revised MS. received May 19, 1955]

Recent work suggests that it is possible to find a close relation between the location of etch pits and the points at which dislocations emerge through the surface of slightly deformed metallic or ionic crystals. Examples are experiments on 35% Zn brass (Jacquet 1954), on ionic crystals (Amelinckx 1953) and on pure single crystals of Zn (Abdou 1954).

In the course of the present work, it has become clear that in the particular case of Al, great care must be taken in the interpretation of etch pits formed by dipping specimens into acid. In previous publications (Wyon and Marchin 1954, Wyon and Lacombe 1954) it has been shown that for Al the presence of impurities on dislocations appears to be the cause of the localization of etch pits on grain boundaries and sub-boundaries and even of the etch pits distributed at random on crystals' surfaces. On the other hand the experiments of Amelinckx on etching of slip bands in Al seem to indicate that dislocations alone are responsible for the localization of etch pits on slip lines.

In order to verify this very important point, these experiments have been repeated and the following method has been used : refined aluminium samples (0·004% Fe and 0·005 Si) in sheets about 1 mm thick were recrystallized with large grains by annealing at 620°c for eight days. The samples were electro-polished in a cooled Jacquet bath (666 cm^3 of $(CH_3CO)_2O$ and 333 cm^3 ClO_4H) and subsequently slightly deformed in tension to produce some slip lines. In this condition, the sheets were immediately etched, first in fluorated aqua regia (Wyon 1953), then in a reagent derived from the preceding one and including a wetting agent which emphasizes the grain and sub-grain boundaries, and which also produces micro-etch pits (Wyon 1953). This etching was preceded by an electrolytical re-polish after the deformation in order to determine the part played by the dislocations locked on the slip planes inside the crystals. On the basis of these experiments, the following observations could be made.

Etching after Deformation without Repolishing

We have found that generally the slip lines apparent on the surface are only etched if the crystal has an orientation such that a (100) axis is approximately parallel to the surface. After etching, micro-etch pits appear with indefinite shapes as observed by Amelinckx (fig. 1 (figs. 1–3, Plate 23)). In certain very rare cases, there occur for grains with any orientation, true micro-etch pits along the slip bands (fig. 2). The distribution of etch pits along the slip bands can vary widely.

---

* Communicated by Professor P. Lacombe.

We have observed :

(*a*) compact local alignments of etch pits, as seen by Amelinckx (fig. 1),

(*b*) alignments similar to (*a*) but continuous along some slip lines (fig. 3),

(*c*) clearly marked micro-etch pits occur well separated from each other.

(*d*) micro-etch pits arranged in a broader and more diffuse cluster. overlapping in the region of crystal around the slip line.

Generally several slip lines remain unetched along their length. and the following remarks can be made.

1. When several slip planes are acting in the same grain :

(*a*) one system out of two, or two systems out of three may be etched (fig. 3) ; all active systems may be attached but not all the slip lines of a single system may show the same phenomenon,

(*b*) etch pits may or may not be observed at the ends of cross-slip lines.

2. When a slip line stops in front of a crystalline boundary, the micro-etch pits, when they occur, are spaced further and further apart while at the same time the line disappears (fig. 5 (figs. 4–6, Plate 24)). There is never a concentration of etch pits at the end of such slip lines.

3. At the point at which a slip line meets a grain boundary, the micro-etch pits on those lines which show them suddenly stop at the boundary. even if the lines cross the boundary (fig. 6). But not all the slip lines have micro-etch pits up to the grain boundary (fig. 6).

Etching on Surface Re-polished after Deformation

Figure 7 (figs. 7, 8, Plate 25) shows the appearance of an electrolytically polished specimen slightly deformed in order to develop some slip lines, then repolished in a Jacquet bath in order to smooth out any slips on the surface. The sample has also been etched and no alignment of etch pits is observed. A second deformation is then carried out, in order to show the direction of the active slip lines : these are the last formed slip lines seen on fig. 7. Starting with the idea that dislocations by themselves cannot (in the case of Al) be revealed individually by an acid, we attempted to reveal the slip lines obliterated by polishing. For this purpose an ageing treatment was applied after deformation to enable impurities to diffuse to dislocations. The samples were then polished and etched again. In the case of refined Al, it was never found possible to reveal the slip markings by this method. In fact the impurity content is very small. The impurities (generally iron) have a low mobility at the low ageing temperatures which one is obliged to use to prevent other effects, e.g. ' polygonization ', from occurring (15 days at 100° for instance). The experiment gave a positive result, however, with an alloy of Mn (0·56%) : fig. 8 shows the slip markings observed on a sample repolished and etched after the deformation and subsequent ageing treatment.

CONCLUSIONS

From the experiment described above it appears that dislocations alone are not sufficient to explain the localization of some etch-pits on the slip-lines of aluminium. If it were so, at least sometimes a concentration of etch-pits should be observed at the ends of the slip lines stopped at grain boundaries (Jacquet 1954). The etch pits should continue to be localized on the slip planes in the areas under the surface. On the other hand, the etch figures seem to occur only on the slip lines in crystals having a fairly particular orientation and even then some slip systems do not show these etch-pits. Nevertheless, the influence of some factors should not be disregarded, for instance the rupture of the surface oxide film at the slip lines or the 'microgeometric' factor caused by the undulations of the surface at these slip lines, can modify profoundly the local reactivity of the metal.

In the light of some previous results (Wyon and Lacombe 1954) and others to be published soon, it may be concluded that dislocations alone cannot modify the reactivity of Al with regard to the acid reagents sufficiently to give rise to etch-pits at the points of emergence of the dislocations. But in Al alloys with small amounts of the alloying element such as the above-mentioned Al 0·56% Mn, the Al 3% Mg alloy studied by Crussard and Aubertin (1951) and alloys of Zn (6–12%) (Berghezan 1952) it is possible to demonstrate without any doubt the alignment of etch-pits on slip-band markings, even in the areas of crystals lying under the surface. But this result is only obtained if the samples are aged after the deformation; this ageing treatment promoting without doubt the combination of dislocations with impurities which can be detected by etching. From this point of view, Jacquet's work on 65–35 brass also shows that impurities play their part in corrosion phenomena on the slip lines; the reagent used by Jacquet is unable to reveal dislocations in the case of fairly pure copper. For this purpose, it is necessary that the Zn-content is sufficiently high and close to the content at which the beta-brass phase appears.

It is known that in the copper lattice, the dislocations are easily split up into half-dislocations giving rise to 'stacking faults' (Heidenreich and Shockley 1948). Nevertheless these stacking faults alone do not cause dislocations to be revealed by etching with hyposulphite reagent. On the other hand, in the case of 65–35 brass, the presence of a high proportion of Zn atoms in the face-centred cubic matrix enables isolated dislocations to be revealed by etching.

All these experimental results show that the problem of revealing the dislocations by micrography in metallic lattices is rarely simple and that it is necessary to perfect etching reagents which are more and more sensitive, reproducible and selective.

REFERENCES

ABDOU, A. H., 1954, *Phil. Mag.*, **45**, 105.
AMELINCKX, S., 1953, *Phil. Mag.*, **44**, 1048; 1954, *Acta Met.*, **2**, 848.

Aubertin, F., and Crussard, C., 1951, *Congress of Venice.*

Berghezan, A., 1952, *Revue Met.*, **49**, 99.

Heidenreich, R. D., and Shockley, W., 1948, *Report on Strength of Solids* (London : Physical Society), p. 57.

Jacquet, P. A., 1954, *Acta Met.*, **2**, 752.

Lacombe, P., and Berghezan, A., 1949, *Alluminio*, 4.

Wyon, G., 1953, *Metaux et Corrosion*, **28**, 143.

Wyon, G., and Marchin, J. M., 1954, *C. R. Acad. Sciences, Paris*, **238**, 2420.

Wyon, G., and Lacombe, P., 1954, *Report of Conference on ' Defects in Crystalline Solids '* (London : Physical Society), p. 187.

CXXV. *Combination Spectra in Long-Period Variable Stars* *

By C. E. R. Bruce
The British Electrical and Allied Industries Research Association †

[Received in revised form July 27, 1955]

Summary

The electrical discharge theory of the variation in excitation observed in the atmospheres of the long-period variable stars offers an explanation for the combination spectra exhibited by many of these stars, which is in accord with several of the most outstanding changes in their spectra and magnitude.

§ 1. Introduction

In an earlier note (Bruce 1955 a) it was shown that the hypothesis of electrification due to freezing in low temperature stellar atmospheres would account for many of the phenomena observed in the spectra of the long-period variable stars. Subsequently it was suggested (Bruce 1955 b) that the simpler and better established phenomenon of electrification due to asymmetrical impacts will probably account satisfactorily for all the electrical phenomena observed in dust storms, volcanoes and terrestrial thunderstorms, as well as those already mentioned in the atmospheres of the long-period variable stars.

It is the purpose of the present report to suggest that the electrical discharge theory may account for the puzzling combination spectra observed in some of these stars. The states of excitation indicated by these spectra are so diverse that they have been, and often still are, believed always to have their origin in a binary star and an associated nebula. However, a consideration of the nature of the long electrical discharges, already postulated to account for the general characteristics of long-period variable stars, suggests that they may sometimes account for both the nebular spectrum, and for the spectrum which has hitherto been attributed to a companion star.

§ 2. Generation of Stellar Atmospheric Electric Fields

It is well known that asymmetrical interactions between pieces of the same material can lead to separation of electric charge (Shaw 1926); the two pieces of material carry away the complementary charges of opposite polarity. Impacts between particles of different sizes and shapes are an example of such asymmetrical interaction, and it is well known that electrification does result from such impacts (Shaw 1928). It is thus to be expected that the larger particles will on an average carry one charge and the smaller particles will carry the complementary charge of opposite polarity. When such impacts take place in a gravitational field, then extensive electric fields will be built up. In sand and dust storms and in the debris which is ejected from volcanoes, electric fields generated in this way can reach values which lead to electrical breakdown of air at atmospheric pressure, and to long electrical discharges.

---

* Based on E.R.A. Report, Reference Z/T 101.

† Communicated by the Author.

Though the electrification in terrestrial thunderstorms is often attributed to charge separation occurring in the freezing process itself, it would appear that the same process of electrification by asymmetrical impacts will account satisfactorily for the separation in that case also, as was indeed in effect suggested by Simpson and Scrase (1937), when they first showed that ice particles, rather than water drops, must be involved in the separation process. Shaw (1928) found that the electrification of cold dry ice particles seemed to be of the same order as that observed with sand particles in his experiments with particles blown by air blasts.

The same conclusion applies regarding the electrification processes in stellar atmospheres which have been invoked to account for the phenomena observed in the atmospheres of long-period variable stars (Bruce 1955 a), though the actual freezing out of solid particles from the atmosphere remains of fundamental importance. The particles involved will be the oxides, carbides, hybrides of the metals, as well as carbon and other materials, and ultimately the metals themselves, which freeze at temperatures from about 4000° K downwards. Electric fields will only be built up, however, when the electrical conductivity of the atmosphere with electric fields up to that required for breakdown, has fallen below the rate of charge separation due to impacts. The breakdown field in an atmosphere which is largely composed of hydrogen will be given approximately by (PX_0/T), in which P is the pressure in atmospheres, T the absolute temperature, and X_0 is the potential gradient required for breakdown in a uniform field at atmospheric pressure, i.e. it will be of the order of $(10^4P)/T$ volts per cm, where P is in atmospheres.

The rate of freezing and of charge generation will depend on the frequency of collisions between particles and will therefore probably increase with the square of the gas pressure, as well as with the gravitational force. Both will increase towards lower regions of the stellar atmosphere. The rate will also increase with the velocities of the particles. The breakdown field itself is proportional to the gas pressure, so that it is to be expected that the time required for the electric field to reach the breakdown value will vary inversely as the gravitational force and gas pressure and inversely too as the velocity of the particles or as some power of that velocity.

In terrestrial thunderclouds the time required for freezing and field generation is of the order of minutes or tens of minutes while the electrical status quo is reconstituted after the occurrence of a lightning flash in a few seconds. The values of the above three quantities are not known precisely in the atmospheres of the long-period variable stars. If we may assume that the pressure is of the order of 10^{-6} atmosphere, that gravity is of the order of 10^{-4} the value in the earth's atmosphere, and that the velocities involved are of the order of about 10^3 times those observed in thunderclouds, then the time required for the process of freezing and charge generation in the stellar atmosphere would be of the order of 10^4 to 10^7 times that required in a terrestrial thunderstorm according as the electrification process increases linearly with, or as the second power of the velocity. Taking the critical time required in a thundercloud as 10^2 seconds, the time required in the stellar atmosphere will be of the order of 10^6 to 10^9 seconds, in general agreement with the observed values for the periods of those stars of the order of 10^7 seconds.

§ 3. Characteristics of Long Electrical Discharges

In considering the effects which the extensive electrical discharges will have in the atmospheres of long-period variable stars it is necessary first to describe an important characteristic of long electrical discharges to which the writer first called attention in relation to the leader stroke of the lightning discharge (Bruce 1944). It had been generally believed (Loeb and Meek 1941) that, in order to produce electrical breakdown in a long gap, a field of the order of that required for breakdown in a homogeneous gap under the existing conditions of temperature and pressure had to exist throughout the whole gap, and remnants of this belief still are expressed (Loeb 1954). For air at atmospheric pressure this field is of the order of 10 000 volts/cm even with water drops present, and fields of the order of 3 500 volts/cm have actually been observed during aeroplane flights through thunderstorms.

However, when the field at one point rises to such a value as to give rise to corona currents reaching some critical value, a value such that the temperature of the gas reaches that required for adequate thermal ionization to carry the discharge, then the discharge becomes an electric arc (Bruce 1941). That portion of the channel already formed is thus no longer a column of corona-like discharge requiring for its maintenance a field of several thousand volts per cm, but one requiring a potential gradient of the order of only 10 volts/cm. The propagation of the leader stroke thus represents a partial short circuit of the pre-discharge field, and the discharge becomes, so to speak, self-propagating. It also causes an increase of the electric field concentration at its tip, over that which originally initiated the discharge, and transfers that field concentration into regions of the atmosphere in which the electric field was initially quite small. Thus if X volts/cm is the average value of the predischarge field throughout the length, l, in cm, traversed by the advancing tip of the leader stroke, and x volts/cm is the potential gradient required to maintain the column of thermally ionized arc discharge, then the tip will be at a potential relative to the surrounding atmosphere, which is greater by the amount $l\,(X-x)$ than the value at the initiation of the discharge.

The theory explained how breakdown could occur between thunderclouds and earth with average potential gradients of the order of only 100 volts per cm. Even with such an average predischarge field of 100 volts/cm, the difference in potential between the discharge tip and its surroundings builds up at the rate of about 100 volts/cm travelled. By the time the leader stroke travels the two kilometres or so to earth this potential difference has reached 20×16^6 volts, and potentials of half this value at least have been recorded on overhead transmission lines struck by lightning.

The large differences in potential between the channel and its surroundings have an important consequence (Bruce 1944), in that they cause corona currents to flow laterally from the leader stroke channel. These too are probably of astrophysical importance.

This thermal ionization, or arc, theory of the leader stroke has been verified experimentally by Komelkov (1947) in the case of the laboratory spark discharge, while the complete theory of thermally ionized column surrounded by lateral corona currents has been found by Pierce (1955) to account for the observations made at Cambridge on the electric field changes caused by the leader strokes of lightning flashes.

This property of long electrical discharges of concentrating pre-existing differences in potential across relatively small spaces, and of transferring these electric field concentrations into regions which were initially subject to only small electric stresses, is of considerable astrophysical importance. In very extensive atmospheres the result of the field concentration and transference will be enhanced when the discharge is propagated into regions of lower pressure, and also for the further reason that the thermal losses from the very extensive discharge channels become very small. In the small laboratory arc discharge, or the leader stroke of the lightning discharge, in which the current reaches hundreds, or in intense flashes possibly thousands of amperes, the temperature gradients are high (King 1954) and the thermal losses correspondingly large. Despite such relatively large losses the potential gradient required for its maintenance is as we have seen a very small fraction, of the order of 10^{-3}, of that required for the initiation of the discharge. In the very large stellar discharge channels of fairly uniform temperature and therefore very small lateral temperature gradients, the only losses will ultimately be those due to radiation, and the potential gradient required for their maintenance will be correspondingly small. The process of electric field concentration and transference will therefore be effected by the long electrical discharges which occur in these stellar atmospheres, even more pronouncedly than it is by the leader stroke of the lightning discharge.

§ 4. Duration of the Electrical Discharges

Though the breakdown field will be reached first at some region relatively low down in the stellar atmosphere, considerable fields will in the same interval have been reached throughout much of that atmosphere. The effect of the important characteristic of these long leader strokes discussed in the preceding section will be that, when once the discharge or discharges are started, they will be propagated throughout practically the whole stellar atmosphere. The velocity of propagation of such a discharge is not known accurately, but, since it depends on the product of the breakdown field and the mean free path (Schonland 1938), and since the former of these varies directly, and the latter inversely with pressure there is no reason to believe that this velocity will differ greatly from the value observed at atmospheric pressure, i.e. of the order of 10^7 cm/sec. Since the dimensions involved in these atmospheres are of the order of 10^{14} cm, the discharges will last for a period of the order of 10^7 sec or 100 days, in agreement with the times during which emission line spectra are observed in the long period variable stars.

§ 5. Combination Spectra

During the propagation of these long discharges the excitation of the matter in and around the discharge channel will not remain uniform. As a result of the intensification and projection outwards of the field-concentration caused by the discharge, discussed in § 3, and because the discharge is being propagated outwards into regions of lower gas pressure, the excitation of the gas is increased. The spectrum of the discharge will therefore change during the outburst from one of high temperature at relatively high pressure, to one of high excitation at low pressure, with forbidden lines entering as the very low pressures of the outer regions of the stellar atmosphere are reached. It is suggested that the theory will thus account for the combination spectra in such stars as R Aquarii, Z Andromedae, BF Cygni and AX Persei. In these the initial bright line spectrum comprising lines of H, He I, Fe II, Ti II and Si II gives place, after a period of the order of 100 days, to a spectrum of higher excitation, containing lines of He II, N III, C III, [O III], [Ne III] and [Fe III]. The nature of this latter ‘ nebular ’ spectrum with its forbidden lines will be seen to be in accord with the suggestion that it originates in regions of very low pressure, far out in the star's atmosphere, towards the completion of electrical neutralization.

The stars showing these spectral combinations and variations thus probably differ from ordinary long-period variables in degree rather than in kind. They are stars in which the atmosphere outside the photosphere is in a more advanced stage of development. The inner atmospheric pressure is higher and the atmosphere is radially more extensive. The discharges in the inner regions then give rise to the spectrum, which has normally been attributed to a small hot ‘ companion ’ star, while the later stages of the discharge yield the ‘ nebular ’ spectrum.

In a study of some of the better known of these combination-spectra stars—AX Persei, RW Hydrae, CI Cygni, and Z Andromedae—Merrill (1944) concludes that the “ maxima and minima of the forbidden lines occur about one-fifth of the period after the corresponding phases of the permitted lines ". The periods lie between about 650 and 900 days. The observed time intervals are thus in good agreement with the rough estimate given above for this interval, namely of the order of 100 days. The time intervals between the velocity-curves for the two sets of lines, between 120 and 200 days are also in agreement with this interval.

It may be pointed out that, though the belief that in all cases two stars and a nebula are required to explain the spectra is widespread, Merrill himself in his monograph (Merrill 1940) and papers has been careful to emphasize that in many cases, including R Aquarii itself, there is no positive evidence for the existence of the 'companion' star, as he has usually so written it, and that all might in fact come from one M-Type star and its atmosphere.

Thus on one occasion Merrill (1935) wrote that "the procedure (i.e. the 'analysis of the light curve of R Aquarii into two curves') has a hypothetical basis: that is to say, it assumes the existence of two light sources. It does not, however, postulate the exact character of the source of the companion spectrum. This source may be a separate companion star, itself variable in light, or possibly small areas of high temperature within the outer limits of the tenuous red variable".

Recently, regarding the same star, he wrote: "It is somewhat uncertain whether the bright lines . . . should be ascribed to the Me star or to the nebula. Perhaps the question is without meaning." (Merrill 1950.) Summing up his discussion of this type of star in his monograph, Merrill concluded that "it would be inadvisable at the moment to accept without reserve the hypothesis of actual duplicity for all combination spectra". (Merrill 1940, p. 105.)

§ 6. CHARACTERISTICS OF STARS WITH COMBINATION SPECTRA

6.1. *Relation between M-Type and 'Companion' Spectra*

Several characteristics of the variations of the light of these stars possessing 'combination' spectra are in accord with the proposed explanation of their origin, in addition to those already described.

Perhaps the most important is the relationship between the intensities of the M-type and 'companion' spectrum observed in R Aquarii by Merrill. He writes: "A remarkable fact is that during the years 1931–33, when the companion was especially bright, the Me variable had a succession of remarkably low maxima. Whether this was more than a coincidence cannot be ascertained until the physical nature of the companion and its relationship to the red variable are better understood." (Merrill 1940, p. 84.) On the present theory the relationship referred to in that quotation is more than a coincidence. It was emphasized in an earlier note (Bruce 1955 a) that the electrical discharge theory is in accord with the suggestion put forward by Merrill to account for the marked falling off in the magnitude of M-type stars at their minimum. He suggested that this abnormal decrease is due to the formation of a cloud of particles or drops in their atmospheres. The denser this cloud of particles becomes, the lower is the magnitude of the M-star at minimum, and the greater will be the effect of the processes of static electrification occurring during the minimum period. The average electric fields generated throughout the atmosphere, during this period will also be greater, and therefore the intensity of—or electric currents in—the ensuing electrical discharges will also be greater. It is therefore to be expected that abnormally low minima of the M-type star will be associated with the abnormal increases in the intensity of the electrical discharges and hence of the ' companion ' spectrum ; as was observed by Merrill in R Aquarii.

Furthermore, the existence of these variations in magnitude are in accord with the general electrical discharge theory of the cause of this type of stellar variation, just as earlier, when applied to the lightning discharge (Bruce 1944), the theory of the initiation and propagation of the leader stroke accounted for the very marked variation observed in the currents in lightning flashes to earth. For the initiation of these long atmospheric electrical discharges there are two requisites : First, an extensive electric field which is adequate to maintain the discharge once it is initiated, and secondly an electric field concentration at one point in that general field of sufficient magnitude to initiate the discharge. The more uniform the atmospheric conditions in any one cycle, the longer will the formation of the region of intense initiatory electric field concentration be delayed, and the larger will be the general average electric field throughout the whole atmosphere, and hence the greater will be the electrical discharges, when they do occur.

6.2. *Effects of Atmospheric Absorption on the Spectra*

Another characteristic of the spectra of long period variable stars, which is in good accord with the discharge theory has been observed by Merrill in many of their spectra. The discharges originate far down inside the stars' atmospheres and are propagated outwards mainly. As they progress, not only are the oxides and other particles vapourized and dissociated by the energy liberated in the discharge, so that the ' veiling ' is diminished, and the stars increase in magnitude, but the discharges emerge from the clouds of TiO and ZrO in the lower atmospheres, and ultimately yield light which is little affected by the absorption bands of these oxides. This effect is, for example, well illustrated by the variation in the intensities of the individual lines of multiplet (2) of Fe I (Merrill 1947, Table 4) of which Merrill writes : " In the last column, phase+162 days (i.e. 162 days after maximum light) the relative intensities are nearly the same as in the laboratory. At earlier phases the intensities are modified, probably by TiO band absorption, as in R Leonis. The behaviour of this multiplet presents another example of the general tendency of bright lines to escape from the effects of the reversing layer as the phase advances."

The same explanation probably will account for the well-known variation in the relative intensities of Hγ : Hδ at different phases of the brightness cycle of these stars (Merrill 1930). It is only some considerable time after maximum light that this ratio approaches the value observed in the laboratory, when the lines are freed from the effects of atmospheric absorption as the discharge rises in the star's atmosphere.

6.3. *Rapid Changes in Spectrum Line Intensities*

The occurrence of discharges in these extensive stellar atmospheres will result in their atmospheres possessing considerable variations in density. Along one discharge channel the current will flow for periods of several months, resulting in a considerable change in gas density relative to that in neighbouring regions of the atmosphere. When the next cycle of discharges occurs the leader strokes will be propagated through regions varying considerably in density. As each region of relatively high gas pressure is encountered there will result a considerable increase of the current density in that region and a consequent brightening of the light from the discharge. As distances of the order of one to ten million kilometres are covered in a day by the advancing head of the discharge column, the effect of changes in density can be considerable in times of this order. Rapid changes in line intensities are observed in many of these stars, and particularly well in BF Cygni (Merrill 1943).

§ 7. CONCLUSIONS

1. The combination spectra observed in several long period variable stars can be explained on the basis of the electrical discharge theory of their variability.

2. On this theory the 'companion' spectrum is emitted from the electrical discharges at relatively low levels in the star's atmosphere. The nebular spectrum containing forbidden lines is emitted when the discharge reaches the extremely low pressures of the outer regions of the star's atmosphere.

3. The theory explains the observed time interval between the maxima of these two spectra.

4. It explains the observed relationship between the intensities of the M-type and 'companion' spectra observed by Merrill in R Aquarii.

5. The theory explains the variation in the relative intensities of the individual lines of multiplets as the outburst progresses.

ACKNOWLEDGMENTS

The author wishes to acknowledge his indebtedness to the Council of the E.R.A. for their support of this work and to the Director of the E.R.A. for permission to publish this paper.

REFERENCES

BRUCE, C. E. R., 1941, *Nature, Lond.*, **147,** 805; 1944, *Proc. Roy. Soc.* A, **183,** 228; 1955 a, *Observatory*, **75,** 82; 1955 b, *Quart. J. Roy. Met. Soc.*, **81,** 265.

KING, L. A., 1954, *Nature, Lond.*, **174,** 1008.

KOMELKOV, V., 1947, *Dok. Akad. Nauk. U.S.S.R.*, **68,** 57.

Loeb, L. B., 1954, *Modern Physics for Engineers* (New York: McGraw-Hill), p. 347.

Loeb, L. B., and Meek, J. M., 1941, *The Mechanism of the Electric Spark* (Oxford: University Press), p. 98.

Merrill, P. W., 1930, *Ap. J.*, **71**, 285; *M.W.C.*, No. 399 (with Burwell, Cora G.); 1935, *Ap. J.*, **81**, 312; *M.W.C.* No. 513, p. 17; 1940, *Spectra of Long-Period Variable Stars* (Chicago: University of Chicago Press); 1943, *Ap. J.*, **98**, 334; *M.W.C.* No. 687; 1944, *Ap. J.*, **99**, 15; *M.W.C.* No. 688; 1947, *Ap. J.*, **106**, 274; *M.W.C.* No. 735; 1950, *Ap. J.*, **112**, 515; *M.W.* and *P.* Reprint No. 27.

Pierce, E. T., 1955, *Quart. J. Roy. Met. Soc.*, **81**, 229.

Schonland, B. F. J., 1938, *Proc. Roy. Soc.* A, **164**, 132.

Shaw, P. E., 1926, *Nature, Lond.*, **118**, 659; 1928, *Proc. Roy. Soc.* A, **122**, 49.

Simpson, G. C., and Scrase, F. J., 1937, *Proc. Roy. Soc.* A, **161**, 309.

[Under Merrill, P. W., the *M.W.C.* references are alternatives to the *Ap. J.* references.]

CXXVI. CORRESPONDENCE

The Decay Scheme of ^{140}La

By C. F. Coleman
Atomic Energy Research Establishment, Harwell

[Received July 4, 1955]

An investigation of the decay scheme of ^{140}La, prepared by slow neutron irradiation of Johnson Matthey Specpure La_2O_3, has been carried out with sodium iodide scintillation spectrometers. Gamma rays of energies 328, 486, 815, 893±40, 1597, and 2570±150 kev were found, with relative intensities of 25±10, 48±8, 27±5, 11±4, 100, and 4±1. No others were observed with energies greater than 50 kev, and in particular the intensity of the 2900 kev radiation reported by Wattenberg (1947) was found to be less than 1% of that of the 1597 kev radiation. The only previous report of a gamma ray with an energy of about 900 kev was made by Cork *et al.* (1951), who observed conversion electrons of a 920 kev radiation. Since the ratio of the heights of the 815 and 893 kev photopeaks in the lanthanum spectrum changed by less than 20% over a period of three half-lives, the 893 kev radiation is assumed to belong to the ^{140}La decay, and is identified with Cork's 920 kev radiation.

Coincidence studies were then carried out by setting a single channel pulse analyser on each photopeak in turn, and observing the coincident spectrum in a second counter by means of a thirty channel pulse analyser. The 1597 kev line was found to be in coincidence with all the lines of lower energy, including the 920 kev line (fig. 1). The other coincidence spectra showed that coincidences also occurred between the 328 and 486 kev gamma rays, and that, within the experimental error caused by the presence of the 1597 kev Compton distribution below the photopeaks of the lower energy gamma rays, both the 815 and the 920 kev lines were in coincidence with the 1597 kev line alone. These results, together with the beta–gamma coincidence measurements of Robinson and Madansky (1951) and the beta-ray energy measurements of Peacock *et al.* (1954), strongly support the decay scheme given in fig. 2, proposed by the latter group of workers.

Values obtained for the angular correlation of the 815, 1597 kev gamma ray cascade have differed widely (Robinson and Madansky 1951, Bishop and Perez 1955), probably because the observed correlations include different contributions from the 920, 1597 kev cascade. The correlation of this latter cascade was isolated and measured by feeding the output of one detector to a single channel pulse height analyser arranged to accept as much of the 920 kev photopeak as was consistent with complete rejection of the 815 kev photopeak. A rate controlled gain stabilizer was used to minimize the effect of amplifier and multiplier gain drifts. The observed correlation, after correction for finite angular resolution, is given by

Fig. 1

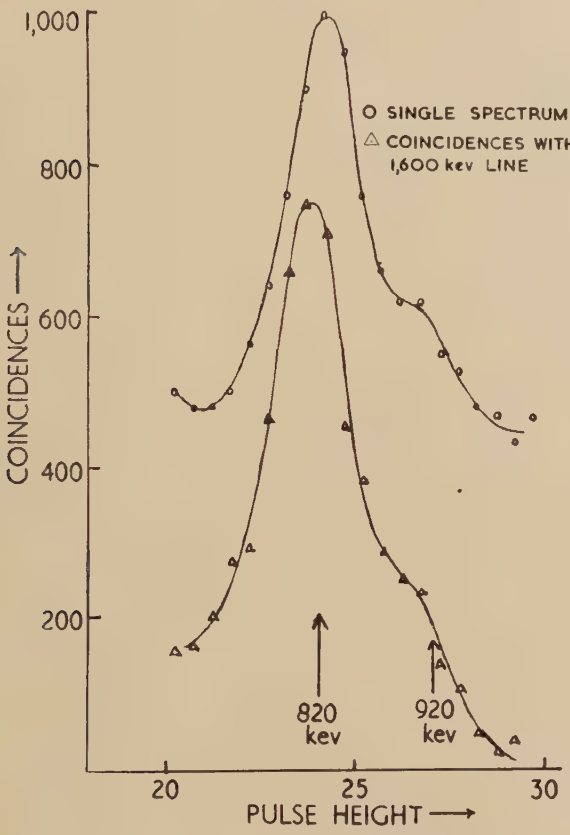

^{140}La—Coincidence spectrum near 860 kev.

$$W(\theta)=(1{\cdot}000\pm0{\cdot}010)+(0{\cdot}200\pm0{\cdot}035)P_2(\cos\theta)-(0{\cdot}002\pm0{\cdot}043)P_4(\cos\theta)$$

which can be fitted by the spin sequence for the 2517 and 1597 kev levels, 2{M1+(0·1% to 1·0%)E2}2{E2}0. where the M1 and E2 components in the first transition are in antiphase according to the convention of Biedenharn and Rose (1953). The spin shown in fig. 2 for the 2083 kev level is that which Bishop and Perez derive from their measurements on the angular correlation of the 486, 1597 kev cascade.

From the above decay scheme over 95% of all ^{140}La disintegrations are accompanied by emission of the 1597 kev gamma ray, and fewer than 5% by the emission of any other gamma radiations with energies greater than 920 kev. Thus it should be possible to estimate the absolute disintegration rates of ^{140}La sources to within 5% by beta–gamma coincidence measurements if a thallium activated sodium iodide crystal

Fig. 2

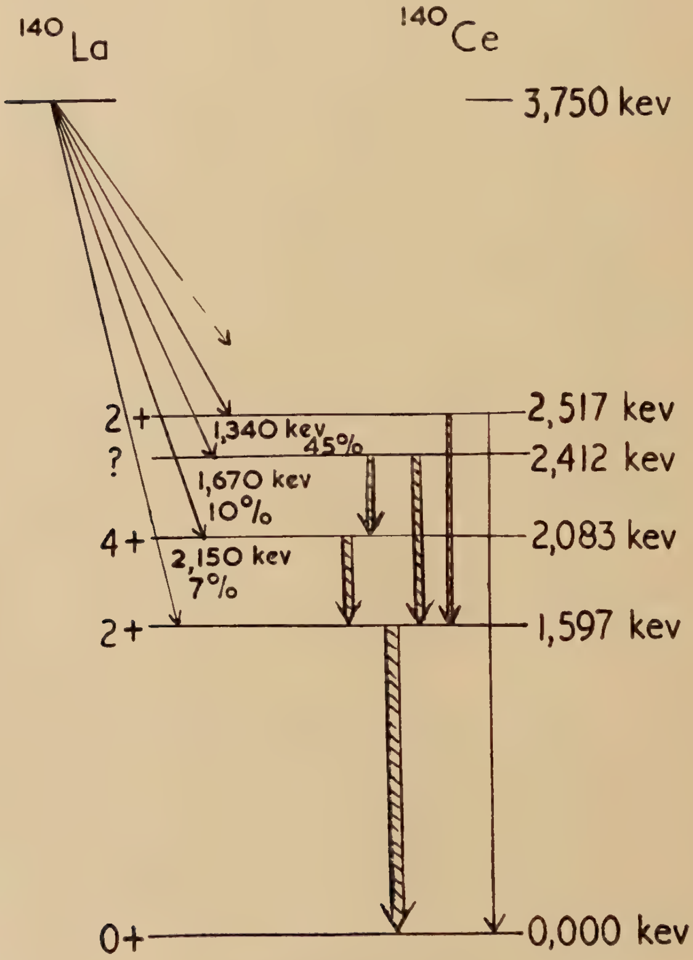

Decay scheme of ^{140}La.

is used as the gamma ray detector, and only those pulses are accepted which correspond to an energy release in the crystal greater than about 1000 kev.

REFERENCES

BIEDENHARN, L. C., and ROSE, M. E., 1953, *Rev. Mod. Phys.*, **25,** 729.
BISHOP, G. R., and PEREZ Y JORBA, J. P., 1955, *Phys. Rev.*, **98,** 89.
CORK, J. M., STODDARD, A. E., LEBLANC, J. M., BRANYAN, C. E., MARTIN, D. W., and CHILDS, W. J., 1951, *Phys. Rev.*, **83,** 856.
PEACOCK, C. L., QUINN, A. F., and OSER, A. W., 1954, *Phys. Rev.*, **94,** 372.
ROBINSON, B. L., and MADANSKY, L., 1951, *Phys. Rev.*, **84,** 1067.
WATTENBERG, A., 1947, *Phys. Rev.*, **71,** 497.

Electric Quadrupole Lifetimes in Even–Even Nuclei

By C. F. Coleman
Atomic Energy Research Establishment, Harwell

[Received July 4, 1955]

Two groups of coincidence measurements have been carried out in an attempt to determine the lifetimes of a number of E2 gamma ray transitions. In the first group, values of mean lifetimes were obtained from the side slopes of coincidence curves with a full width at half height of 2×10^{-8} seconds, taken using T.P.B.D. phosphors, E.M.I. 6260 photomultipliers, and 30 Mc/sec fast amplifiers in a parallel coincidence arrangement. With this equipment mean lifetimes $\gtrsim 6\times10^{-10}$ seconds could be detected. In the second group, for which the corresponding limit was $\sim3\times10^{-11}$ seconds, the lifetimes were deduced from the centroid shifts (Bay 1950) between pairs of beta–gamma coincidence curves with effective full widths of $1{\cdot}6\times10^{-9}$ seconds, taken under comparable experimental conditions, using T.P.B.D. phosphors, R.C.A. 5819 photomultipliers, and 200 Mc/sec fast amplifiers, again in a parallel coincidence arrangement. The differences ($\sim5\times10^{-11}$ seconds) between the flight times of beta rays and gamma rays were calculated from the energy bands selected by the slow channels (widths $\sim20\%$) and the geometry of the equipment. In most cases the paired curves were taken from a single source (‘ self-comparison ’), a beta absorber being placed before each detector in turn to exchange the functions of the beta and gamma counters, but the coincidence curves from ^{76}As and ^{124}Sb were paired with comparable curves from ^{24}Na. The experimental technique used in these measurements will be described in detail in a later paper. The quoted uncertainties in the mean life-times for this group arise from the different distributions within the phosphors of the points of origin of light photons produced by beta and by gamma irradiation. The statistical uncertainties are usually less than 10^{-11} seconds, going down to 2×10^{-12} seconds for the ^{24}Mg measurement. Where two gamma rays are emitted in cascade*

Nucleus	τ_{obs}	E_γ(Mev)	τ_{exp}	τ_{E2}(S.P.M.)	$\|M\|^2$	Method
^{24}Mg	$(3\pm2)\times10^{-11}$ sec	1·38*	$(3{\cdot}6\pm2{\cdot}5)\times10^{-11}$ sec	$1{\cdot}6\times10^{-11}$ sec	$\gtrsim0{\cdot}25$	Self Compn.
^{46}Ti	$<2\times10^{-11}$ sec	0·89*	$<4\times10^{-11}$ sec	$5{\cdot}9\times10^{-11}$ sec	$>1{\cdot}5$	Self Compn.
^{56}Fe		0·85	$<6\times10^{-10}$ sec	$6{\cdot}0\times10^{-11}$ sec	$>0{\cdot}10$	
		1·26	$<3\times10^{-10}$ sec	$8{\cdot}3\times10^{-12}$ sec	$>0{\cdot}02$	
^{60}Ni	$<2\times10^{-11}$ sec	1·17*	$<4\times10^{-11}$ sec	$1{\cdot}0\times10^{-11}$ sec	$>0{\cdot}25$	Self Compn.
^{76}Se	$(3\pm2)\times10^{-11}$ sec	0·56*	$(3{\cdot}3\pm2{\cdot}2)\times10^{-11}$ sec	$3{\cdot}0\times10^{-10}$ sec	$\gtrsim5$	Compn. ^{24}Na
^{88}Sr		1·85	$<6\times10^{-10}$ sec	$6{\cdot}9\times10^{-13}$ sec	$>0{\cdot}001$	
^{114}Cd		0·55	$<6\times10^{-10}$ sec	$2{\cdot}0\times10^{-10}$ sec	$>0{\cdot}3$	
^{122}Te	$(20\pm2)\times10^{-11}$ sec	0·57*	$(22\pm3)\times10^{-11}$ sec	$1{\cdot}4\times10^{-10}$ sec	$0{\cdot}64\pm0{\cdot}1$	Self Compn.
^{124}Te	$<2\times10^{-11}$ sec	0·60	$<2\times10^{-11}$ sec	$1{\cdot}1\times10^{-10}$ sec	>5	Compn. ^{24}Na
^{131}Cs		0·122	$(5{\cdot}9\pm0{\cdot}8)\times10^{-9}$ sec	—		

τ_{obs}—See text.
τ_{exp}—Mean lifetime deduced from experiment.
τ_{E2}(S.P.M.)—Theoretical mean lifetime for E2 radiation deduced from the Single Particle Model.
$|M|^{-2}$—Ratio τ_{exp}/τ_{E2}(S.P.M.).

a value for the mean life-time of the softer transition has been calculated from the experimental average of the two lifetimes, τ_{obs}, by taking the lifetime of the harder transition as zero. The metastable level found in ^{131}Cs is fed by the 0·494 MEV gamma ray from the decay of ^{131}Ba, confirming the decay scheme proposed by Lu *et al.* (1955).

Most of the data presented here are for transitions between the first excited states and ground states of even–even nuclei. It will be seen that several of the observed lifetimes are comparable with those estimated from the single particle model, or even smaller, in two cases by a factor of five, giving strong evidence for the existence in these nuclei of collective motion (Goldhaber and Weneser 1955).

REFERENCES

BAY, Z., 1950, *Phys. Rev.*, **77**, 419.
GOLDHABER, G., and WENESER, J., 1955, *Phys. Rev.*, **98**, 212.
LU, D. C., KELLY, W. H., and WIEDENBECK, M. L., 1955, *Phys. Rev.*, **97**, 139.

The X-ray Spectra of μ-mesonic Copper and Lead

By F. D. S. BUTEMENT
Atomic Energy Research Establishment, Harwell

[Received July 27, 1955]

THE theoretical significance of measurements of the 2P–1S radiative transition energies of μ-mesonic atoms of the heavier elements (from which the nuclear radius may be calculated) has been discussed theoretically by Wheeler (1953), Cooper and Henley (1953), and Hill and Ford (1954). Experimental measurements for a number of elements have been made by Fitch and Rainwater (1953). This letter describes measurements made on copper and lead.

The arrangement of the apparatus is shown in fig. 1. The external π^- and μ^- meson beam of the University of Liverpool cyclotron (after passing through a channel in the 12 ft. thick iron loaded concrete shielding and deflection by an analysing magnet) was filtered through 48 mm of copper (1) in order to stop the π^- mesons. The emergent beam of μ^- mesons and fast electrons in approximately equal proportions passed through a collimator in a wall of iron loaded concrete (2), then through scintillation counters with plastic scintillators 8 mm thick and 63 mm diameter (3 and 4) and fell on a slab of the target element 75 mm square and 10 g cm^{-2} thick (5). The mesonic x-rays emitted were detected by a NaI(Tl) crystal 44 mm in diameter and 47 mm thick (7) viewed by a type 6260 E.M.I. photomultiplier tube. Events were selected by coincidence between counters 3, 4 and 7, with a resolving time of 3×10^{-7} sec. Counter 6 with a plastic scintillator 6 mm thick and 8 cm square operated as an anticoincidence counter to reject events due to a charged particle traversing 5 and entering 7. About 400 μ^- mesons per minute stopped in the target. The pulse height distributions from counter 7 was analysed on a 100 channel analyser similar to that described by Wilkinson (1950). Energy calibrations were made with the 1·33 Mev γ-ray of ^{60}Co and the 4·43 Mev γ-ray from a Po–Be source. The attenuator scale of the spectrometer amplifier and the linearity of the pulse analyser were calibrated and found to be accurate to better than one part in a thousand. The main source of error was due to slight drifts in the gain of the photomultiplier, but numerous calibrations showed that this did not exceed 1%.

Fig. 1

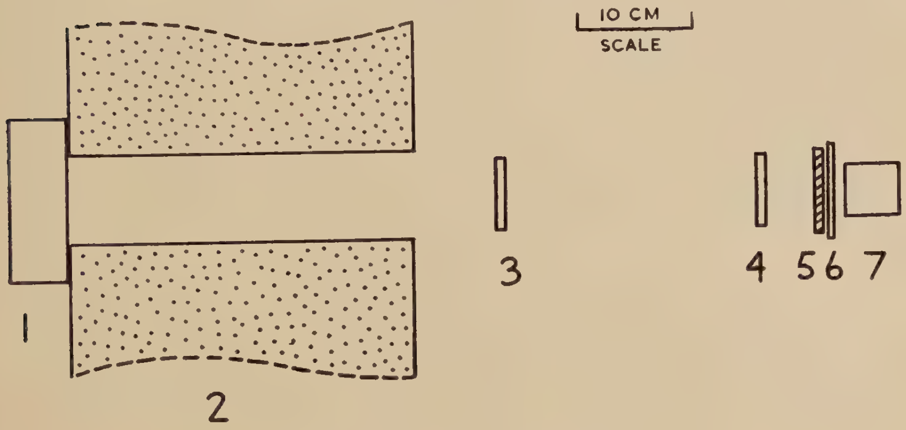

Arrangement of apparatus.

The mesonic x-ray spectra observed were superimposed on a continuum of pulses extending to above 10 Mev, due to bremsstrahlung produced by high energy electrons. Nuclear γ-rays following various modes of nuclear disintegration caused by eventual nuclear capture of the mesons must also have been recorded, but these γ-rays would have individual intensities considerably less than those of the mesonic x-rays, and were not observed.

The spectrum of copper (fig. 2) shows the (unresolved) 2P–1S transition as a photoelectric peak at 1·55 Mev together with the corresponding Compton peak at lower energy. Fitch and Rainwater (1953) also obtained a value of 1·55 Mev.

Figure 3 shows the 2P–1S transition of lead. At high γ-ray energies (E) there is a peak due to pair production at ($E-1{\cdot}02$) Mev, a peak of almost equal intensity at ($E-0{\cdot}51$) Mev due to pair production with subsequent absorption of one of the annihilation quanta and a weak peak at the full energy due partly to photoelectric absorption and partly to pair production with absorption of both annihilation quanta. The resolution on a single peak was 8% (width at half maximum intensity) and it was therefore not possible to resolve the $2P_{1/2}$–1S and $2P_{3/2}$–1S components, which should theoretically have a separation of about 3·6% for the pair production peak (assuming that the μ meson is a Dirac type particle of spin $\frac{1}{2}$).

Fig. 2

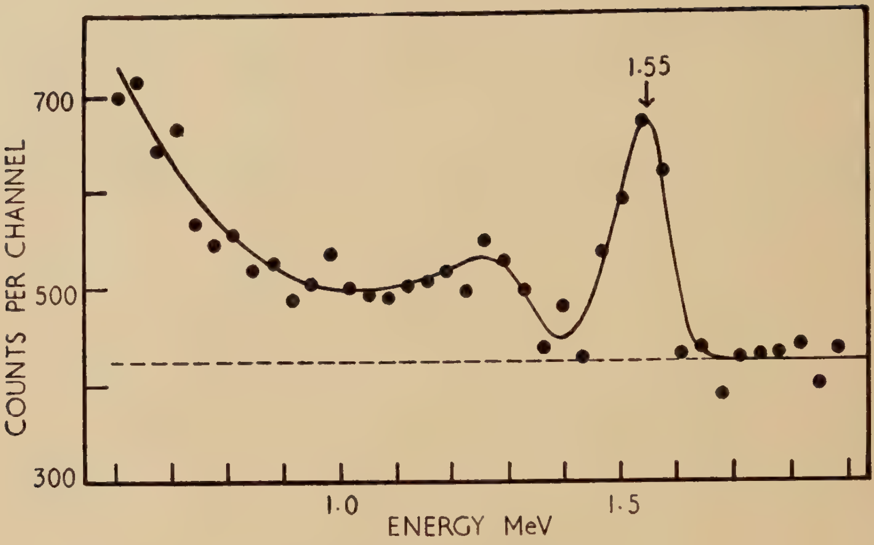

Spectrum of μ-mesonic copper.

Fig. 3

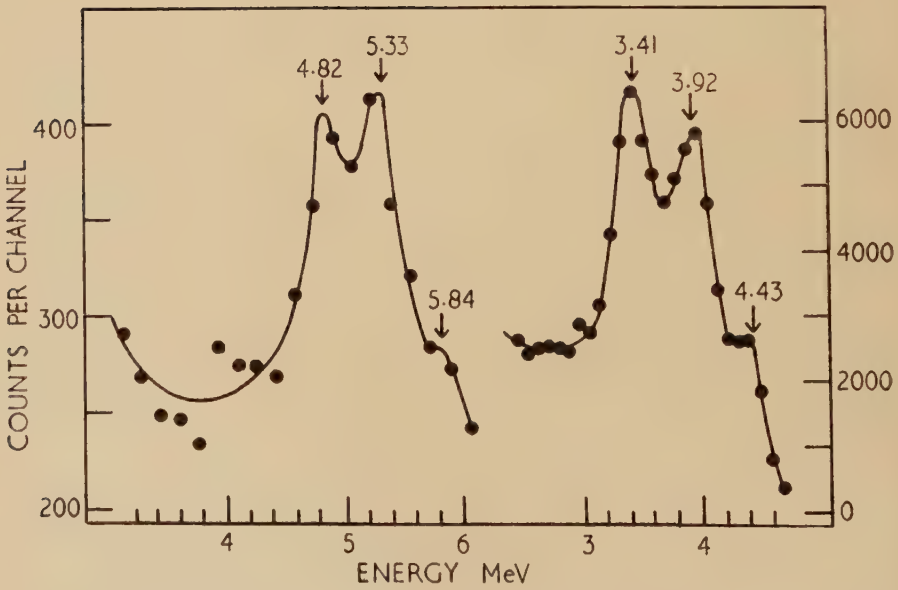

Spectra of μ-mesonic lead and of 4·43 MEV γ-ray.

Study of the peak profile for the 4·43 Mev γ-ray from a Po–Be source, obtained with good counting statistics, indicated that the most reliable method of determining the energy of a statistically imperfect profile was to determine the centre of the composite $(E-1{\cdot}02)$ and $(E-0{\cdot}51)$ Mev peak at a level of 80% of the maximum peak height. The value thus obtained was very close to the mean, i.e. $(E-0{\cdot}77)$ Mev. Application of this method to the lead spectrum gave a value of 5·84 Mev for the unresolved 2P–1S transition. Hill and Ford have shown that for any plausible nuclear model the $2P_{3/2}$ and $2P_{1/2}$ levels have a separation of between 0·176 and 0·186 Mev and relative statistical weights of 2 : 1. With the resolution quoted above, the $2P_{3/2}$–1S transition should then be approximately 0·05 Mev higher than the unresolved peak, i.e. at 5·89 Mev. Fitch and Rainwater found 6·02 Mev.

The author wishes to thank Professor H. W. B. Skinner for providing the facilities of the University of Liverpool cyclotron, and Mr. D. West and Mr. E. F. Bradley for help with the operation of the apparatus.

REFERENCES

COOPER, L. N., and HENLEY, E. M., 1953, *Phys. Rev.*, **92,** 801.
FITCH, V. L., and RAINWATER, J., 1953, *Phys. Rev.*, **92,** 789.
HILL, D. L., and FORD, K. W., 1954, *Phys. Rev.*, **94,** 1617.
WHEELER, J. A., 1953, *Phys. Rev.*, **92,** 812.
WILKINSON, D. H., 1950, *Proc. Camb. Phil. Soc.*, **46,** 508.

A Note on the Ground State Spin of ^{177}*Hafnium*

By B. HARTMANN and T. WIEDLING
Laboratory of Physics, University of Stockholm, Sweden

[Received July 28, 1955]

RASMUSSEN made spectroscopic fine structure measurements on ^{177}Hf and reported a ground state spin of $\leqslant 3/2$ (Rasmussen 1935). It is well known that angular correlation measurements are a method of determining spins not only of excited states but under favourable conditions of ground states as well. Some experiments of this kind were made on ^{177}Hf some years ago in a trial to exclude one of the proposed spins given above (McGowan *et al.* 1951, Wiedling 1952). According to the results obtained it seemed possible to exclude spin 1/2.

We have now made a reinvestigation of the angular correlation of ^{177}Hf with the use of some different chemical compounds. The measurements were made on the two strong gamma lines in the well-known decay scheme of ^{177}Hf (Douglas 1949, Marmier and Boehm 1955). The investigation was made with two scintillation spectrometers coupled in coincidence. One spectrometer accepted only the full energy photopeak of 113 kev and the other spectrometer only the peak of 208 kev.

Measurements were made on the following chemical compounds: Lu_2O_3, $Lu(NO_3)_3$ as a powder, $Lu(NO_3)_3$ in water solution, and $Lu(NO_3)_3$ in water solution mixed with glycerine.

The two sources mentioned last were chosen because of the fact that the attenuation of an angular correlation is a function of the viscosity of the solution under some circumstances. The angular correlation measurements were made on several sources of each compound. Data were taken for every fifteen degrees. A least squares fit of the experimental points to the function $W(\theta)=1+A_2P_2(\cos\theta)$ was made. The results are shown in the table.

Source	$-A_2$
Lu_2O_3	0·147
$Lu(NO_3)_3$ (powder)	0·142
$Lu(NO_3)_3$ (in water solution)	0·176
$Lu(NO_3)_3$ (25% water and 75% glycerine)	0·140
	The errors of A_2 are about ±4%

Within the experimental errors the value of A_2 obtained here for Lu_2O_3 is in agreement with earlier results. However, the less pronounced anisotropy obtained for $Lu(NO_3)_3$ as a powder and for $Lu(NO_3)_3$ in water solution mixed with glycerine is remarkable as well as the stronger anisotropy found for a dilute solution of $Lu(NO_3)_3$ in water. This last mentioned anisotropy may be a maximum because of the fact that solutions often give maximum anisotropy. The fact that the attenuation of the angular correlation is less pronounced when the crystalline source is dissolved in water shows that the source effect may be an interaction of the electric quadrupole moment of the first excited level of the nucleus with an electric field gradient.

As pointed out earlier Rasmussen proposed a ground state spin $\leqslant 3/2$. The shell model prefers spin 1/2. If we suppose the spin sequences of the levels of ^{177}Hf to be $5/2\rightarrow 7/2\rightarrow 3/2$ or $3/2\rightarrow 5/2\rightarrow 1/2$ and assume the emitted gamma-rays to have pure character the angular correlation theory gives $A_2=-0{\cdot}153$ and $A_2=-0{\cdot}200$, respectively, compared with our maximum value $-0{\cdot}18$. Thus our measurements show that at present it is not possible to draw any certain conclusions about the ground state spin of ^{177}Hf from angular correlations measurements but that it is necessary to use other experimental methods to get information about this. It seems, however, to be possible to get other valuable information about the ^{177}Hf nucleus from correlation measurements and for this reason our investigations continue.

REFERENCES

DOUGLAS, D. G., 1949, *Phys. Rev.*, **75,** 1960.
MARMIER, P., and BOEHM, F., 1955, *Phys. Rev.*, **97,** 103.
McGOWAN, F. K., KLEMA, E. D., and BELL, P. R., 1951, *Phys. Rev.*, **85,** 152.
RASMUSSEN, E., 1935, *Naturwiss.*, **23,** 69.
WIEDLING, T., 1952, *Ark. Fys.*, **6,** 39.

Screw Dislocations and Polytypism of Cadmium Iodide

By RICHARD S. MITCHELL
Department of Geology, University of Virginia, Charlottesville

[Received July 28, 1955]

INTRODUCTION

SINCE the appearance of a previous summary on polytypism of cadmium iodide (Mitchell 1954), many new forms of this substance have been identified, and the stacking structures have been determined for several of these. In this note the writer plans to summarize this new information and then draw some conclusions concerning the relationship of screw dislocations to the formation of these polytypes. In order to avoid repetition of the previous summary of this subject no space groups or unit cell constants are given here for the different polytypes. All of the determined stacking structures are summarized, however, since these are essential to the discussion of the dislocation theory. Each structure is represented both by the classical A, B, C notation and the iodine atom zigzag sequence. Details on the determination of these structures will be published in the future. The crystals used in this investigation were grown from aqueous solutions at room temperature, and were picked at random from these solutions for study by the Weissenberg x-ray method.

SUMMARY OF POLYTYPES

The writer has encountered a few crystals of type 2H. Each of these has the structure $[(A\gamma B)]_n$, (11), which was first determined by Bozorth (1922).

Type 4H is by far the most common modification of cadmium iodide. This type has the stacking structure $[(A\gamma B)(C\alpha B)]_n$, (22). Several earlier investigators reported cadmium iodide crystals with this structure.

Two specimens of 6H were recently found. Both of these have a $[(A\gamma B)(C\alpha B)(A\gamma B)]_n$, (2211), structure. This stacking sequence differs from Pinsker's (1941 a, b) 6H type which has the arrangement $[(A\gamma B)$

$(C\beta A)\ (C\alpha B)]_n$, (33). Theoretical considerations for the existence of these two types will be given later in this note. In the future the writer will designate the (2211) type as $6H_{(a)}$ and the (33) type as $6H_{(b)}$. This follows a scheme used by Ramsdell and Kohn (1952) for naming two polytypes of silicon carbide with equal numbers of layers but different stacking.

Two crystals of type 8H have been noted. One of these, reported previously, has the structure $[(A\gamma B)\ (C\alpha B)\ (A\gamma B)\ (A\gamma B)]_n$, (221111). The second example appears to have an identical structure, but, because it is syntactically coalesced with 4H, a good evaluation of the intensities of some of the x-ray reflections is impossible.

Type 10H has been encountered twice. Both crystals have a structure represented by $[(A\gamma B)\ (C\alpha B)\ (A\gamma B)\ (C\alpha B)\ (A\gamma B)]_n$, (222211).

Three structural variations of type 12H have been identified. Type $12H_{(a)}$ has the structure $[(A\gamma B)\ (C\alpha B)\ (A\gamma B)\ (C\alpha B)\ (A\gamma B)\ (A\beta C)]_n$, (222123). In this particular case the iodine zigzag sequence is not, by itself, a sufficient symbol for designating the complete structure. The zigzag arrangement does not fix the cadmium atom positions when there is no horizontal plane of symmetry for the iodine atoms, and, hence, the cadmium atoms may lie on one of two groups of positions. The A, B, C notation, however, gives an unambiguous designation. Type $12H_{(b)}$ has the structure $[(A\gamma B)\ (A\gamma B)\ (C\alpha B)\ (C\alpha B)\ (A\gamma B)\ (A\beta C)]_n$, (22121121). The structure of type $12H_{(c)}$ appears to be $[(A\gamma B)\ (C\alpha B)\ (A\gamma B)\ (C\alpha B)\ (A\gamma B)\ (A\gamma B)]_n$, (22221111), but this is still uncertain because the crystal is syntactically coalesced with 4H which makes the intensity evaluation of certain x-ray reflections difficult.

One crystal of 14H was identified. This has a structure represented by $[(A\gamma B)\ (C\alpha B)\ (A\gamma B)\ (C\alpha B)\ (A\gamma B)\ (C\alpha B)\ (A\gamma B)]_n$, (22222211).

In addition to the aforementioned crystals, the writer has also observed types 16H, 18H, 20H, $24H_{(a)}$, $24H_{(b)}$, $24H_{(c)}$, $24H_{(d)}$, 26H, $28H_{(a)}$, $28H_{(b)}$, $32H_{(a)}$, $32H_{(b)}$, $40H_{(a)}$, $40H_{(b)}$, $40H_{(c)}$, 44H, 50H, 56H, 62H and 64H, and is working on the structures of some of these at the present time. There is still some uncertainty about the identity of a rhombohedral type, 24R, and several other types consisting of many layers.

EXPLANATION OF POLYTYPISM

This study has not only proved Forty's (1952) idea that cadmium iodide exhibits polytypism, but also now virtually proves his explanation for this phenomenon. He suggested that various slips in the [0001] direction of the 'ideal structure' 4H, $[(A\gamma B)\ (C\alpha B)]_n$, would produce different kinds of steps on the (0001) surface, and the crystal generated by spiral growth on this surface would have a structure controlled by the structure of these steps. In fig. 1 atoms below line ABCDEF are arranged according to the 4H stacking sequence (JKLM outlines a 4H unit cell). This structure has been dislocated in the [0001] direction along BG and DH. BC represents a slip of the structure equal to a Burgers vector of unit strength (equal to one sandwich of atoms or 6·835 Å), and DE is a similar slip equal to a vector of strength three. The structure at step BC is (AγB) or (11). If the crystal grows on this step alone a 2H type would be generated. A unit cell of this is outlined by NPQR in fig. 1. Step DE has the structure (AγB) (CαB) (AγB) or (2211). If this step existed by itself type 6H (STUV) would be generated. One should also notice how well the atoms fit together along the planes of dislocation. Following is a summary of the structures that would be produced by single slips of different magnitudes of the type illustrated below.

Fig. 1

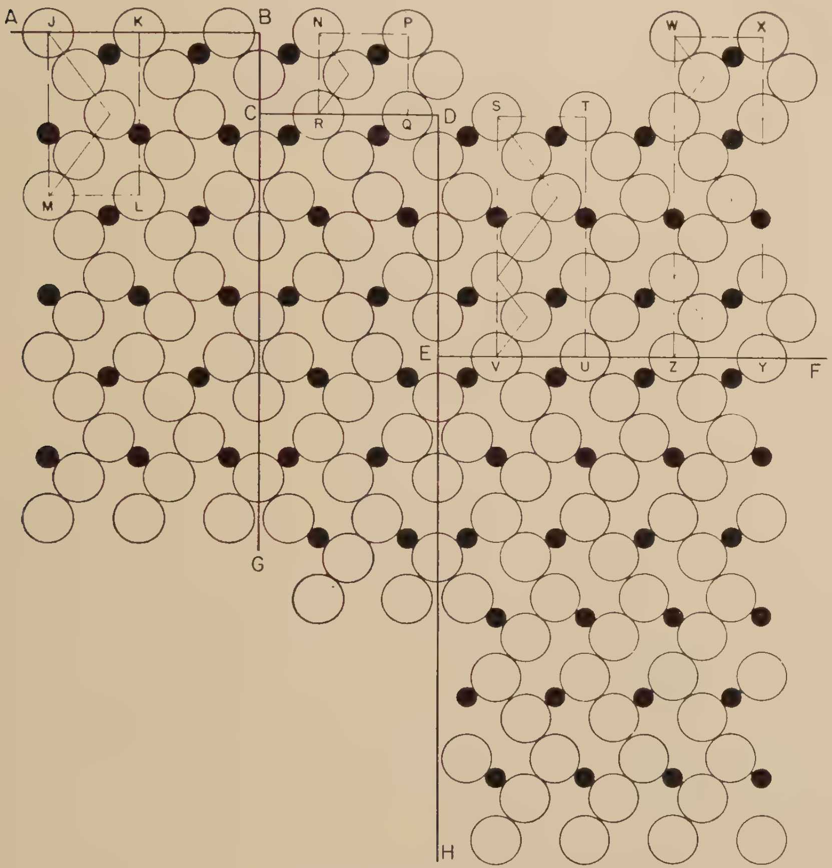

A (11$\bar{2}$0) cross section of a dislocated 4H cadmium iodide structure. White circles represent iodine atoms while black circles represent cadmium atoms. The atoms and unit cell dimensions are drawn to scale relative to each other.

It should be noted that every time the strength of the Burgers vector is equal to 2n the 4H structure results, and, therefore, a single dislocation of this type would never produce an 8H, 12H, 16H . . . 4nH polytype.

From the theory, one might also expect to encounter type 4H more frequently than other modifications.

A close examination of the experimental results, outlined in the earlier part of this note, will reveal that experimental observation completely supports the above theory with a few modifications. Types 2H, 4H, $6H_{(a)}$, 10H and 14H have been found and have structures identical with those predicted by the theory. In addition type 4H is by far the most abundant polytype of this compound.

Burgers vector strength	Resulting step structure	Polytype generated
1	(AγB) (11)	2H
2	(AγB)(CαB) (22)	4H
3	(AγB)(CαB)(AγB) (2211)	6H
4	(AγB)(CαB)(AγB)(CαB) (2222)	4H
5	(AγB)(CαB)(AγB)(CαB)(AγB) (222211)	10H
6	(AγB)(CαB)(AγB)(CαB)(AγB)(CαB) (222222)	4H
7	(AγB)(CαB)(AγB)(CαB)(AγB)(CαB)(AγB) (2222211)	14H
etc.		

Polytypes 8H and $12H_{(c)}$, reported above, can easily be explained by assuming the presence of two simple screw dislocations of the same hand. In fig. 1 it was illustrated how 2H and 6H each originated by a single dislocation. Now if both dislocations occurred in the same crystal and close enough together to co-operate (Frank 1951), the final effect would be an addition of the two step structures, resulting in a step with the structure (AγB) (AγB) (CαB) (AγB), (112211). This is illustrated in fig. 1 where a unit cell of the structure is outlined by WXYZ. This is the structure that was determined experimentally for 8H. A step needed to generate the $12H_{(c)}$ structure will result from a similar combination of two dislocations whose steps have the 2H and 10H structure.

To explain types $6H_{(b)}$, $12H_{(a)}$ and $12H_{(b)}$ one must consider a further complication of the theory. In all the cases up to this point one will notice that when atoms began to take their place on the newly formed step they fell into the position of atom g in fig. 2, which is the position to be expected by the control of the exposed step. However, if the first atom fell into position h certain variations in the growing crystal would result. Also it should be noted that the arrangement of neighbours around atom h is similar to arrangements in the dislocated region along BG. A structure of this kind, built upon a dislocation with a Burgers vector of unit strength, would give an (AβC), (11), arrangement which is equivalent to the simple 2H structure. A unit cell of this type is outlined by NPQR in fig. 2. Likewise, a structure of this type built upon a dislocation with a vector strength of three would produce a 6H type with the structure [(AγB) (CαB) (AβC)]$_n$, (33), which is equivalent to the 6H$_{(b)}$ structure reported by Pinsker (1941 a, b).

Fig. 2

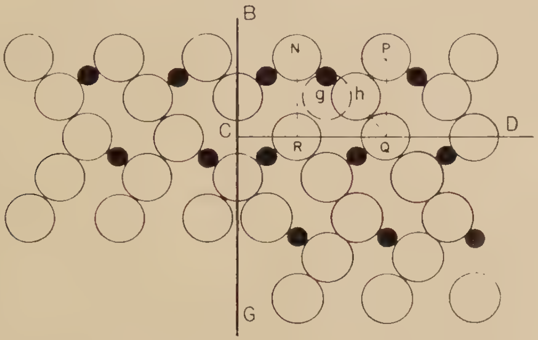

Similar to fig. 1, but showing a different arrangement of atoms growing on the dislocation step BC.

The 12H$_{(a)}$ structure [(AγB) (CαB) (AγB) (CαB) (AγB) (AβC)]$_n$ is equivalent to the simple 10H structure plus one (AβC) sandwich. A step with an arrangement necessary to generate this stacking could be formed by the combination of two dislocations of the same hand. One of these would have a dislocation strength of one and would grow by adding the first atom in the h position. The other dislocation would involve a slip equal to a vector strength of five and would grow by adding atoms in the normal g position. Type 12H$_{(b)}$ could result from the combination of five small dislocations, the growth of three involving atoms in the g position and the growth of the other two involving atoms in the h position. This does not seem to be unreasonable. Forty (1952) has stated that if a crystal plate buckles fairly uniformly the resultant slip will produce several screw dislocation groups of about the same size.

Because polytypes can be generated both from multiple dislocations. and growth in g and h positions, it is easily understood why one polytype may have several structures. The fact that type 26H, for example, fits in the series 2H, 6H, 10H, 14H, etc., but does not have the structure (22222222222211) of this series, does not invalidate the theory. Its structure, still undetermined, could be one resulting from multiple dislocations.

It is interesting to note that Forty (1952) measured spiral step heights on cadmium iodide and found values ranging in magnitude corresponding all the way from 16H to 96H. Values corresponding to types less than 16H were not determined because of limitations in the method of measurement. Some of his steps no doubt occurred on pure 4H crystals which had one dislocation with a Burgers vector strength equal to 2n, while others were no doubt present on polytypes of many layers, yet to be discovered. He found steps equal in value to the writer's types 16H, 24H, 28H, 32H, 40H, 44H, 50H, 56H, 62H, and 64H.

The writer feels that the observations presented in this note reasonably prove the theory that polytypism of cadmium iodide is a phenomenon that results directly from screw dislocations of a variety of magnitudes in the ' ideal structure ', 4H. In addition to explaining polytypism, this work also seems to validate the more general theory that crystals grow from screw dislocations. A more detailed discussion of this work will be published in the future.

References

Bozorth, R. M., 1922, *J. Amer. Chem. Soc.*, **44,** 2232.
Forty, A. J., 1952, *Phil. Mag.*, **43,** 377.
Frank, F. C., 1951, *Phil. Mag.*, **42,** 1014.
Mitchell, R. S., 1954, *Phil. Mag.*, **45,** 1093.
Pinsker, Z. G., 1941 a, *J. Phys. Chem.* (*U.S.S.R.*), **15,** 559 ; 1941 b, *Acta Phys. U.R.S.S.*, **14,** 503.
Ramsdell, L. S., and Kohn, J. A., 1952, *Acta Cryst.*, **5,** 215.

Ionization at the Origin of Electron Pairs, and the Lifetime of the Neutral Pion

By D. H. Perkins
H. H. Wills Physical Laboratory, University of Bristol

[Received August 12, 1955]

It was first suggested by King (1950) that, as a result of the close proximity of the trajectories of the unlike charges of the electron and positron created in the materialization of a high-energy photon, the ionization near the origin of such a pair might be less than that of the two particles separately.

During an investigation of the soft component associated with high energy ' jets ' produced by cosmic rays in nuclear emulsions, preliminary results had suggested that the lifetime of the neutral pion, as measured by Anand (1953 a), might be an overestimate. Anand's method consisted essentially in measuring the length of the gap between the centre of a star and the first clearly resolved grain in the track of a ' direct ' electron pair originating from the alternative mode of decay $\pi^0 \rightarrow e^+ + e^- + \gamma$. The gap distribution was compared with that of the tracks of protons of twice-minimum ionization projected from the same stars, and it was a possible point of objection that the method depended on the assumption of a constant ionization along the path of the 'direct' pair. It was therefore decided to make measurements of the ionization along a number of tracks of pairs of energy of the order of 100 Bev, for in such conditions the effect suggested by King, if indeed it existed at all, might be present for a considerable distance from the pair origin and so be accessible to measurement.

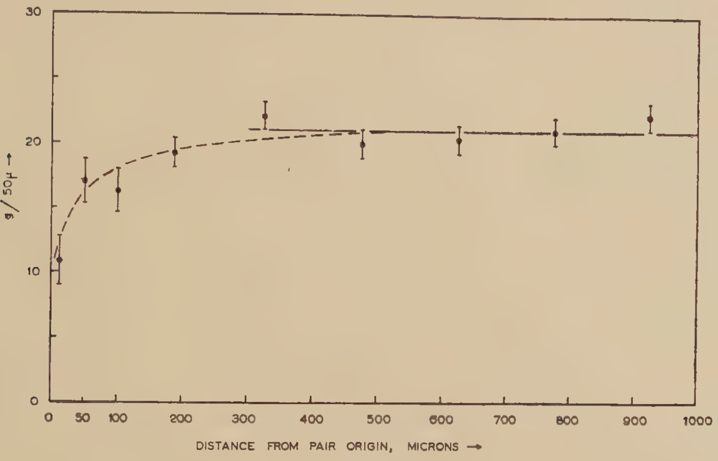

In the figure is displayed the result of measurements on seven energetic electron pairs, the coefficient g of the gap-length distribution (Fowler and Perkins 1955) being plotted against distance x from the pair origin. The full line in the graph refers to the mean value of g for x between 0·3 and 1·0 mm, and the reduction in the value of g, and hence of ionization, for values of $x<0{\cdot}3$ mm is at once apparent. The energies of the pairs were estimated from the relative scattering of electron and positron over the first radiation length or so, and from the features of the soft cascade at greater distances. They lay within the range 80–400 Bev, with a mean value of the order of 180 Bev. At such energies, the relative scattering of the two particles is quite small, and the tracks to which they give rise are unresolvable for a distance of several mm from the origin.

Theoretically, the reduction in ionization near the origin must presumably arise from the fact that for large impact parameters between the pair and the target electrons of the emulsion, the incident field is that of an electric dipole, whereas at greater distances from the origin, the electron and positron are well separated and behave as two independent monopoles. The ionization is expected to increase with x approximately as $\log d/d_{\max}$, where d is the lateral separation of the electrons, roughly proportional to x, and $d_{\max}$ is the maximum effective value of the impact parameter for momentum transfers contributing to the activation of the silver bromide crystals traversed. The dotted curve indicates the form of the expected variation of ionization with distance, calculated from the opening angle of the pairs and for an arbitrary value of $d_{\max}=5\times10^{-7}$ cm.

As stated above, the mean energy of the pairs examined was 180 BEV, whereas that of the direct pairs in Anand's experiment was about 200 MEV. Thus, assuming the relation between opening angle and energy for direct pairs to be similar to that of pairs produced by external conversion of photons (Anand 1953 b), the reduction in ionization in Anand's experiment would only be serious within less than $0{\cdot}5\,\mu$ of the pair origin. This distance is small compared with the mean gap-length ($\sim 2{\cdot}5\,\mu$) in a twice-minimum track. What is more important, the proximity of the parent star very often obscured the first micron or so of the path of the direct pair. Taking these two factors into account, it turns out that, although Anand's assumption of a constant ionization along the path of the pair must lead to an overestimate of the lifetime of the neutral pion, the error introduced is very small in comparison with the statistical errors of his measurements.

Recently, an independent estimate of the lifetime of the neutral pion, based on a modification of the intercept method of Carlson, Hooper and King (1950), has been carried out in this laboratory (Brisbout *et al.* 1955). The value so deduced falls with a 90% probability within the limits 1·2 and 5×10^{-15} sec, in fair agreement with Anand's value of between 2·5 and 14×10^{-15} sec for the same confidence limits.

If the effect described above can be considered as established, it offers a useful alternative method of estimating the energy of γ-rays in the region above 10^{12} ev, subject of course to large statistical fluctuations. At such energies, the conventional measurement of pair energy based on the relative Coulomb scattering of the two particles, has to be carried out over distances greater than or comparable with one radiation length (3 cm). Thus confusion arises because of the presence of bremsstrahlung pairs, and recourse must be had to estimation of the energy from the somewhat tedious analysis of the ensuing soft cascade.

REFERENCES

ANAND, B. M., 1953 a, *Proc. Roy. Soc.* A, **220**, 183 ; 1953 b, *Ph.D. Thesis*, University of Bristol.

BRISBOUT, F., DAHANAYAKE, C., ENGLER, A., FUJIMOTO, Y., and PERKINS, D. H., 1955, *Phil. Mag.*, in the press.

CARLSON, G., HOOPER, J., and KING, D. T., 1950, *Phil. Mag.*, **41**, 701.

FOWLER, P. H., and PERKINS, D. H., 1955, *Phil. Mag.*, **46**, 587.

KING, D. T., 1950, Private communication.

On the Magneto-resistance Effect in Metals

By Rosemary A. Coldwell-Horsfall and D. ter Haar
Department of Natural Philosophy, St. Salvator's College, St. Andrews

[Received August 15, 1955]

One often finds in the literature the statement that the magneto-resistance effect in metals will be zero, if the one-band model is used. This statement is only true, if one understands it to mean that magneto-resistance is really a second-order effect in the same way as are the thermo-electric power and thermal conductivity. Indeed one finds in Seitz (1940) a formula for the magneto-resistance derived on the basis of the one-band model which is stated to be correct in the general case of an energy-dependent mean free path, and which is quoted from an earlier paper by Sommerfeld and Frank (1931). However, Sommerfeld and Frank's derivation is only correct in the case of a constant mean free path. It therefore seemed to us to be of some interest to derive a general formula for the magneto-resistance in a metal with an energy-dependent mean free path derived from the one-band model in the usual way. We have found, up to terms of higher order,

$$[\sigma(\mathrm{H})-\sigma(0)]/\sigma(0)=-D\mathrm{H}^2/(1+C\mathrm{H}^2) \tag{1}$$

in which

$$D=B(1-\tfrac{1}{2}\,[d\ \ln l/d\ \ln \epsilon']_{\varepsilon'=\varepsilon_0'})^2, \tag{2}$$

where all symbols have the same meaning as in Seitz's book.*

From eqns. (1) and (2) it is clear (i) that the magneto-resistance calculated in this way will never be of the same order of magnitude as the observed effects which is the reason why Jones (1936) and Sondheimer and Wilson (1947) developed the two-band model; and (ii) that the effect always has the conventional sign and can thus not be used to explain the recently found effects of opposite sign in In–Sb (Lark-Horovitz, private communication) and Sb (Steele 1955).

References

Jones, H., 1936, *Proc. Roy. Soc.* A, **155,** 653.
Seitz, F., 1940, *The Modern Theory of Solids* (New York: McGraw-Hill), p. 184.
Sommerfeld, A., and Frank, N. H., 1931, *Rev. Mod. Phys.*, **3,** 1.
Sondheimer, E. H., and Wilson, A. H., 1947, *Proc. Roy. Soc.* A, **190,** 435.
Steele, M. C., 1955, *Phys. Rev.*, **97,** 1720.

---

* There are two misprints in formula (12) on p. 184 of Seitz's book: the exponent of π should be 2, and a factor c is missing from the denominator of the expression in square brackets.

Slip in the Interior of Aluminium–Silver Single Crystals

By N. A. McKinnon
Aeronautical Research Laboratories, Australia

[Received August 2, 1955]

The mechanism of deformation in the interior of metal crystals has given rise to much speculation in recent years (Brown and Honeycombe 1951, Kuhlmann-Wilsdorf *et al.* 1952). However a reliable method for disclosing the distribution of slip bands in the interior of, for example, super purity aluminium single crystals has not yet been found. The author has been investigating a possible technique which involves the addition to super purity aluminium of a solute element, which, after deformation has been carried out in the solution treated and quenched condition, will precipitate at a suitable temperature on any dislocations remaining in the crystal. Subsequent removal of the surface by electropolishing and conventional metallographic procedures enables the location of the precipitate and hence the distribution of dislocations to be found.

An alloy of aluminium with 3·8 wt. % of silver was used. Single crystals with a gauge length of 2·3 in. and cross section 0·3 in. × 0·1 in. were grown by a modified strain anneal procedure, electropolished, solution treated, quenched at a rate not fast enough to cause detectable quenching strains, and then quickly repolished and strained in tension. Part of one surface of the single crystals used had been abraded before the final polish during a study of the effects of such abrasion on the nature of slip bands, but in view of later work to be described separately it is not believed that this abrasion had any effect on the results to be detailed.

A typical surface micrograph after an elongation of 5% of crystal LG103 whose orientation, fig. 1 (Plate 26), is towards the middle of the stereographic triangle is shown in fig. 2 (Plate 26). Under oblique illumination it was found that some slip bands were more prominent than others. No slip bands on other systems could be detected. After ageing and repolishing with an accentuation of the structure by an anodising treatment, the interior micrograph of fig. 3 (Plate 26) was obtained.

This shows heavily developed primary slip bands, obviously related to the prominent bands of fig. 2, (Plate 26) but no trace of the other more closely spaced surface slip bands between the prominent ones. Whether closely spaced bands exist in the interior is the subject of further investigation. For the moment, the important feature of fig. 3 (Plate 26) is the indication in this crystal of ‘ middle ’ orientation of short slip bands on the conjugate (Rosi and Mathewson 1950) system lying across the primary system. The slip bands on the conjugate system became continuous as the edge of the crystal was approached and here evidence was also found of slip on the cross slip system (fig. 4 (Plate 27)). This effect at the specimen edges has not been found for other crystals –it may be related to the fact that the glide direction was towards a corner of the test specimen and not, as in the other cases, towards the surface being examined.

Crystal LG81, of orientation near the [100]–[110] side of the stereographic triangle, showed only primary slip bands on the surface after an extension of 2%, but in the interior short slip bands were again found on the conjugate system crossing the primary one (fig. 5 (Plate 27)).

For crystal LG80 on the [111]–[110] side of the stereographic triangle, primary slip only was observed on the surface after an extension of 7%. In the interior no evidence was found of any aggregation of dislocations on other than the primary system (fig. 6 (Plate 27)).

None of the 3·8% silver crystals so far tested have shown any deformation bands of the S-type either on the surface or in the interior but bands of secondary slip of the step ladder type (Calnan 1952) are sometimes observed. The stress strain curves for the particular crystals described were not determined, but in more recent experiments, the shape of the curves has been consistent with linear hardening, the slope being approximately the same as that for super pure aluminium crystals of similar orientations.

Part of the explanation of these results is believed to be that at the applied stress which is necessary for several per cent elongation on the primary system the total resolved stress on other less favourably oriented systems due to the applied stress plus that set up by groups of dislocations on the primary system, is large enough to cause the generation on such a system of a limited number of dislocations. These dislocations are apparently not sufficient in number to produce a detectable step on the surface. Experimental evidence for the generation of slip bands in the interior prior to the applied stress exceeding the conventionally determined yield stress has been reported in sodium chloride by Pratt (1952).

For crystal LG81 where short slip bands on the conjugate system were observed the second most favoured slip system is the conjugate system. For crystal LG80, on the other hand, where only the one set of slip bands was found in the interior the slip system with the second highest resolved shear stress is a different direction in the same slip plane and this of course cannot be distinguished from the primary system. Crystal LG103, though further from the [111]–[110] boundary than LG80, shows a similar order of favoured slip systems. However the interior metallography results differ from those for LG80 in that slip on the conjugate system which is the third favoured one was actually found in the interior while at the edges of the crystal some slip on the cross slip system was also detected. The specimen shape and the orientation of glide plane and direction towards that shape as they affect the rotation of the gauge length relative to the shoulders during plastic extension is being further investigated.

The detection of less favourably oriented slip systems in the interior of crystals for which only primary slip was observed on the surface provides experimental justification for the model used by Haasen and Leibfried (1951–52) to explain the orientation dependence of strain hardening curves.

The interactions between dislocations on secondary systems with the primary system clearly provide a source of work hardening although, if the preliminary stress strain curves are typical of all orientations of alloy crystals, then these results provide experimental evidence for a mechanism of linear hardening only.

ACKNOWLEDGMENTS

This work was commenced in the Department of Metallurgy at the University of Birmingham under the direction of Professor A. H. Cottrell and has been continued at the Department of Supply Laboratories, Melbourne, Australia.

The author is indebted to the Chief Scientist, Department of Supply, for permission to publish.

REFERENCES

BROWN, A. F., and HONEYCOMBE, R. W. K., 1951, *Phil. Mag.*, **42,** 1146.
CALNAN, E. A., 1952, *Acta Cryst.*, **5,** 557.
HAASEN, P., and LEIBFRIED, G., 1951–52, *Z. Phys.*, **131,** 538.
KUHLMANN-WILSDORF, D., VAN DER MERWE, J. H., and WILSDORF, H., 1952, *Phil. Mag.*, **43,** 632.
PRATT, P. L., 1952, *A.E.R.E. Harwell Report* M/R 883.
ROSI, F. D., and MATHEWSON, C. H., 1950, *Trans. A.M.I.E.*, **188,** 1159.

ERRATA

Photometric Measurement of Ionization in Cloud Chambers, by I. BUTTERWORTH, 1955, *Phil. Mag.*, **46,** 884.

In the table of mass measurements, p. 892, the figures in the column "Mass from visual estimation" are upper limits, no lower limit being assignable. The limits given do not apply. The same applies to the value 1220 in the photometric measurements.

In the abscissae of fig. 2 the small divisions represent 200 electron masses.

CXXVII. REVIEWS OF BOOKS

Annual Review of Nuclear Science, Volume 4, 1954. Editor JAMES G. BECKERLEY. Published by Annual Reviews Inc., Stanford, California in co-operation with the National Research Council of the National Academy of Sciences. [Pp. 483.] Price (outside the U.S.A.) $7.50 postpaid.

THE contents of the fourth volume of the Annual Review of Nuclear Science cover an exceptionally wide range as will be seen from the following list :

Recent developments in proton synchrotrons by J. P. Blewett.
Theories of photonuclear reactions by J. S. Levinger.
Radiofrequency and microwave spectroscopy of nuclei by G. E. Pake.
Standardization of radioactive sources by G. G. Manov.
Fission radiochemistry (*low-energy fission*) by L. E. Glendenin and E. P. Steinberg.
Stable isotope dilution as an analytical tool by M. G. Inghram.
Nuclear particle detection (*fast electronics*) by R. E. Bell.
Nuclear particle detection (*characteristics of scintillators*) by R .K. Swank.
Nuclear particle detection (*characteristics of Cerenkov counters*) by J. Marshall.
Alpha radioactivity by I. Perlman and F. Asaro.
Positronium by S. DeBenedetti and H. C. Corben.
The interactions between pi-mesons and nucleons by M. Gellmann and K. M. Watson.
Heavy mesons by C. Dilworth, G. P. S. Occhialini and L. Scarsi.
Penetration of heavy charged particles in matter by E. A. Uehling.
Biochemical effects of radiation by K. P. DuBois and D. F. Petersen.
Vertebrate radiobioloyg (*lethal actions and associated effects*) by J. F. Thomson.
Radioactivity in geology and cosmology by T. P. Kohman and N. Saito.

N. F. M.

Radioisotope Conference 1954. Sponsored by the Atomic Energy Research Establishment, Harwell. Proceedings of the Second Conference, Oxford, 19–23 July. Edited by J. E. JOHNSTON, with the assistance of R. A. FAIRES and R. J. MILLETT. Vol. 2, *Physical Sciences and Industrial Applications*. [Pp. ix+223.] (London : Butterworths Scientific Publications, 1954.) Price 45*s*.

THE second volume of papers presented at the Radioisotope Conference at Oxford in 1954 presents a fascinating account of the use of radioisotopes in Physical Sciences and Industrial Applications. The twenty-four papers presented cover four main fields : Chemistry, especially exchange reactions and polymerization ; Metallurgy, including segregation, purification and self-diffusion in metals and alloys ; Physics, including some new technical devices and Industrial Applications. To physicists these papers appear to form a more united group than the medical, agricultural and biological papers contained in volume 1. Nevertheless, it is already clear that radioisotope methods, as a tool of scientific research has reached roughly the same position as electron microscopy. The basic techniques and underlying principles are well established. Modifications and improvements of general importance may from time to time be reported. But on the whole individual applications of the technique to a particular field form an integral part of the field itself rather than another facet of radioisotopy. With the growing application of this technique to numerous branches of scientific research it will become increasingly difficult to convene further Radioisotope Conferences of this type.

The volume is well produced, the papers are brief and clear and the discussions lively—where necessary persistent—and stimulating. The reviewer found particular pleasure in reading Dr. D. S. Taylor's account of a novel use of radioactive phosphorus to study the movement of wool fibres during the process of drafting.

D. TABOR.

Linearized Theory of Steady High-Speed Flow. By G. N. WARD. (Cambridge: University Press.) [Pp. xv+243.] Price 30*s*.

FOR a decade, the linearized theory of compressible fluid motion has been intensively pursued by a large body of aerodynamicists throughout the world. The pioneering exploration seems now to be mainly completed, and it is proper that summaries are beginning to appear in book form. High-speed aerodynamic theory in general has been the subject of several recent treatises of an encyclopaedic nature. Professor Ward has chosen instead to produce a single volume of moderate size by confining attention to steady motions and to the linearized theory only.

The linearized equation of fluid motion is simply Laplace's equation for subsonic flows and the wave equation for supersonic flows; all the complications arise in the bondary conditions. It is therefore appropriate that the first part of the monograph, devoted to general theory, concludes with a careful discussion of boundary conditions and the various subtle points connected with singularities at wing and wake edges, shock waves, and conditions far from the body. The second part treats special methods for thin wings, conical fields, and nearly cylindrical shapes. The last part is devoted to slender-body theory, a useful further approximation beyond linearization that is valid only near the surfaces of smooth slender shapes. A selected bibliography lists 200 original papers.

The monograph is based upon an Adams Prize essay, and the author consequently admits to a strong personal bias in the selection of material. However, conciseness demands some definite viewpoint, and the author's own well-known researches do serve as a suitable basis for a connected account. The mathematical apparatus includes vector notation and Hadamard's finite part of a divergent integral, but the physically more intuitive concept of sources, sinks, and vortices is also discussed. M. D. V. D.

BOOK NOTICES

Harmonic Analysis and the Theory of Probability. By S. BOCHNER. (Berkeley and Los Angeles: University of California Press.) [Pp. viii+176.] Price 35*s*.

Degradation of Vinyl Polymers. By H. H. G. JELLINEK. Volume III of a series of monographs on physical chemistry edited by Eric Hutchinson of Stanford University. (London: Academic Books Ltd.) [Pp. 329.] Price $8.50.

Applied Mass Spectrometry. The report of a conference organized by the Mass Spectrometry Panel of the Institute of Petroleum and held in London from 29th–31st October, 1953. Published by the Institute of Petroleum. [Pp. vii+333.] Price not stated.

Science and its Background. By H. D. ANTHONY. 2nd edition. (London: Macmillan and Co. Ltd.) [Pp. ix+337.] Price 20*s*.

Bessel Functions for Engineers. By N. W. McLACHLAN. [Pp. xii+239.] (Oxford: Geoffrey Cumberlege, Clarendon Press.) 2nd Edition. Price 35*s*.

[*The Editors do not hold themselves responsible for the views expressed by their correspondents.*]

Fig. 2

Electron micrograph of 60 Å gold film (×10 000).

Fig. 3

Electron micrograph of 100 Å bismuth oxide film (×10 000).

Fig. 4

Electron micrograph of 60 Å gold film on 100 Å bismuth oxide (×10 000).

Fig. 5

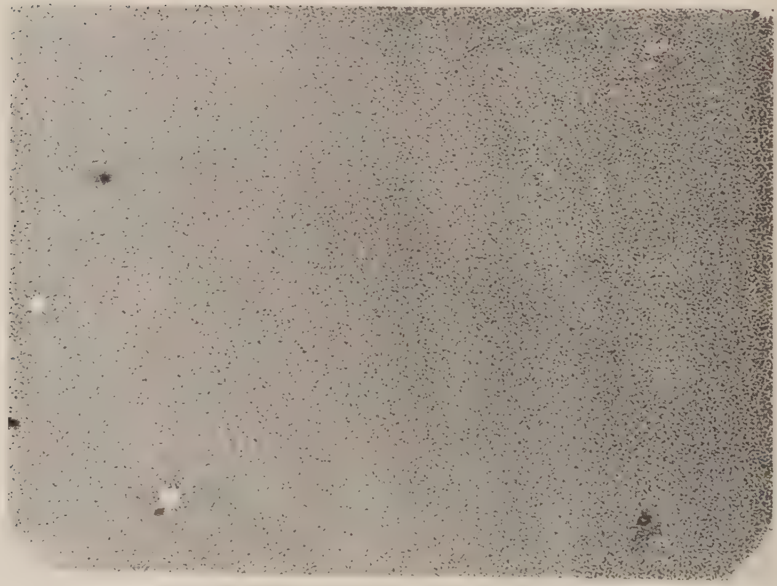

Electron micrograph of 60 Å gold film on 100 Å bismuth oxide, after inadvertent overheating (×10 000).

Fig. 6

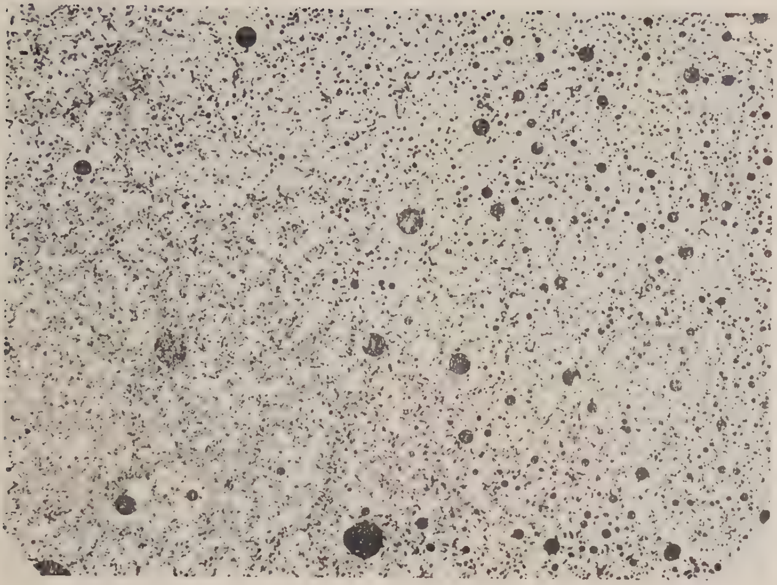

Same as fig. 5, after intense electron bombardment.
(Figures 2–6 on formvar pellicle base.)

Fig. 7

Electron micrograph of 100 Å gold film, between two 100 Å bismuth oxide films after annealing at 450°c (×10 000). (On carbon pellicle base.)

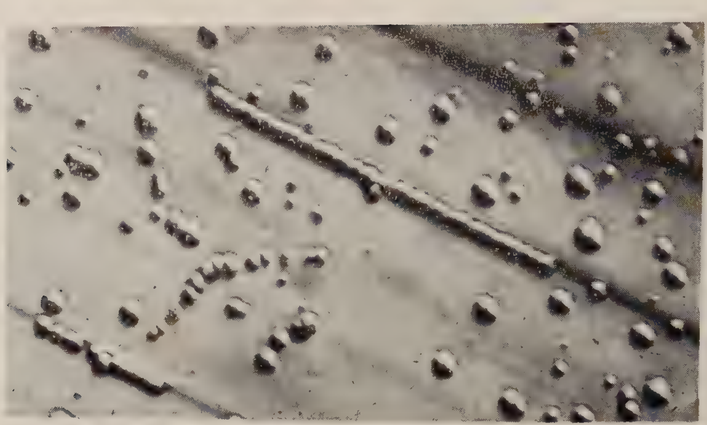

Fig. 1 ×1200

Preferential alignment of 'microetchpits' on the slip lines (Al etched immediately after deformation).

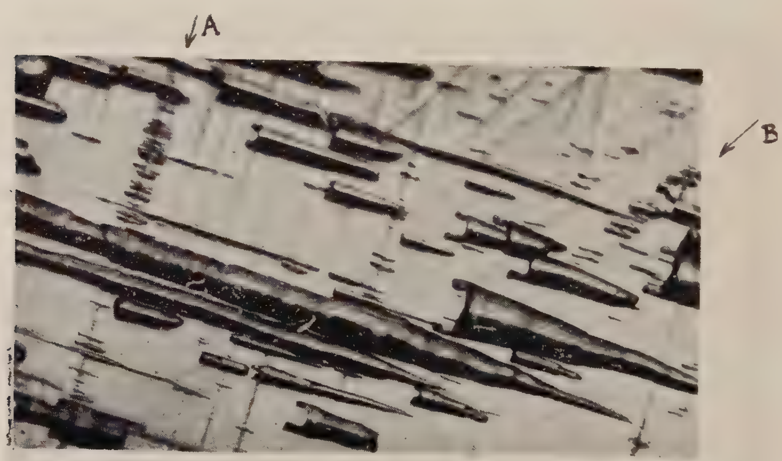

Fig. 2 ×600

Small etchpits on two slip systems A and B.

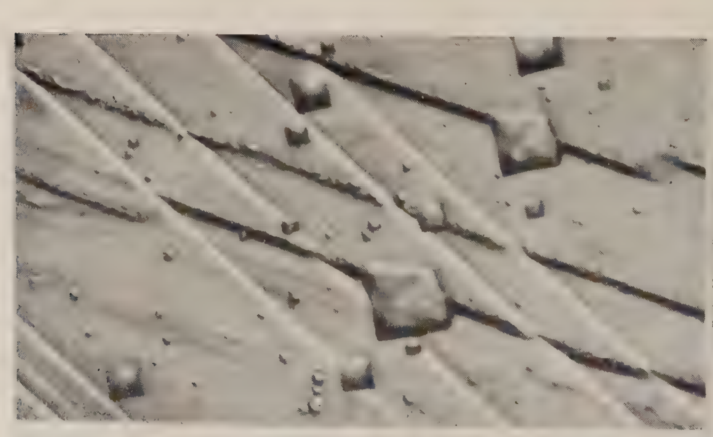

Fig. 3 ×1200

Microetchpits aligned on a single slip system. (Notice the difference between etchpits with a geometrical outline and the smaller and rounder microetchpits.)

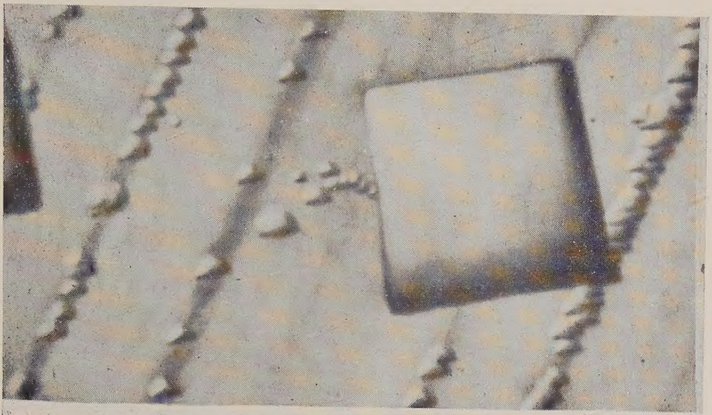

Fig. 4

Various examples of alignments of microetchpits, either continuous or separate.

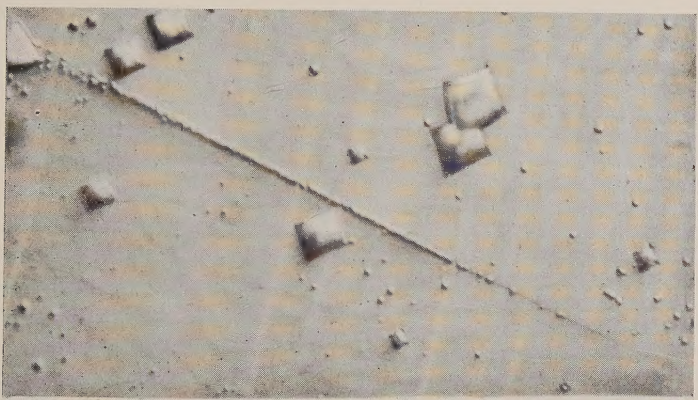

Fig. 5

End of a slip line: no accumulation of etchpits is observed there.

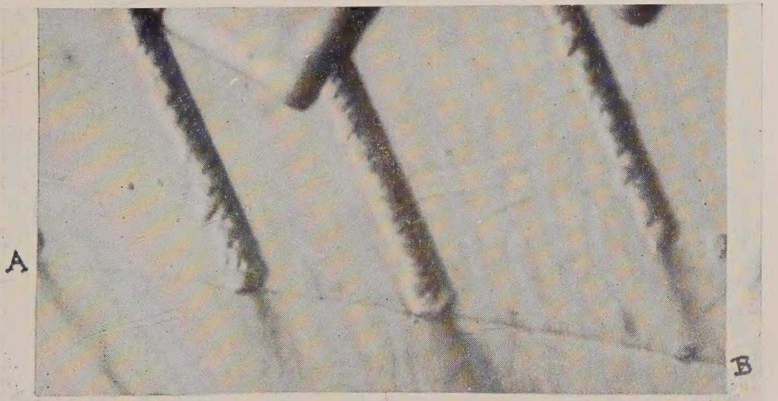

Fig. 6

Arrival of slip lines at a grain boundary A, B. One of the slip lines shows no etchpits except at the point of intersection.

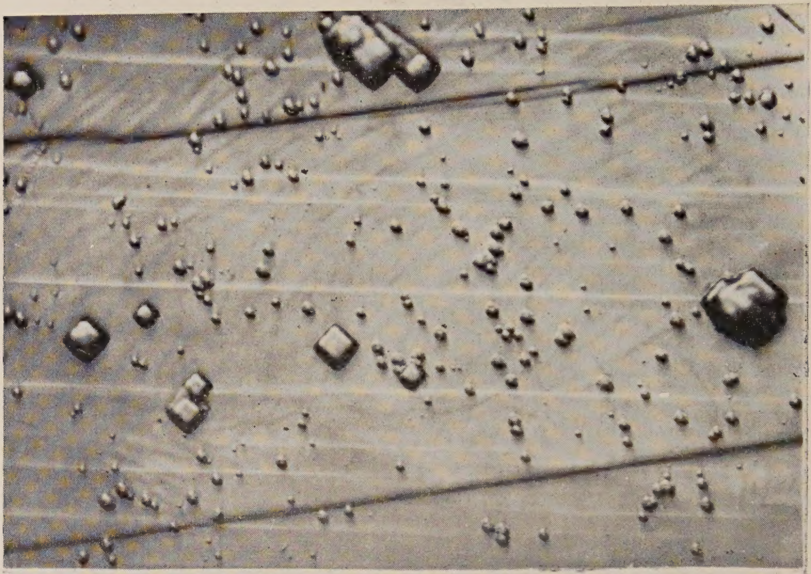

Fig. 7 ×600

Electrolytically polished specimen, weakly stretched, polished again and etched. A new deformation after etching shows the direction of the slip lines.

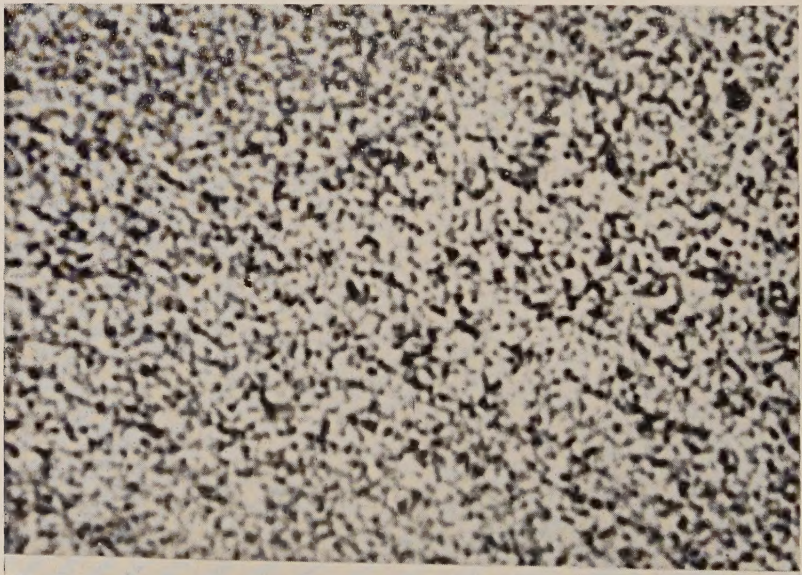

Fig. 8 ×600

Al–Mn 0·56% alloy homogenized, weakly stretched, polished and aged. Microetchpits are aligned along the direction of the previously active slip lines.

Fig. 1

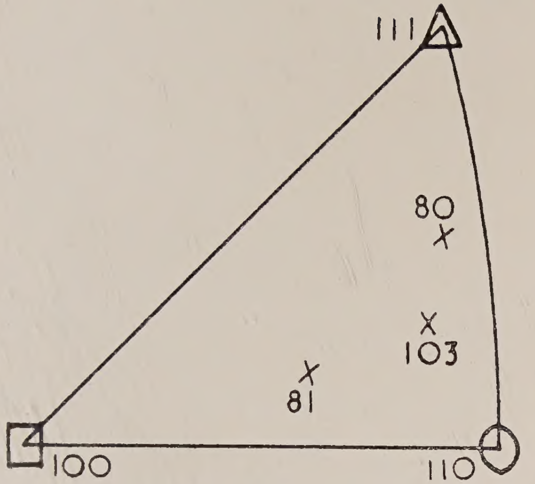

Orientation of specimen axis of single crystals.

Fig. 2

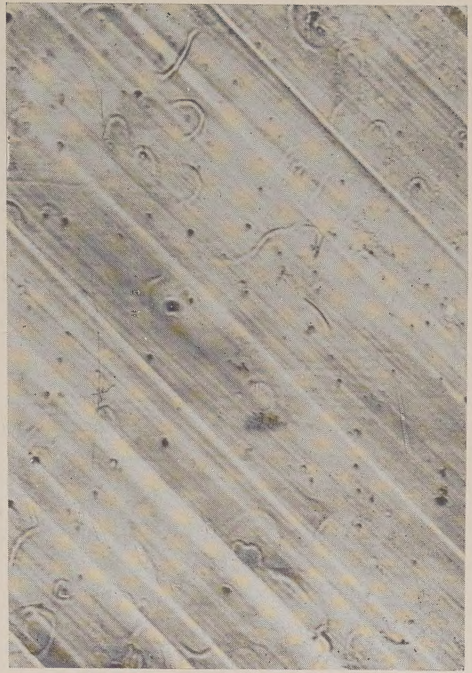

×250

Surface micrograph of crystal LG103 after an extension of 5%.

Fig. 3

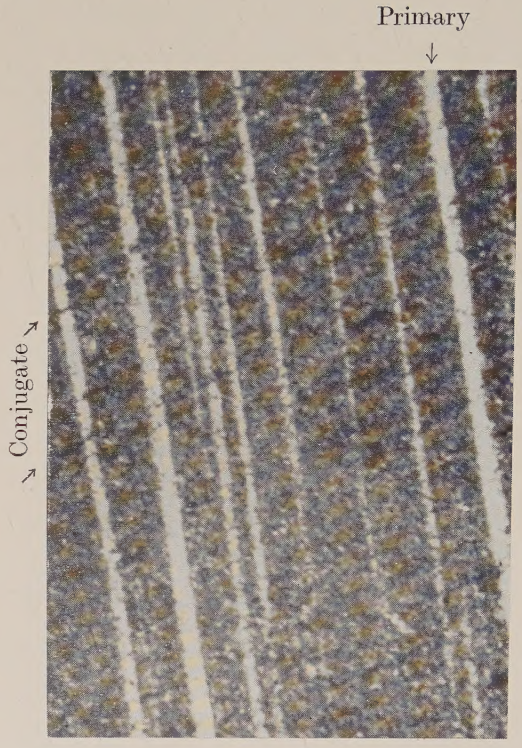

×250

Interior micrograph of crystal LG103 showing primary slip bands related to the prominent bands of fig. 2 and short bands on the conjugate system.

Fig. 4

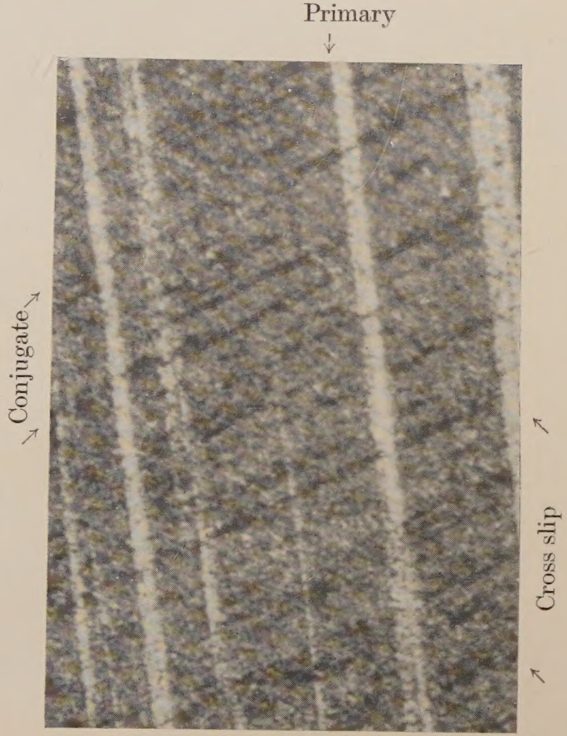

×250

As fig. 3 but towards the edge of the crystal. Conjugate slip continuous and two traces on the cross slip system.

Fig. 5

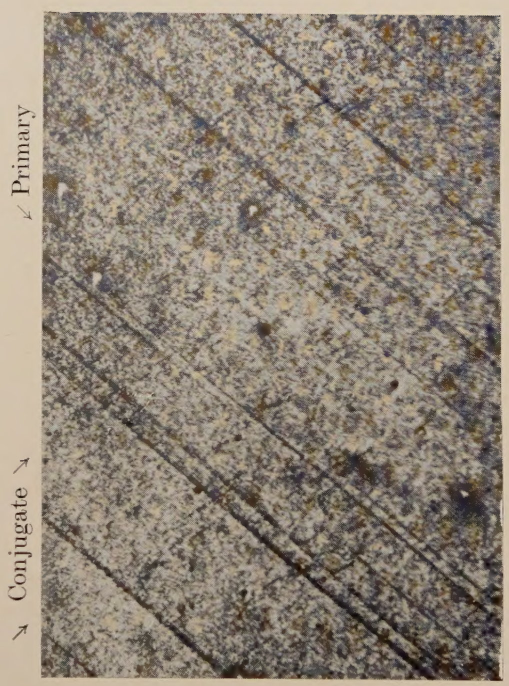

×150

Interior micrograph of crystal LG81 showing short slip bands on the conjugate system lying across the primary system.

Fig. 6

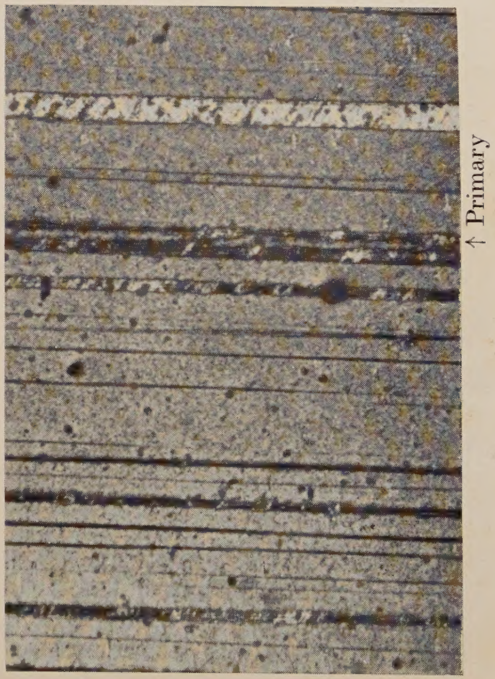

×150

Interior micrograph of crystal LG80 showing only the primary system.